Polymer nanocomposites with fibrillar inclusions generated during compounding

Kinga Jurczuk
PhD Thesis

Advisor: Prof. dr hab. Andrzej Gałęski

Centre of Molecular and Macromolecular Studies
Polish Academy of Sciences
Polymer Physics Department

Łódź, 2012

I am heartily thankful to my advisor,
Prof. dr hab. Andrzej Gałęski, whose encouragement,
guidance and support from the initial to the final level
enabled me to develop an understanding of the subject.

I am also grateful to Prof. dr hab. Ewa Piórkowska-Gałęska,
for all helpful discussions we have sheared.

Lastly, I offer my regards to all of those, especially
my husband, my parents and my brother, who supported me
in any respect during the completion of this thesis.

Contents

General introduction **7**

Chapter 1 State of knowledge **11**

1.1 Mixing of polymers 11
1.1.1 Capillary instabilities and breakup 13
1.1.2 Dispersive mixing 15
1.1.3 References 18
1.2 Polytetrafluoroethylene, PTFE 20
1.2.1 Synthesis of polytetrafluoroethylene 20
1.2.2 Morphology of nascent PTFE particles 21
1.2.3 Crystalline structure of PTFE 23
1.2.4 Properties of polytetrafluoroethylene 25
1.2.5 PTFE processing and its applications 26
1.2.6 References 27
1.3 Mechanisms of plastic deformation in semicrystalline polymers 31
1.3.1 Deformation of amorphous phase 33
1.3.2 Deformation of polymer crystals 34
1.3.3 References 38
1.4 Scope of the thesis 45

Chapter 2 Experimental Section **47**

2.1 Materials 47
2.2 Apparatus and experimental techniques 51
2.2.1 Scanning Electron Microscopy (SEM) 51
2.2.2 Mechanical properties 52
2.2.3 Instruments for rheological tests 53
2.2.4 Wide-angle X-ray Scattering (WAXS) 55
2.2.5 Differential Scanning Calorimetry (DSC) 55
2.2.6 Polarized Light Microscopy (PLM) 56

2.2.7 Dynamic Mechanical Thermal Analysis (DMTA) 57

Chapter 3 Results and Discussion 58

3.1 Nascent polytetrafluoroethylene powders 58
3.2 Deformation of polytetrafluoroethylene crystals 63
3.3 Structure of the nanocomposites with PTFE inclusions 66
3.3.1 Type of polytetrafluoroethylene powder 66
3.3.2 Thermoplastic matrix and its viscosity 68
3.3.3 Shear rate and compounding time 71
3.4 Thermal properties of the nanocomposites with PTFE inclusions 75
3.5 Mechanical properties of the nanocomposites with PTFE inclusions 80
3.6 Rheological properties of the nanocomposites with PTFE inclusions 86
3.6.1 Oscillatory shear flow 86
3.6.2 Uniaxial extensional flow 88
3.7 Conclusions 95
3.8 References 97
3.9 Nomenclature 103
3.10 List of publications and patents 105
3.11 Summary 106

General introduction

The properties of thermoplastic polymers can be modified by means of filling. A type and a content of filler used, and also shapes of filler grains and mutual interactions between a filler and a polymer matrix affect the properties of filled polymers. Fillers can be classified as powders, composed of spherical or flaky grains, or short cut fibers, and as continuous unidirectional fillers, called also fibers. A content of powders or continuous fillers in composites ranges typically from 5 to 60 wt. %. Commonly used fillers comprise various chemical compounds (e.g. talc, chalk, volcanic minerals, metal powders and others) [Rothon 1999], carbon fibers, glass fibers or polymeric fibers (e.g. polypropylene PP, polyethylene PE, polyamide PA, poly(ethylene terephthalate) PET, and poly(buthylene terephthalete) PBT, and also natural fillers (e.g. cellulose, wood flour etc.) [Klason 1984].

Polymer nanocomposites represent a new and attractive alternative to conventionally filled polymers. A characteristic feature of polymeric nanocomposites is that filler particles are of nanometer sizes (typically 1÷100 nm thick in at least one dimension). Nowadays, most often used are inorganic nanofillers including silicates, clays, carbon nanotubes and carbon nanofibers. Owing to a large surface area of interactions between filler nanoparticles and a polymer a desirable modification of properties including increased modulus and strength, toughness, outstanding barrier properties, improved solvent and heat resistance, reduced weight and improved dimensional stability, induced electrical conductivity, thermal conductivity, scratch resistance and other properties, can be achieved at low filler loadings (1÷5 wt. %) [Friedrich 2005].

The virtue of polymer nanocomposites is neither solely based on the mechanical enhancement of the neat resin nor based on the direct replacement of current filler or blend technology. Rather, its importance comes from providing value-added properties not present in the neat resin, without sacrificing thee resin's inherent processability and mechanical properties or by adding excessive weight. Polymer nanocomposites contain substantially less filler and thus enabling greater retention of the inherent processability and toughness of the neat resin than conventional polymer composites [Usuki 1993a; Usuki 1993b; Pinnavaia 2001; Ray 2003; Lee 2005; Sanchez 2005; Mai 2006; Moniruzzaman 2006; Manias 2007; Morgan 2007; Leszczynska 2007; Utracki 2007; Darder 2007; Okada 2007; Vaia 2007; Schaefer 2007].

Polymer-polymer composites are rear and known only when ready-made nanofibers or nanodroplets are dispersed in the matrix. Polymer nanofibers are now produced by

electrospinning only. “All-polymer” nanofiber composites are only known from 3 papers [Iwatake 2008; Jenoobi 2010; Kowalczyk 2011], all of them describing composites containing cellulose nanofibers.

In mixing of immiscible polymers, drops of dispersed phase are extended but they do not preserve the shape after deformation. The occurrence of capillary instabilities phenomenon leading to the disintegration of liquid extended threads causes that polymer inclusions finally appear in a form of droplets instead of fibers. The idea is to find a way to preserve the shape of polymer inclusions after deformation, i.e. act against capillary instabilities. A range of means can be proposed but there are limits of achievable deformation: (a) fast crosslinking while deformed inclusions, (b) fast solidification of a matrix, (c) fast solidification of inclusions, (d) use of crystalline but easy to deform inclusions, (e) very viscous matrix and inclusions subjected to shear, (f) drastic change of surface tension and (g) use of liquid crystal (LC) polymers as a dispersed phase. (a-c) and (f-g) are unrealistic, (e) could be considered but difficult to perform on existing equipments, while (d) seems to be a promising case to generate polymer nanofibers through shearing the medium in which crystalline inclusions are dispersed (a polymer matrix). The higher the capillary number the more efficient is the stress transfer from sheared polymer matrix to the crystal inclusions. If the shear stress overrules the interfacial stress the inclusion can be deformed. In order to deform polymer crystals embedded in a viscous media a critical shear stress, resolved in a slip plane of the respective slip systems to be activated, must be reached and exceeded. There is only one paper published describing a possibility of deformation of a sheet crystal embedded in viscous matrix under shearing flow [Harrowell 1990]. Shearing of the matrix was found to lead to a mechanical instability of a crystal which results in a continuous decrease in the coherence length of crystalline order in the sliding layers as the shear rate increases. The shear modulus and shear yield stress of the sheet crystal was at the level of 2 MPa which value is characteristic for crystals of many polymer at temperatures few tens of degrees below their melting. The above estimation makes the idea to transform polymer crystals into nanofibers by shear deformation quite realistic.

The state of knowledge of the mixing of immiscible polymers, polytetrafluoroethylene used in the thesis as an easy deformable crystalline inclusions, and the deformation of semicrystalline polymers, especially mechanisms o polymer crystals deformation, will be described for proper understanding the subject of further studies presented in this thesis.

References

Darder M., Aranda P., Ruiz-Hitzky E., **2007**. *Bionanocomposites: A New Concept of Ecological, Bioinspired, and Functional Hybrid Materials.* Adv. Mater. *19*, 1309-1319;

Friedrich K., Fakirov S., Zhang Z., **2005**. *Polymer Composites. From Nano- to Macro-Scale*. Springer, New York;

Harrowell P., **1990**. *Mechanical instability of colloidal crystals under shear flow.* Phys. Rev. A 42, 3427–3431;

Iwatake A., Nogi M., Yano H., **2008**. *Cellulose nanofiber-reinforced polylactic acid.* Comp. Sci. Tech. 68, 2103-2106;

Jenoobi M., Harun J., Mathew A.P., Oksman K., **2010**. *Mechanical properties of cellulose nanofiber (CNF) reinforced polylactic acid (PLA) prepared by twin screw extrusion.* Comp. Sci. Tech. 70, 1742-1747;

Klason C., Kubat J., Strömvall H.E., **1984**. *The efficiency of cellulosic fillers in common thermoplastics. Part 1. Filling without processing aids or coupling agents*. Int. J. Polym. Mater. 10, 159-187;

Kowalczyk M., Piorkowska E., Kulpinski P., Pracella M., **2011**. *Mechanical and thermal properties of PLA composites with cellulose nanofibers and standard size fibers.* Composites Part A 42, 1509-1514;

Lee L.J., Zeng C., Cao X., Han X., Shen J., Xu G., **2005**. *Polymer nanocomposite foams.* Comp. Sci. Tech. 65, 2344-2364;

Leszczynska A., Njuguna J., Pielichowski K., Banerjee J.R., **2007**. *Polymer/montmorillonite nanocomposites with improved thermal properties Part I. Factors influencing thermal stability and mechanisms of thermal stability improvement*. Thermochimca Acta *435*, 75-96;

Mai Y.-W., Yu Z.-Z., **2006**. *Polymer Nanocomposites.* Woodhead Publ., ISBN 978-1-85573-969-7;

Manias E., **2007**. *Nanocomposites: Stiffer by design*. Nature Materials 6, 9–11;

Moniruzzaman M., Winey K.I., **2006**. *Polymer Nanocomposites Containing Carbon Nanotubes*. Macromolecules *39*, 5194-5205;

Morgan A.B., Wilkie C.A., **2007**. *Flame Retardant Polymer Nanocomposites.* Wiley, ISBN 978-0-471-73426-0;

Okada A., Usuki A., **2007**. *Twenty Years of Polymer-Clay Nanocomposites.* Macromol. Mater. Eng. 291, 1449-1476;

Pinnavaia T.J., Beall G.W., **2001**. *Polymer-Clay Nanocomposites.* Wiley, ISBN 978-0-471-63700-4;

Ray S.S., Okamoto M., **2003**. *Polymer/layered silicate nanocomposites: a review from preparation to processing.* Prog. Polym. Sci. 28, 1539-1641;

Rothon R.N., **1999**. *Mineral Fillers In Thermoplastics: Filler Manufacture and Characterisation*. Adv. Polym. Sci. 139, 67-107;

Sanchez C., Julian B., Belleville P., Popall M., **2005**. *Applications of hybrid organic-inorganic nanocomposites.* J. Mater. Chem. *15,* 3559-3592;

Schaefer D.W., Justice R.S., **2007**. *How Nano are Nanocomposites?*. Macromolecules *40*, 8501-8517;

Usuki A., Kawasumi M., Kojima Y., Okada A., Kurauchi T., Kamigaito O., **1993a**. *Swelling behavior of montmorillonite cation exchanged for ω-amino acids by ε-caprolactam*. J. Mater. Research 8, 1174-1178;

Usuki A., Kojima Y., Kawasumi M., Okada A., Fukushima Y., Kurauchi T., **1993b**. *Synthesis of nylon 6-clay hybrid*. J. Mater. Research 8, 1179-1184;

Utracki L.A., Sepehr M., Boccaleri E., **2007**. *Synthetic, layered nanoparticles for polymeric nanocomposites (PNCs).* Polym. Adv. Technol. *18*, 1-37;

Vaia R.A., Maguire J.F., **2007**. *Polymer Nanocomposites with Prescribed Morphology: Going beyond Nanoparticle-Filled Polymers.* Chem. Mater. *19*, 2736-2751;

Chapter 1
State of knowledge

1.1 Mixing of polymers

Mixing is a key step in almost every polymer processing operation, affecting material properties, processability and cost. The development of new materials seems to rely nowadays more on modification, blending and compounding rather than on the synthesis of chemically new polymers. Polymers are blended with other polymers to combine their properties and sometimes to even synergistically increase their physical characteristics. Also various additives and reinforcing agents are mixed with polymers to improve mechanical performance and impart specific properties to the mixture.

The words: mixing, blending and compounding are synonyms and according to the English dictionaries are defined as “an action to combine ingredients into one mass, so that the constituent parts are indistinguishable”. However, in the plastic processing, these three terms have different meanings. While mixing indicates the physical act of homogenization, e.g., mixing of fractions, blending commonly specifies preparation of polymer blends or alloys, while compounding means incorporation of additives into polymeric matrix, i.e. antioxidants, lubricants, pigments, fillers, or reinforcements.

There are two basic mechanisms of mixing polymers. First involves the reduction in size of a cohesive minor component such as liquid drops or agglomerates of solid particles, and is called dispersive or intensive mixing. The second, referred to as distributive, laminar or extensive mixing, is the process of spreading the minor component throughout the matrix in order to obtain a good spatial distribution. In any mixing device, these two mechanisms may occur simultaneously. In distributive mixing the second component is usually a powder whose particles cannot be further broken down.

The spherical liquid drops are usually the starting morphology of dispersed phase. Their deformation in flow field is promoted by the shear stress, τ, and counteracted by the interfacial stress, σ/R. The ratio between these two stresses is called the capillary number, Ca:

$$Ca = \frac{\tau R}{\sigma} = \frac{\eta_c \dot{\gamma} R}{\sigma} \tag{1.1}$$

where R is the local radius of a drop, σ is the interfacial tension, η_c is the viscosity of matrix (or continuous phase), and $\dot{\gamma}$ is the shear rate.

Taylor [Taylor 1932; Taylor 1934; Taylor 1954] and others [Cerf 1951; Travelyan 1951; Bartok 1957; Bartok 1959; Rumscheidt 1961a; Rumscheidt 1961b] extensively studied the process of liquid drop deformation in two basic flow fields: simple shear flow (or rotational flow) and extensional flow (or irrotational flow). Later, Grace [Grace 1982] determined the critical conditions for the affine deformation of drop and breakup phenomena (Figure 1.1).

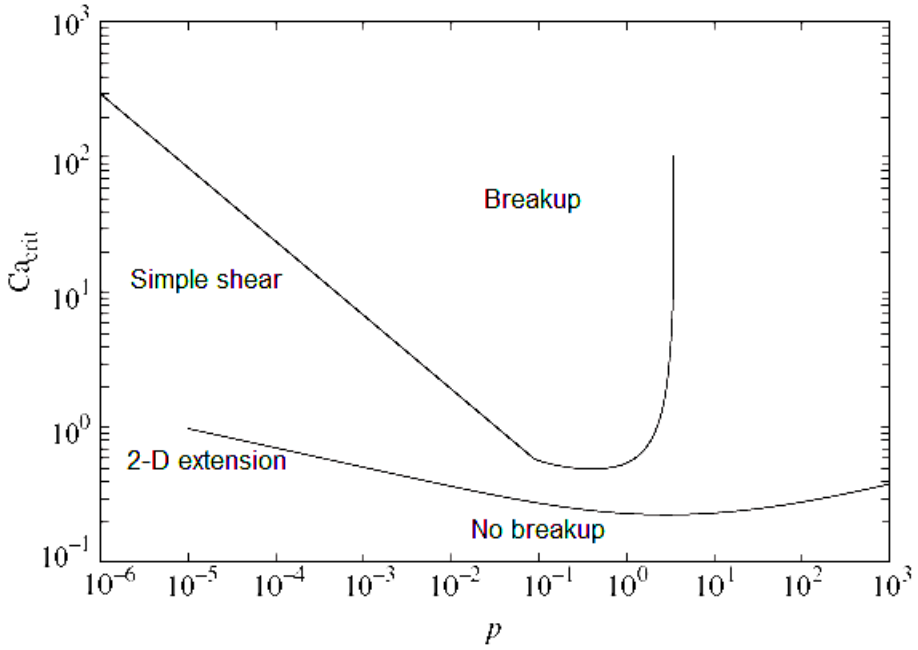

Figure 1.1. *Critical capillary number, Ca_{crit} as a function of viscosity ratio, p [Grace 1982].*

The critical value of capillary number, Ca_{crit}, strongly depends on the viscosity ratio, p, defined as the ratio between viscosity of dispersed phase and viscosity of matrix. Figure 1.1 shows that when the capillary number is lower than its critical value, $Ca < Ca_{crit}$ interfacial stress competes with shear stress and the liquid drop is deformed only slightly in the flow field, yielding a stable drop shape. However, when $Ca >> Ca_{crit}$ the shear stress dominates and the liquid spherical drop is extended into a thread, which can disintegrate into smaller droplets by capillary instability and breakup mechanisms. Karam *et al.* [Karam 1968] found that there are upper and lower limits of the viscosity ratio beyond which no drop breakup can occurs. In simple shear flow, deformed drops will be stable when the viscosity ratio will be $0.005 \leq p \geq 4$.

1.1.1 Capillary instabilities and breakup

The process of dispersing one liquid into another liquid can proceeds by two basic mechanisms [Janssen 1993] as illustrated in Figure 1.2. The first is steady breakup, or drop splitting, and the later is the disintegration of extended thread into series of fine droplets, also known as capillary instability phenomenon.

Since a sphere offers the minimum surface area for a given volume, the interfacial tension between two fluids causes that any nonspherical shape of liquid suspended in another to be unstable. The Lord Rayleigh [Rayleigh 1879] suggested a model for the growth of disturbance in a viscous jet in air. Later, Tomotika [Tomotika 1935] extended this theory to Newtonian fluids.

The instability of a liquid thread has been the object of a large number of theoretical and experimental investigations [Eggers 1997; Lin 1998; Pozrikidis 1999].

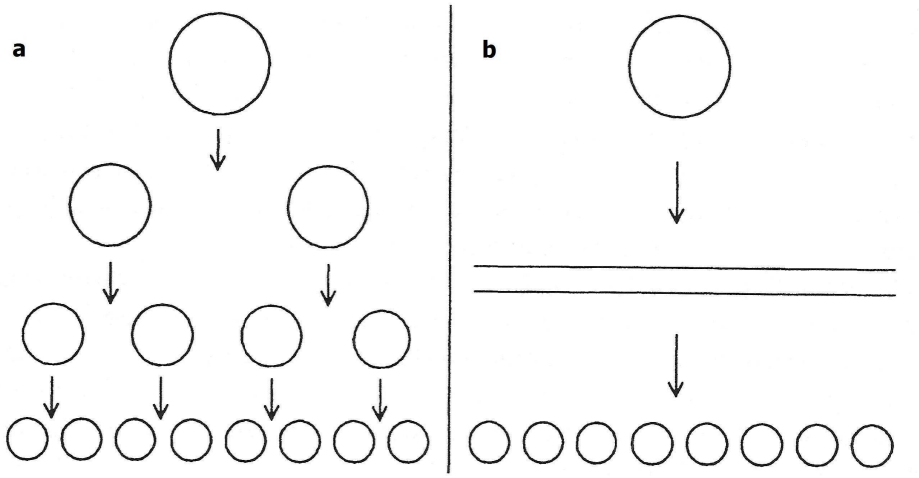

Figure 1.2. *Schematic representation of two dispersion mechanisms: (a) stepwise equilibrium mechanism of repeated drop breakup at Ca = Ca_{crit}, and (b) transient mechanism of extended thread disintegration [Janssen 1993].*

Since local radius, *R*, decreases during affine deformation of spherical drop, the interfacial tension tends to minimize the interface between long filament and liquid matrix. In a consequence, the small disturbances so-called Rayleigh disturbances grow at the interface of a liquid thread.

Figure 1.3 illustrates a sinusoidal Rayleigh disturbance forming on the liquid filament.

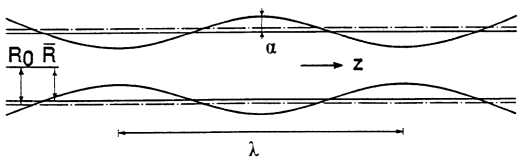

Figure 1.3. *A liquid thread of radius, R_0, with a Rayleigh sinusoidal disturbance [Manas-Zloczower 1994].*

The radius of this small disturbance, *R(z)*, is expressed by:

$$R(z) = \bar{R} + \alpha \sin\left(\frac{2\pi z}{\lambda}\right) = \left(R_0^2 - \frac{\alpha^2}{2}\right)^{0.5} + \alpha \sin\left(\frac{2\pi z}{\lambda}\right) \tag{1.2}$$

where R_0 is the radius of undisturbed thread, $\bar{R}$ is the average radius of disturbed thread ($\bar{R} < R_0$), α is the disturbance amplitude, and λ is the disturbance wavelength. The disturbance amplitude, α, grows exponentially with time:

$$\alpha = \alpha_0 e^{\beta t} \tag{1.3}$$

where α_0 is the original disturbance amplitude, and β is the growth rate given by

$$\beta = \frac{\sigma \Omega(\lambda, p)}{2\eta_c R_0} \tag{1.4}$$

The dimensionless growth rate of the disturbance, Ω, is a function of the wavelength, λ and the viscosity ratio, p. Initially, the small amplitudes of all wavelengths exist, but for a given value of p, only one disturbance with the particular wavelength, λ_m, becomes dominant and grows the fastest, and finally results in disintegration of the liquid filament into droplets. The dominant wave number, X_m $(= 2\pi R_0 / \lambda_m)$ and the corresponding dimensionless growth rate, Ω_m, as a function of viscosity ratio, p are presented in Figure 1.4.

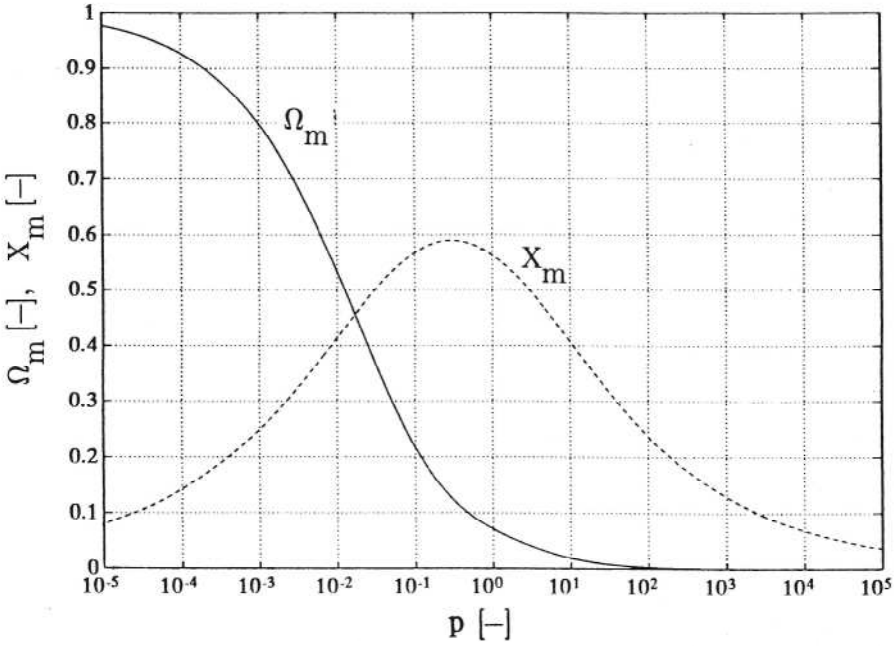

Figure 1.4. *The dimensionless growth rate, Ω_m and the wave number, X_m of interfacial disturbances as a function of viscosity ratio, p [Manas-Zloczower 1994].*

The time required for disintegration of thread, t_b, can be calculated from eq. (1.3):

$$t_b = \frac{1}{\beta}\ln\left(\frac{\alpha}{\alpha_0}\right) \tag{1.5}$$

Tomotika [Tomotika 1935] estimated that the process of thread disintegration occurs when the amplitude of disturbance approaches $0.82R_0$. Hence, the equation for breakup time takes form:

$$t_b = \frac{1}{\beta}\ln\frac{0.82R_0}{\alpha_0} \tag{1.6}$$

Depending on the viscosity ratio, p there are two different modes of drop breakup [Bartok 1959; Rumscheidt 1961b; Grace 1982; Smith 1985]. In the simple shear flow, for $p > 1$ the extended drop having rounded ends disintegrate in the middle in two or three almost equally sized droplets with a few tiny satellite drops between them (Figure 1.5a). The smaller viscosity ratio, p, between extended thread and matrix, the more satellite droplets are formed [Tjahjadi 1992].

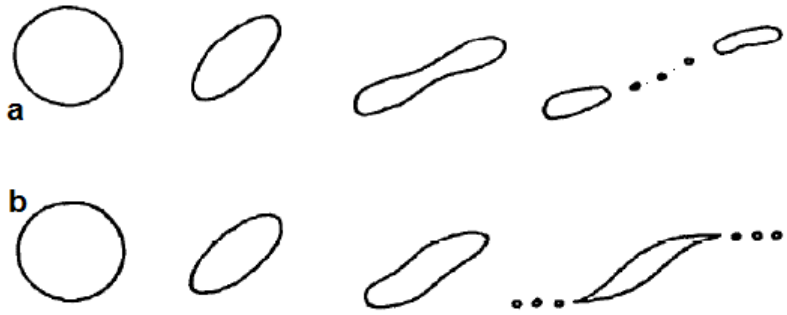

Figure 1.5. *Breakup modes of deformed drop in the simple shear flow: (a) fracture and (b) tipstreaming [Bruijn 1993].*

At low viscosity ratios $p < 0.1$ small droplets are released from the sharply pointed ends (Figure 1.5b). This so-called tipstreaming process is potentially very important since the shear rates required for this type of breakup have in some circumstances been observed to be two orders of magnitude lower than the fracture mode. The tipstreaming may also be useful for separation processes [Srinivasan 1986].

1.1.2 Dispersive mixing

During the initial stages of mixing, the local radius of drop, R, is large ($Ca >> Ca_{crit}$), the shear stress, τ, dominates over the interfacial stress, σ/R, and dispersed drops are affinely deformed in a flow field of the matrix [Janssen 1992]. The affine deformation of a spherical drop with diameter a $(=2R)$ into an ellipsoidal shape under simple shear flow is illustrated in Figure 1.6.

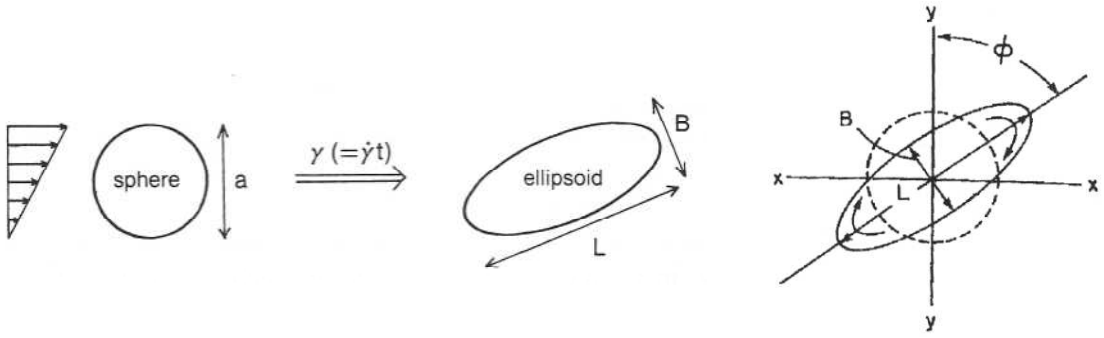

Figure 1.6. *The affine deformation of a sphere in the simple shear flow [Grace 1982; Manas-Zloczower 1994].*

Deformation of a liquid drop, *D*, is defined as:

$$D = \frac{L - B}{L + B} \tag{1.7}$$

where *L* and *B* are length and width of ellipsoid, respectively. It appeared that the drop cannot be deform infinitely. The steady drop deformation for Newtonian fluids [Taylor 1932; Taylor 1934] is finite and is expressed by:

$$D = Ca\frac{19p + 16}{16p + 16} \tag{1.8}$$

Cerf [Cerf 1951] investigated theoretically the rotation phenomenon of affinely deformed drop in simple shear flow and derived the following formula for an orientation angle, ϕ which is applicable only for small deformations:

$$\phi = \frac{\pi}{4} + \left(1 + \frac{2p}{5}\right)D \tag{1.9}$$

At high viscosity ratios, so high that the forces of surface tension counteracting deformation are negligible compared with those due to viscosity, the final deformation becomes a function of *p* only:

$$D = \left(\frac{5}{4}\right)p^{-1} \tag{1.10}$$

and the maximum of orientation angle, ϕ, along the flow direction, reaches $\pi/2$.

Torza *et al.* [Torza 1972] expanded the studies on the liquid drop deformation for Non-Newtonian fluids, e.g. molten polymers and determined the formula for *D*:

$$D = \frac{5(19p + 16)}{4(1 + p)\Big/\left[(19p)^2 + (20/Ca)^2\right]^{0.5}} \tag{1.11}$$

and the corresponding value of the orientation angle, ϕ:

$$\phi = \frac{\pi}{4} + \frac{1}{2}\tan^{-1}\left(\frac{19\,pCa}{20}\right) \tag{1.12}$$

When the deformation $D \geq 0.5$ the liquid drop becomes unstable and breaks up into series of droplets, both for simple shear flow and extensional flow.

Quantitative studies on drop deformation in simple shear and pure extensional flows [Taylor 1934; Rumscheidt 1961b; Grace 1982; Elmendorp 1986; Bentley 1986a; Bentley 1986b; Elemens 1993] have shown that an extension is more effective than a simple shear, especially in the case of high viscosity ratios and low interfacial tensions. However, it is impossible to achieve pure extensional flow in the confined flow geometries encountered in mixing machines and during limited periods of time. So, in practice, shear flow is more important.

The changes of an efficiency parameter, e_f, defined as the scalar product of the principal direction of strain and the transient drop deformation, are presented in Figure 1.7. In extensional flow e_f reaches a value of 1, while in simple shear the rotation of extended drop to the direction of flow causes that the efficiency (initially amounted to 1) ultimately approaches $1/\sqrt{2}$. However, application of the periodical reorientation of extended drops in the simple shear flow enables to obtain the maximum $e_f = 1$ more than once.

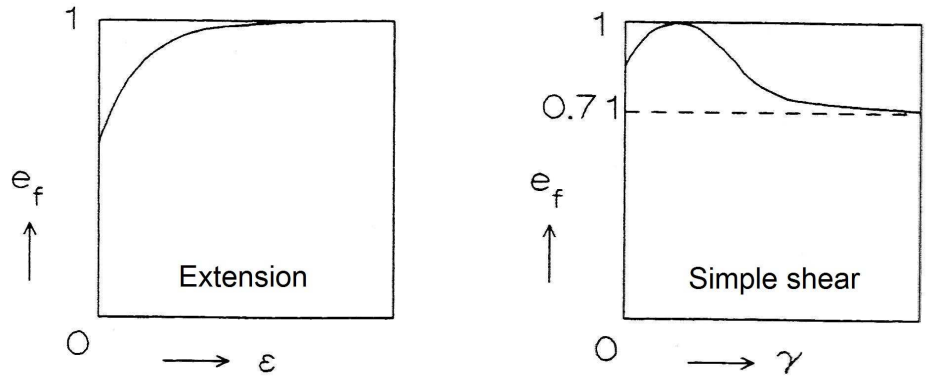

Figure 1.7. *Efficiency, e_f as a function of a total strain, $\varepsilon\left(=\dot{\varepsilon}t\right)$ and a total shear, $\gamma(=\dot{\gamma}t)$ in an extensional flow and a simple shear flow, respectively [Manas-Zloczower 1994].*

In blending of immiscible polymers, morphology of the dispersed phase (i.e. origin being in the form of liquid drops) depends on the blend composition, the rheological characteristics of the components such as viscosity and elasticity, the interfacial tension between the phases, and the intensity and type of flow that is applied. High shear, low surface tension and similar viscosity of the components are required for achieving high deformation of drops of the dispersed phase. These factors also control the breakup phenomena of extended threads. Hence, it is very difficult to select appropriate set of

parameters to act against capillary instabilities and preserve the shape of extended inclusions.

1.1.3 References

Bartok W., Mason S.J., **1957**. *Particle motions in sheared suspensions. V. Rigid rods and collision doublets of spheres.* J. Coll. Sci. 12, 243-262;

Bartok W., Mason S.J., **1959**. *Particle motions in sheared suspensions. VIII singlets and doublets of liquid spheres.* J. Coll. Sci. 14, 13-26;

Bentley B.J., Leal L.G., **1986a**. *A computer-controlled four-roll mill for investigations of particle and drop dynamics in two-dimensional linear shear flows.*
J. Fluid Mech. 167, 219-240;

Bentley B.J., Leal L.G., **1986b**. *An experimental investigation of drop deformation and breakup in steady, two-dimensional linear flows.* J. Fluid Mech. 167, 241-283;

Bruijn de R.A., **1993**. *Tipstreaming of drops in simple shear flows.*
Chem. Eng. Sci. 48, 277-284;

Cerf R., **1951**. *Recherchers theoriques et experimetales sur leffet maxwell des solutions de macromolecules deformables 1. Theorie de leffet maxwell des suspensions de spheres elastiques*. J. Clin. Phys. 48, 59-84;

Eggers J., **1997**. *Nonlinear dynamics and breakup of free-surface flows.*
Rev. Modern Phys. 69, 865-930;

Elemens P.H.M., Bos H.L., Janssen J.M.H., Meijer H.E.H., **1993**. *Transient phenomena in dispersive mixing.* Chem. Eng. Sci. 48, 267-276;

Elmendorp J.J., **1986**. *A study of polymer blending microrheology.*
Polym. Eng. Sci. 26, 418-426;

Grace H.P., **1982**. *Dispersion phenomena in high viscosity immiscible fluid systems and application of static mixers as dispersion devices in such systems.*
Chem. Eng. Commun. 14, 225-277;

Janssen J.M.H., Peters G.W.M., Meijer H.E.H., Baaijens F.P.T., **1992**. *Mixing of immiscible liquids.* Theor. Appl. Rheol. 369-371;

Janssen J.M.H., Meijer H.E.H., **1993**. *Droplet breakup mechanisms: Stepwise equilibrium versus transient dispersion.* J. Rheol. 37, 597-608;

Karam H.J., Bellinger J.C., **1968**. *Deformation and breakup of liquid droplets in a simple shear field.* Ind. Eng. Chem. Fundam. 7, 576-581;

Lin S.P., Reitz R.D., **1998**. *Drop and spray formation from a liquid jet*.
Ann. Rev. Fluid Mech. 30, 85-105;
Manas-Zloczower I., Tadmor Z. **1994**. *Mixing and Compounding of Polymers: Theory and Practice*. Hanser, New York;
Pozrikidis C., **1999**. *Capillary instability and breakup of liquid threads.*
J. Eng. Math. 36, 255-275;
Rayleigh L., **1879**. *On the capillary phenomenon of jets.*
Proc. Roy. Soc. London. 29, 71-97;
Rumscheidt F.D., Mason S.G., **1961a**. *Particle motions in sheared suspensions. XI. Internal circulation of fluid droplets (experimental).* J. Coll. Sci. 16, 210-237;
Rumscheidt F.D., Mason S.G., **1961b**. *Particle motions in sheared suspensions XII Deformation and burst of liquid drops in shear and hyperbolic flow.*
J. Coll. Sci. 16, 238-261;
Smith P.G., Ven T.G.M. van de, **1985**. *Shear induced deformation and rupture of suspended solid/liquid clusters*. Coll. and Surf. 15, 191-210;
Srinivasan M.P., Stroeve P., **1986**. *Subdrop ejection from double emulsion drops in shear flow.* J. Memb. Sci. 26, 231-236;
Taylor G.I., **1932**. *The viscosity of a fluid containing small drops of another fluid.*
Proc. Roy. Soc. London Ser. A 138, 41-48;
Taylor G.I., **1934**. *The formation of emulsions in definable fields of flow.*
Proc. Roy. Soc. London Ser. A 146, 501-523;
Taylor G.I., **1954**. *The two coefficients of viscosity for an incompressible fluid containing air bubbles*. Proc. Roy. Soc. London Ser. A 226, 34-39;
Tjahjadi M., Stone H.A., Ottino J.M., **1992**. *Satellite and sub-satellite formation in capillary breakup*. J. Fluid Mech. 243, 297-317;
Tomotika S., **1935**. *On the instability of a cylindrical thread of a viscous liquid surrounded by another viscous fluid. Proc.* Roy. Soc. London Ser. A 150, 322-337;
Torza S., Cox R.G., Mason S.G., **1972**. *Particle Motions in Sheared Suspensions. XXVII Transient and Steady Deformation and Burst of Liquid Drops.*
J. Coll. Int. Sci. 38, 395-411;
Travelyan B.J., Mason S.G., **1951**. *Particle motions in sheared suspensions. I. Rotations.*
J. Coll. Sci. 6, 354-367;

1.2 Polytetrafluoroethylene, PTFE

Polytetrafluoroethylene is the best known fluoropolymer representing the extreme of known polymers and since its discovery in the half of 20th century [Plunkett 1941] is used as a common engineering material for many demanding applications. PTFE possesses a high thermal stability and chemical inertness, high dielectric strength and extremely low dielectric loss factor. It has also a unique non-adhesion and antifrictional properties. Many of other outstanding properties [Renfrew 1946; Sperati 1961; Smith 1985; Narkis 1995], such as high melting temperature, extremely high molecular weight and melt viscosity, insolubility in all common solvents cause restraints for the processing of polytetrafluoroethylene. Industrial processing of PTFE, including paste extrusion of lubricated fine powders [Lontz 1952b], compression moulding, ram extrusion of granular powders [Ebnesajjad 2005] and coating from aqueous dispersions [Lontz 1952a], is hindered due to high melt viscosity of PTFE and also requires long times and expense, which limit the use of polytetrafluoroethylene for many applications. Cold compaction of polytetrafluoroethylene followed by sintering of the preforms at elevated temperatures is presently a common practice [Bigg 1977; Crawford 1982; Radhakrishnan 1986; Jog 1993; Jog 1994; Hambir 1994; Narkis 1995].

1.2.1 Synthesis of polytetrafluoroethylene

The first report on polytetrafluoroethylene was by Plunkett in 1941 [Plunkett 1941]. He obtained white, opaque powder as a residue from the storage of tetrafluoroethylene monomer under superatmospheric pressure (two or three times atmospheric pressure). After this essential discovery various methods of polymerization were tried and now preferred synthesizes of PTFE involve aqueous media and superatmospheric pressures.

Stable aqueous suspensions of colloidal polytetrafluoroethylene particles can be obtained via emulsion polymerization with minimal quantities of fluorinated surfactants and free-radical initiators such as sodium, potassium, ammonium persulfates, hydrogen peroxide, oxygen or organic peroxy compounds [Brubaker 1946; Hanford 1946; Joyce 1946a; Joyce 1946b; Renfrew 1950].

PTFE dispersions prepared by methods described above contain colloidal, negatively charged particles suspended in water [Lontz 1952a]. These dilute products can be concentrated into dispersions containing from 35 to 75 wt.% of PTFE using methods described by Berry [Berry 1949]. The concentration of dilute aqueous dispersions

comprises: (1) adding a surface-active agent into the dispersion, (2) flocculating the polymer by insolubilizing the surfactant, (3) separating the flocculated polymer from the bulk of aqueous phase, and (4) forming a concentrated dispersion by peptization of the polymer floc. Although, the surface-active agent acting primarily as a stabilizing agent to prevent coagulation can also influence the morphology of PTFE particles [Luhmann 1989]. The absence of any surfactant results in marginal stability of as-polymerized PTFE dispersions and flocculation of the particles into aggregates during high shear mixing and/or addition of the electrolyte. Rinsing, drying and screening of these aggregates lead to the production of fine powder PTFE particles [Lontz 1952b].

1.2.2 Morphology of nascent PTFE particles

The morphology of nascent PTFE dispersions has been extensively studied by different authors. Rahl *et al.* [Rahl 1972] examined emulsion-grade PTFE particles at various stages of polymerization. In the early stages of polymerization the nonspherical, ribbon-shaped objects are formed. Those ribbons are chain-extended single crystals with the chain axis parallel to the long axis of ribbons. The authors suggested that folding of thin ribbons (approximately 60 Å in thickness) occurs as a consequence of hydrodynamic forces acting on extremely thin chain-extended crystals once they exceed a certain aspect ratio and presumably competes with further reaction and crystallization on the surface of the growing particles. At polymerization with low-yields the rod-like particles are formed also as apparently single crystals with the chain axis parallel to the long axis of rod.

Seguchi *et al.* [Seguchi 1974] also suggested that the polymer morphology (shape and molecular weight) strongly depends on the polymerization conditions, especially the concentration of emulsifier as is shown on Figure 1.8. When polymerization is carried out without emulsifier, only nearly spherical to elliptical particles are formed with average diameter of 1000 Å and molecular weight above 10^6 Da. Increasing the concentration of emulsifier, the type of polymer in the latex changes from rods with 300÷600 Å in diameter and molecular weight from 2×10^5 to 5×10^5 Da to fibrils with diameter of 200 Å and molecular weight below 2×10^4 Da.

The influence of emulsifier concentration and polymerization time on the structure of polytetrafluoroethylene was reexamined in the middle of the 1980s by Luhman and Feiring [Luhmann 1989]. The authors observed three types of the particles with different morphology: rod-like, roughly spherical and, in the case of very low molecular weight,

small hexagonal particles. Both hexagonally shaped and short rod-like particles are formed in early stages of polymerization when the initial surfactant concentration is below its critical micelle concentration. An increase in the surfactant chain length and concentration tends to promote the formation of hexagonal particles. Also, at longer polymerization times, roughly spherical particles form dominant population.

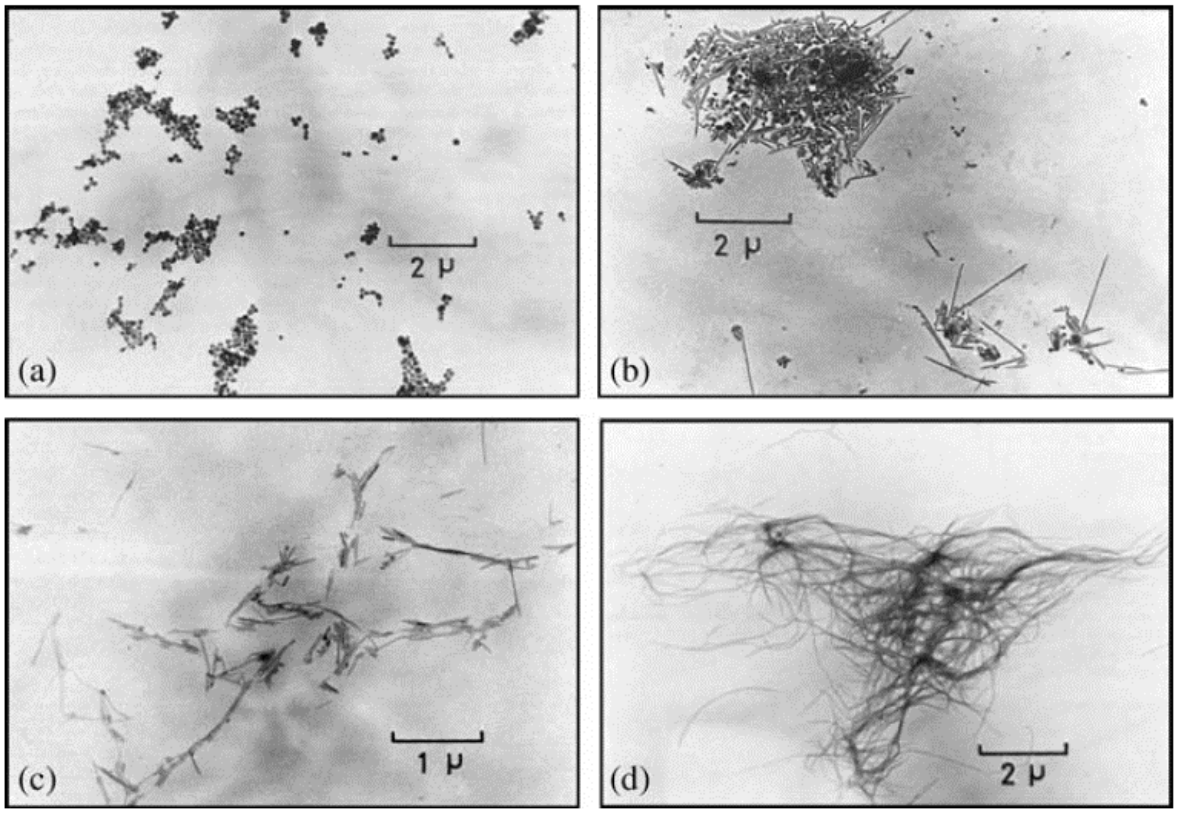

Figure 1.8. *Electron micrographs of nascent radiation initiated PTFE dispersion particles. The polymerization conditions were: (a) 0 % emulsifier, 90 min; (b) 0.5 % emulsifier, 60 min; (c) 1 % emulsifier, 60 min; (d) 2 % emulsifier, 90 min [Seguchi 1974].*

Geil *et al.* [Geil 2005] examined the evolution of nascent PTFE particles morphology in commercial PTFE nanoemulsions as a function of sintering time and temperature. The initial stages of polymerization of standard-size polytetrafluoroethylene resins involve the formation of chain-extended fibrils, rods or ribbons that fold back on themselves to form elliptical or short rod-like particles as the emulsifying agent is used up by the increasing surface area.

It is known that melting of semicrystalline polymers like polytetrafluoroethylene with very high molecular high weight ($M_w \geq 10^6$) leads to the systems with high concentration of entanglements persisting in the amorphous phase and in consequence drastically reduced deformability. Experimental observations and computer simulation revealed that chain-folded crystals “explode” upon melting [Barham 1991]. Figure 1.9

shows a computer generated sketch illustrating typical trajectories of a molecule with molecular weight of 390,000 before and after meting.

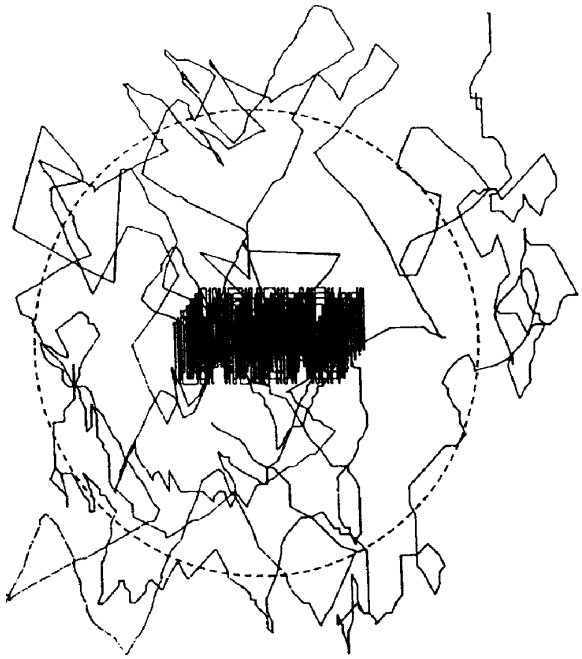

Figure 1.9. *Typical molecular trajectories before and after melting of a polymer of molecular weight 390,000.*

Once the constraints (lattice forces) are removed by melting, folded molecules expand rapidly, driven by the need to increase its entropy. Chain segments are then ejected with a high kinetic energy into the already molten surrounding and interlace with other chains rapidly leading to significant increase of the number of entanglements.

However, utilizing low temperature polymerization of tetrafluoroethylene it is possible to produce highly crystalline polytetrafluoroethylene powders (C ≈ 95 %) showing rod-like whisker or folded ribbon-like morphologies [Rahl 1972; Seguchi 1974; Folda 1988], suggesting a low entangled state with high deformability. In chain-extended crystals the basal planes consist mainly of chain ends instead of folds. Such a crystal plane does not require relaxing of its energy on melting, and chains are not supposed to be translocated to a large extent. Therefore, melting of such crystals does not increase significantly the number of entanglements over that already resident in the amorphous phase prior to melting.

1.2.3 Crystalline structure of PTFE

Polymerization of tetrafluoroethylene is carried out far below the polymer melting temperature, so as-polymerized PTFE possesses a high level of crystallinity [Starkweather 1982] and quite different crystalline morphology [Rahl 1972; Starkweather 1979] than the

same polymer recrystallized from the melt. High crystallinity degree of nascent polytetrafluoroethylene, which has been found to be between 93 to 98 %, can be obtained only when the chain structure is substantially unbranched. Belief that PTFE is an entirely linear polymer with fluorine atoms attached to the carbon chain, was confirmed by the absence of branched-chain compounds in the products of its pyrolysis [Benning 1946].

The temperature-pressure phase behavior of polytetrafluoroethylene has been extensively reported in the literature. Figure 1.10 presents four possible crystalline phases of PTFE. Two first-order crystalline phase transitions at 19 ºC and 30 ºC were first discussed in a report on thermal expansion [Rigby 1949] and confirmed in subsequent studies using dilatometry, calorimetry [Marx 1955] and thermal conductivity [Piorkowska 1986].

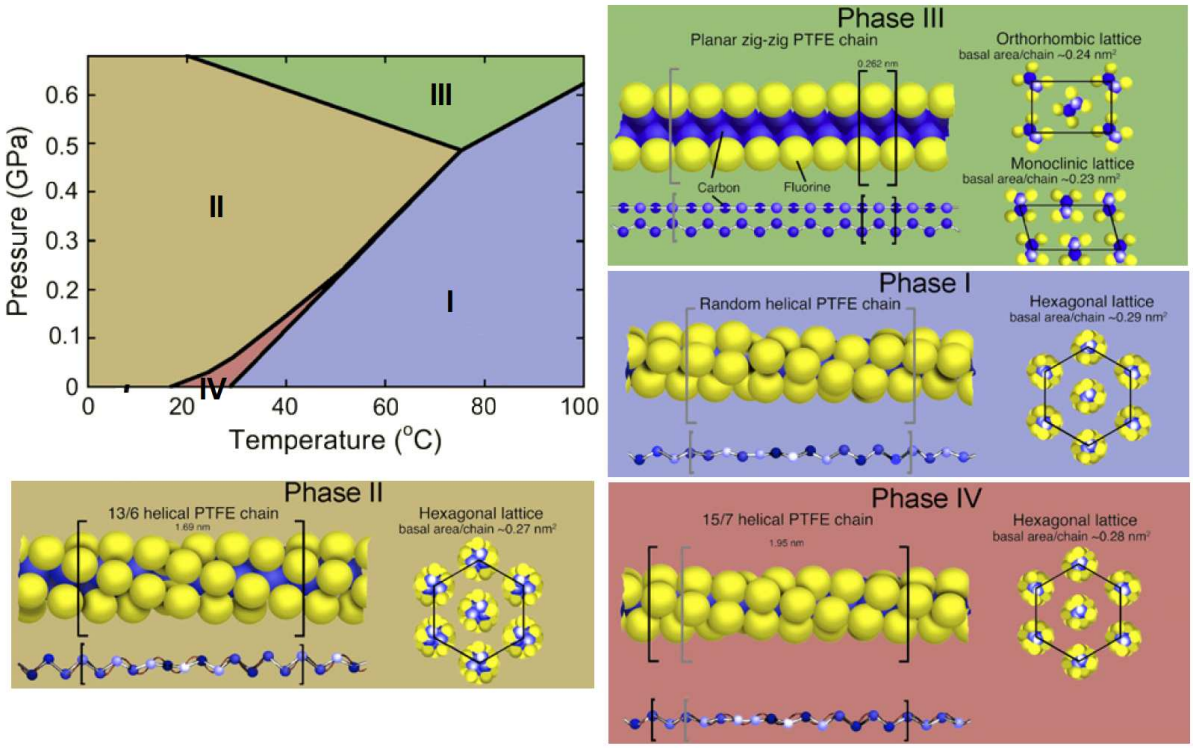

Figure 1.10. *Temperature-pressure phase behavior of crystalline polytetrafluoroethylene [Brown 2007].*

Phase II [Weeks 1981] exists below 19 ºC. The unit cell is hexagonal with PTFE chains arranged in a zig-zag twisted by 180º per 13 carbon atoms. Between 19 ºC and 30 ºC transitions, phase IV [Bunn 1954] is observed with 15/7 helical PTFE chains. Above 30 ºC and up to the melting point a pseudohexagonal very conformationally disordered phase I is the stable one [Bunn 1954; Sperati 1961; Grebowicz 1986].

Studies on the crystalline transitions in polytetrafluoroethylene at high pressures have been reported by Beecroft and Swenson [Beecroft 1959]. Compression measurements made on PTFE samples at various temperatures and pressures up to 2 GPa showed that in

addition to the three crystalline phases which are separated by the 19 ºC and 30 ºC transitions at atmospheric pressure, there is the fourth modification at high pressures. Phase III is present above ~0.65 GPa at room temperature [Rae 2004; Rae 2005]. Brown *et al.* [Brown 2007] reported that the crystalline phase transitions of PTFE can also be activated by tension and compression even at much lower stress levels.

1.2.4 Properties of polytetrafluoroethylene

Polytetrafluoroethylene exhibits many unusual properties such as exceedingly high molecular weight, high melting temperature and melt viscosity, high thermal stability and chemical inertness. Commercial homopolymer fine powders are linear but have molecular weight, M_n exceeding 10^7 Da. The melting point of melt-processed PTFE is about 327 ºC [Suwa 1975] but that of the virgin polymer is considerably higher up to 345 ºC [Weeks 1980]. The melting behavior of PTFE depends on its molecular weight [Suwa 1975] and rises with increasing molecular weight.

The melt viscosity of PTFE typically ranges from 10^{10} to 2×10^{11} poise at 380 ºC [Renfrew 1946]. So high melt viscosity is considered essentially as a consequence of PTFE structure and high chain length [Hanford 1946]. Polytetrafluoroethylene unlike other thermoplastics does not undergo the Newtonian flow at a measurable rate [Tuminello 1988], and is capable of only a very slow plastic flow. The polymer remains in a semisolid gel state, even at temperatures higher than 370 ºC [Lontz 1952a].

Thermal stability of polytetrafluoroethylene is outstanding. Polymer can be held for long period of time at the higher temperatures with relatively little changes of its tensile strength. After one month at 230 ºC, the loss in tensile strength of molded bars is negligible and at 300 ºC will drop only 10 to 20 % in comparison to that at room temperature [Renfrew 1946].

PTFE reveals the almost universal chemical resistance. It has been attributed to the strength of the carbon-fluorine bond and the way in which the fluorine atoms protect carbon chains from attack by highly corrosive chemicals [Renfrew 1946]. However, difficulties in dissolving PTFE arise also from its very high melting temperature which sets a lower limit for the boiling point of solvent candidates. Only some perfluorokerosenes and perfluorinated oils are reported to dissolve 1÷2 wt.% of polytetrafluoroethylene at 290 to 310 ºC [Compton 1950]. It has been shown that PTFE can also dissolve at ambient pressure in its oligomers having a chain length of 21 carbon atoms, or more [Smith 1985].

The dielectric loss factor of PTFE (< 10^{-4}), invariant over the frequency range 60 - 10^6 cycles and the temperature range 25 to 310 ºC [Hanford 1946; Gonon 2002], is one of the lowest known for solid substances. It has also a low dielectric constant (≈ 2) and a very high resistivity (> 10^{18} Ω m).

1.2.5 PTFE processing and its applications

An extremely high melt viscosity and a lack of Newtonian flow at processing temperature cause that polytetrafluoroethylene is hard-to-process polymer and shear processing by either screw extrusion or injection molding is impractical.

Fabrication of PTFE, known as fine or coagulated dispersions powder include powder processing techniques such as compression moulding, preforming, sintering [Sperati 1961; Bigg 1977; Crawford 1982; Radhakrishnan 1986; Jog 1993; Jog 1994; Hambir 1994], ram extrusion [Ebnesajjad 2005] and paste extrusion [Lontz 1952b]. Blending PTFE powder with 18 to 20 wt.% of a lubricant facilitates the process of extrusion below the melting temperature of polymer.

PTFE plays an important role in many industrial and consumer applications. Nonstick surfaces for home cookware is its best-known application. In combination with heat endurance and chemical resistance, polytetrafluoroethylene is favorably used as an electrical insulation in chemical plants [Joyce 1946b].

The aqueous dispersions containing relatively high concentrations of PTFE particles are especially suitable for films forming, dip coating, impregnating applications, and to preparing the mixtures with a variety of fillers, i.e. carbon, silica, clay, and glass fibers. Polytetrafluoroethylene films can be made by casting an aqueous dispersion on a supporting surface such as metal, glass, and ceramics, drying to remove the water, baking, and cooling [Lontz 1952a]. Valves, flexible circuit boards, conveyer belts, tubings are the most common articles coated using polytetrafluoroethylene aqueous dispersions. The main application of filled PTFE is the fabrication of special bearings, and gaskets [Ebnesajjad 2005]. There are a number of other minor uses of PTFE dispersions in fuel cells, batteries, de-dusting, and chloralkali processing.

Formulating dispersions or powders in form which can be spun through the spinneret it is possible to produce PTFE fibers, which can be applied as diaphragms for the electrolysis of alkali chlorides, as well as porous filters for fluids. High strength PTFE fibers can be produced in a fluidized bed [Klatt 2001] or by drawing of monofilament of

polytetrafluoroethylene polymer fabricated in paste extrusion process [Shimizu 1997; Donckers 2009].

Utilizing solid-state extrusion [Starkweather 1979; Mc Gee 1986; Okayama 1994] and two-stage draw [Uehara 1997; Endo 1998; Endo 2001; Sawai 2006] it has been shown that some nascent polytetrafluoroethylene powders are ultradrawable. Morooka *et al.* [Morooka 2011] shown that modifying two-stage draw technique by applying so-called PIN draw above melting temperature, it is possible to achieve a superdrawing of compacted films of nascent PTFE powder, to draw ratios up to 500 and the tensile modulus of 120 GPa. This technique seems to be promising to develop high performance polytetrafluoroethylene fibers.

1.2.6 References

Barham P.J., Sadler D.M., **1991**. *A neutron scattering study of the melting behaviour of polyethylene single mats*. Polymer 32, 393-395;

Beecroft R.I., Swenson C.A., **1959**. *Behavior of Polytetrafluoroethylene (Teflon) under High Pressures.* J. Appl. Phys. 30, 1793-1798;

Benning A.F., Dowing F.B., Park J.D., **1946**. *Pyrolysis of tetrafluoroethylene polymer*. US Patent 2394581;

Berry K.L., **1949**. *Concentrated aqueous colloidal dispersions of polytetrafluoroethylene and methods for their preparation*. US Patent 2478229;

Bigg D.M., **1977**. *A study of the effect of pressure, time, and temperature on high-pressure powder molding*. Polym. Eng. Sci. 17, 691-699;

Brown E.N., Dattelbaum D.M., Brown D.W., Rae P.J., Clausen B., **2007**. *A new path to inducing phase transitions in semi-crystalline polymers*. Polymer 48, 2531-2536;

Brubaker M.M., **1946**. *Process for polymerizing tetrafluoroethylene*. US Patent 2393967;

Bunn C.W., Howells E.R., **1954**. *Structures of molecules and crystals of fluorocarbons.* Nature 274, 549-551;

Compton J.D., Justice J.W., Irwin C.F., **1950**. *Plasticized polymers*. US Patent 2510078;

Crawford R.J., **1982**. *Effect of compaction rate during the cold forming of polymeric powders*. Polym. Eng. Sci. 22, 300-306;

Donckers M., **2009**. *Thermally stable polytetrafluoroethylene fiber and method of making same.* US Patent 7498079;

Ebnesajjad S., Khaladkar P.R., **2005**. *Fluoropolymers Applications in Chemical Processing Industries*. William Andrew Inc., New York;
Endo R., Kanamoto T., Porter R.S., **1998**. *Uniaxial Drawing of Polytetrafluoroethylene Virgin Powder by Extrusion Plus Cold Tensile Draw.* J. Polym. Sci. Part B: Polym. Phys. 36, 2551-2562;
Endo R., Kanamoto T., **2001**. *Superdrawing of Polytetrafluoroethylene Virgin Powder above the Static Melting Temperature.* J. Polym. Sci. Part B: Polym. Phys. 39, 1995-2004;
Folda T., Hoffman H., Chanzy H., Smith P., **1988**. *Liquid crystalline suspensions of poly(tetrafluoroethylene).* Nature 333, 55-66;
Geil P.H., Yang J., Williams R.A., Petersen K.L., Long T.-C., Xu P., **2005**. *Effect of Molecular Weight and Melt Time and Temperature on the Morphology of Poly(tetrafluoroethylene).* Adv. Polym. Sci. 180, 89-159;
Gonon P., Sylvestre A., **2002**. *Dielectric properties of fluorocarbon thin films deposited by radio frequency sputtering of polytetrafluoroethylene.* J. Appl. Phys. 92, 4584-4589;
Grebowicz J., Cheng S.Z.D., Wunderlich B., **1986**. *Kinetics of transitions involving condis crystals.* J. Polym. Sci. Part B Polym. Phys. 24, 675-685;
Hambir S.S., Jog J.P., Nadkarni V.M., **1994**. *Strength development in powder processing of poly(tetrafluoroethylene).* Polym. Eng. Sci. 34, 1065-1069;
Hanford W.E., Joyce R.M. Jr., **1946**. *Polytetrafluoroethylene.* J. Am. Chem. Soc. 68, 2082-2085;
Jog J.P., **1993**. *Solid state processing of polymers: A review.* Adv. Polym. Technol. 12, 281-289;
Jog J.P., Nath K.R., Nadkarni V.M., **1994**. *Solid-state processing of polytetrafluoroethylene Simulation of sintering cycle.* Itern. J. Mater. Prod. Technol. 9, 155-169;
Joyce R.M. Jr., **1946a**. *Process for polymerizing tetrafluoroethylene.* US Patent 2394243;
Joyce R.M. Jr., **1946b**. *Electrical apparatus.* US Patent 2392388;
Klatt B., Horx M., Koelling H., Berndt K., Krueger G., Kuenne H.-J., Moerl L., Backhauss L., **2001**. *Method for physically converting PTFE particles to fibers.* US Patent 6187238;
Lontz J.F., Happoldt W.B. Jr., **1952a**. *A new aqueous colloidal dispersion of polytetrafluoroethylene.* Ind. Eng. Chem. 44, 1800-1805;
Lontz J.F., Jaffe J.A., Robb L.E., Happoldt W.B. Jr., **1952b**. *Extrusion properties of lubricated resin from coagulated dispersion.* Ind. Eng. Chem., 44, 1805-1810;

Luhmann B., Feiring A.E., **1989**. *Surfactant effects in polytetrafluoroethylene dispersion polymerization*. Polymer 30, 1723-1732;
Marx P., Dole M., **1955**. *Specific Heat of Synthetic High Polymers. V. A Study of the Order-Disorder Transition in Polytetrafluoroethylene.* J. Am. Chem. Soc. 77, 4771-4774;
Mc Gee R.L., Collier R., **1986**. *Solid state extrusion of polytetrafluoroethylene fibers.* J. Polym. Eng. Sci. 26, 239-242;
Morooka N., Sawai D., Ohama T., Sano A., Matsuura K., Kanamoto T., **2011**. *Processing of nascent polymer powders to high performance fibers*, in: Myasnikowa L., Lemstra P.J. (Eds.), *Reactor Powder Morphology*. Nova Science Publishers, Inc, New York, pp. 295-316;
Narkis M., Rosenzweig N., **1995**. *Polymer Powder Technology*. John Wiley & Sons Ltd., Chichester;
Okayama H., Kanamoto T., Porter R.S., **1994**. *Solid-state deformation of polytetrafluoroethylene powder. Part I Extrusion drawing*. J. Mater. Sci. 29, 6485-6494;
Piorkowska E., Galeski A., **1986**. *Measurements of thermal conductivity of materials using a transient technique. II. Description of the apparatus*. J. Appl. Phys. 60, 493-498.
Plunkett R.J., **1941**. *Tetrafluoroethylene polymers.* US Patent 2230654;
Radhakrishnan S., Nadkarni V.M., **1986**. *Modification of Crystallinity and Structure in Powder Processing of Polytetrafluoroethylene*. Inter. J. Polym. Mater. 11, 79-94;
Rae P.J., Dattelbaum D.M., **2004**. *The properties of poly(tetrafluoroethylene) (PTFE) in compression*. Polymer 45, 7615-7625;
Rae P.J., Brown E.N., **2005**. *The properties of poly(tetrafluoroethylene) (PTFE) in tension.* Polymer 46, 8128-8140;
Rahl F.J., Evanco M.A., Fredericks R.J., Reimschuessel A.C., **1972**. *Studies of the Morphology of Emulsion-Grade Polytetrafluoroethylene.* J. Polym. Sci. Part A-2: Polym. Phys. 10, 1337-1350;
Renfrew M.M., Lewis E.E., **1946**. *Polytetrafluoroethylene. Heat-Resistant, Chemically Inert Plastic.* Ind. Eng. Chem. 38, 871-877;
Renfrew M.M., **1950**. *Polymerization of tetrafluoroethylene with dibasic acid peroxide catalysts.* US Patent 2534058;
Rigby H.A., Bunn C.W., **1949**. *A Room-Temperature Transition in Polytetrafluoroethylene*. Nature, 164, 583;
Sawai D., Watanabe D., Morooka N., Kuroki H., Kanamoto T., **2006**. *Superdrawing*

of Polytetrafluoroethylene Nascent Powder by Solid-State Coextrusion.
J. Polym. Sci. Part B: Polym. Phys. 44, 3369-3377;
Seguchi T., Suwa T., Tamura N., Takehisa M., **1974**. *Morphology of Polytetrafluoroethylene Prepared by Radiation-Induced Emulsion Polymerization*.
J. Polym. Sci. Polym. Phys. Ed. 12, 2567-2576;
Shimizu M., **1997**. *Process of making PTFE fibers.* US Patent 5686033;
Smith P., Gardner K.H., **1985**. *Dissolution of Poly(tetrafluoroethylene).*
Macromolecules 18, 1222-1228;
Sperati C.A., Starkweather H.W. Jr., **1961**. *Fluorine-Containing Polymers. II. Polytetrafluoroethylene*. Fortschr. Hochpolym.-Forsch. Bd. 2, 465-495;
Starkweather H.W. Jr., **1979**. *A Comparison of the Rheological Properties of Polytetrafluoroethylene below Its Melting Point with Certain Low-Molecular Smectic States.* J. Polym. Sci. Polym. Phys. Ed. 17, 73-79;
Starkweather H.W. Jr., Zoller P., Jones G.A., Vega A.J., **1982**. *The Heat of Fusion of Polytetrafluoroethylene.* J. Polym. Sci. Polym. Phys. Ed. 20, 751-761;
Suwa T., Seguchi T., Takehisa M., Machi S., **1975**. *Effect of Molecular Weight on the Crystalline Structure of Polytetrafluoroethylene As-Polymerized.*
J. Polym. Sci. Polym. Phys. Ed. 13, 2183-2194;
Tuminello W.H., Treat T.A., English A.D., **1988**. *Poly(tetrafluoroethylene): Molecular Weight Distributions and Chain Stiffness.* Macromolecules 21, 2606-2610;
Uehara H., Jounai K., Endo R., Okuyama H., Kanamoto T., Porter R.S., **1997**. *High modulus films of polytetrafluoroethylene prepared by two-stage drawing of reactor powder.* Polym. J. 29, 198-200;
Weeks J.J., Sanchez I.C., Eby R.K., Poser C.I., **1980**. *Order-disorder transitions in polytetrafluoroethylene*. Polymer 21, 325-331;
Weeks J.J., Clark E.S., Eby R.K., **1981**. *Disorder in the crystal structures of phases I and II of copolymers of tetrafluoroethylene and hexafluoropropylene.*
Polymer 22, 1496-1499;

1.3 Mechanisms of plastic deformation in semicrystalline polymers

The understanding of the basic mechanisms of deformation in semicrystalline polymers has been a subject of intense interest since at least four decades. Plastic deformation in semicrystalline materials is a complex phenomenon because of their complicated structure and morphology. Presently, the structure of bulk-crystallized polymer is described by two-phase model: where the crystalline lamellae are separated from each other by a layer of amorphous polymer and held together by tie molecules [Keller 1968].

In the past, three principal conceptions were worked out to explain the nature of plastic deformation in semicrystalline polymers. The first so-called "micronecking" model proposed by Peterlin [Peterlin 1969; Peterlin 1971; Peterlin 1977] assumes that at large strains the initial chain-folded lamellar structure is discontinuously transformed into microfibrils. These catastrophic process occurring during tensile drawing is schematically presented in Figure 1.11.

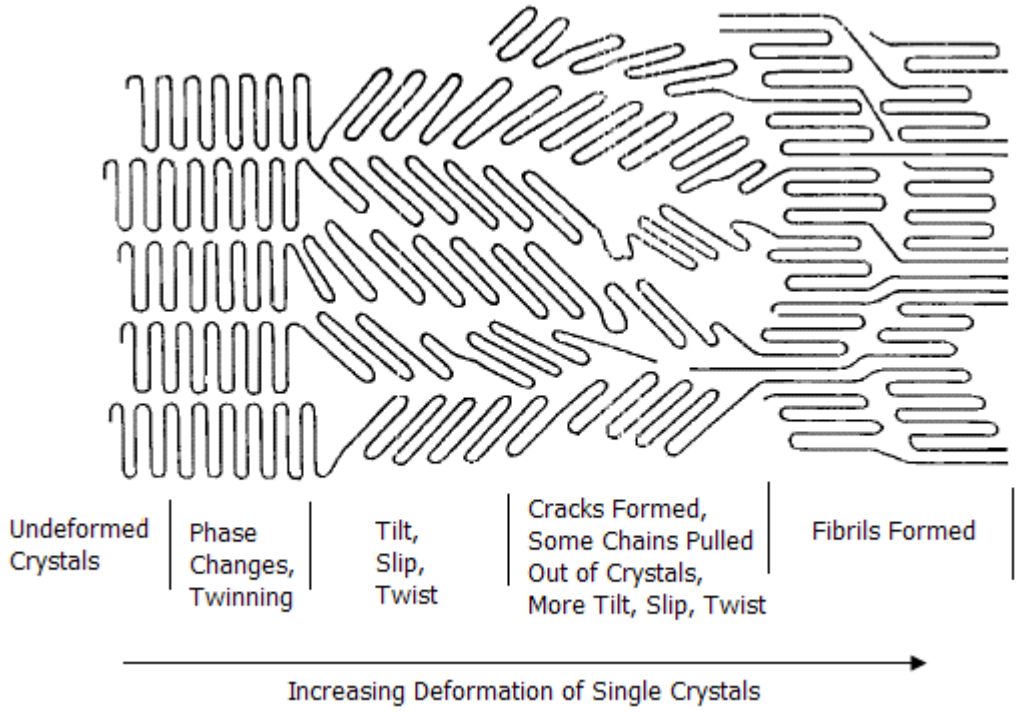

Figure 1.11. *Schematic illustration of 'micronecking' model [Peterlin 1969].*

The second model assumes that the plastic deformation is connected with the melting of polymer crystals and simultaneous recrystallization during tensile drawing [Flory 1978; Popli 1987; Gent 1989; Wu 1992; Kennedy 1994; Annis 1996; Peacock 1998]. The third conception based on the idea that the deformation of crystals proceeds by crystallographic

mechanisms, was adopted to polymers by Young and others [Young 1974b; Bowden 1974; Lin 1994] from the science of metals and other low molecular materials.

The nature of mechanisms accompanying deformation of crystalline polymers and the factors affecting them were intensively studied [Bowden 1974; Escaig 1982; Galeski 1992; Lin 1994; Porter 1995; Oleinik 2003; Galeski 2003; Pawlak 2005]. The mechanical behavior of semicrystalline polymers in tension, is influenced by a number of factors such as molecular weight [Capaccio 1975; Capaccio 1976; Fu 2003; Stern 2007; Pawlak 2008], thermal history [Capaccio 1975; Capaccio 1976; Fu 2003; Davies 2004; Pawlak 2007; Stern 2007], orientation of lamellar structure [Hobeika 2000], deformation rate [Hobeika 2000; Viana 2005; Stern 2007] and temperature of deformation [Hartmann 1987; Hobeika 2000; Schneider 2010].

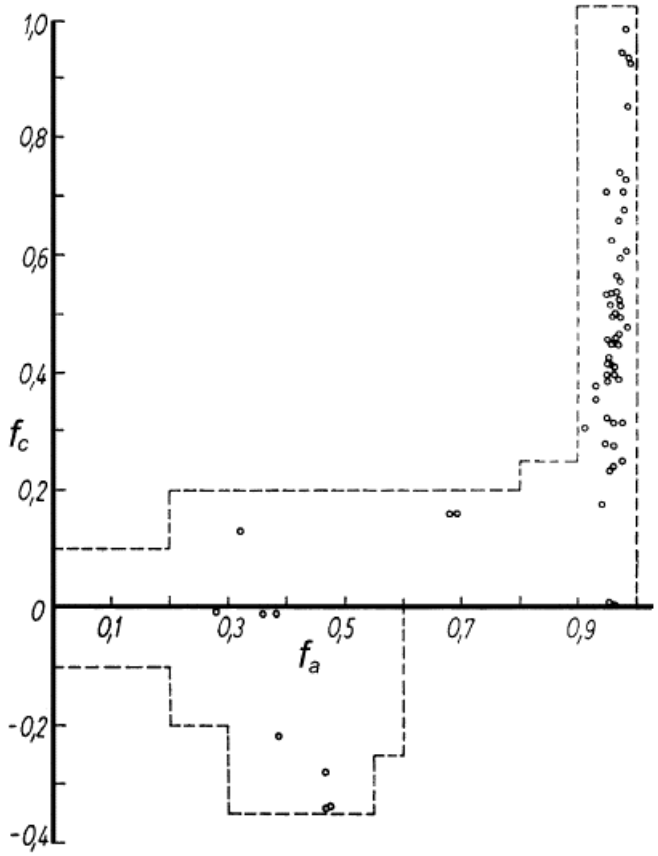

Figure 1.12. *Hermans orientation parameters of the crystalline phase, f_c and amorphous phase, f_a for a series of isotactic polypropylene samples uniaxially deformed to a different degree of orientation. The region surrounded by the dotted lines represents the course of deformation starting from f_c and f_a equal 0 [Kryszewski 1978].*

Deformation in semicrystalline polymers takes place firstly in the amorphous phase, since the stress required to initiate this process constitutes from 2 to 10 % of the value of stress needed to activate the deformation modes in crystallites [Peterson 1966b].

This predictions were confirmed experimentally by Kryszewski *et al.* [Kryszewski 1978] and also by Bartczak [Bartczak 1992a; Bartczak 1992b; Bartczak 1994].

Figure 1.12 presents the Hermans orientation parameters for the crystalline and amorphous phases of a series of tensile deformed samples of isotactic polypropylene. In the initial stage of deformation, the amorphous phase becomes oriented while the crystalline phase remains very slightly oriented or oriented in the transverse direction. Further increase in the draw ratio results in almost entirely stretched out amorphous phase and beginning of orientation process of the crystalline phase. Finally, at high draw ratio the macromolecular chain fragments embedded in both phases become highly oriented.

1.3.1 Deformation of amorphous phase

The structure of amorphous phase and mechanisms of their plastic deformation in polyethylene has been intensively studied by Fisher and others [Fisher 1988; Lin 1994; Bartczak 1997]. The amorphous regions above glass transition temperature, T_g, exhibit a rubber-like behavior, hence their plastic deformation takes place according to the three principal mechanisms: interlamellar slip (or interlamellar shear), interlamellar separation and lamellae-stack rotation [Bowden 1974; Lin 1994; Bartczak 1996] which are schematically illustrated in Figure 1.13.

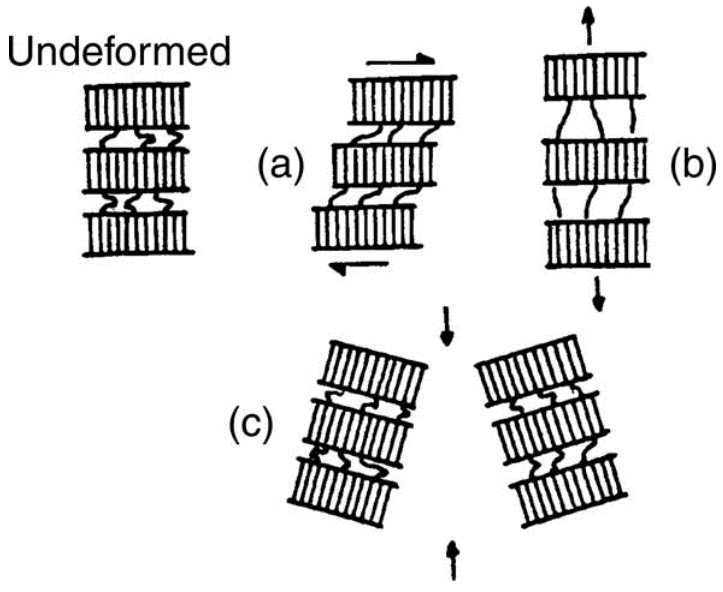

Figure 1.3. *Deformation mechanisms of the amorphous phase in semicrystalline polymers: (a) interlamellar slip, (b) interlamellar separation and (c) lamellae-stack rotation [Bowden 1974].*

Interlamellar slip involves a simple shear of amorphous layers between crystalline lamellae parallel to each other and causes rotation of crystalline lamellae around the direction of deformation. These deformation mode is not observable below T_g of the

amorphous phase [Keller 1971; Young 1973; Bowden 1974; Pope 1975]. Keller and Pope [Keller 1971] showed that above 80 ^{o}C in the early stage of deformation, interlamellar slip is the dominant mode of deformation of oriented low density polyethylene, LDPE and can be completely reversible up to deformation, $\varepsilon < 0.6$ [Bartczak 2005].

The second deformation mode of amorphous phase is interlamellar separation which involves a change of the distance between adjacent lamellae parallel to each other, when the direction of stress is perpendicular to their surface [Quynn 1971; Keller 1971; Kaufman 1973; Pope 1975; Petermann 1978]. The deformation resistance to interlamellar separation depends upon the detailed structure of the material, including the amount of an active, taut tie molecules between the lamellae, distribution of their chain lengths, and on the lateral dimension of crystalline lamellae. The implementation of this deformation mode is possible by two processes: either a large density fluctuations (cavities) leading to the formation of voids [Pawlak 2005; Pawlak 2007; Pawlak 2008] or a flow of the amorphous material into structural traps, i.e. opening gaps between lamellae [Pope 1975].

In contrast to interlamellar slip and interlamellar separation, a lamellae-stack rotation requires the cooperative movement of amorphous phase and crystalline lamellae. The crystallites are embedded in the amorphous phase in the form of stacks, and they are free to rotate under the influence of stress [Cowking 1968; Groves 1969; Keller 1971]. Tagawa showed that the stack rotation involves three to ten crystallites [Tagawa 1980].

1.3.2 Deformation of polymer crystals

Plastic deformation of polymer crystals proceeds by three basic mechanisms, i.e. crystallographic slip, twinning and stress-induced martensitic transformation, but slip mode is predominant since it can generate larger plastic strains than two others.

Crystallographic slip is identified as (*hkl*)[*uvw*] which is a combination of the slip plane (*hkl*) and the slip direction [*uvw*] in these plane where *h*, *k*, *l*, *u*, *v* and *w* are the Miller indices.

The crystallographic slip, schematically presented in Figure 1.14, takes place when the actual shear stress acting on the slip plane reaches a critical value, known as the critical resolved shear stress τ_c or plastic resistance [Bowden 1971; Young 1973; Young 1974a] and afterwards two parts of crystal separated by the slip plane undergo a relative translation.

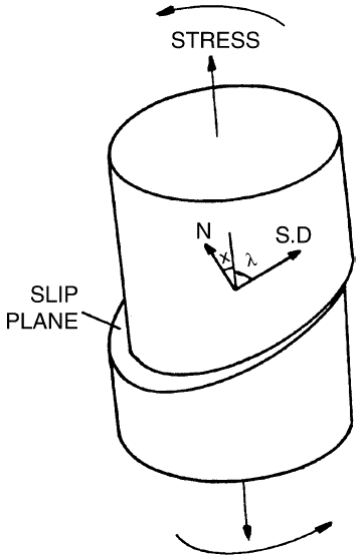

Figure 1.14. *Single slip under a uniaxial tensile stress, σ. N is the normal to the slip plane and S.D is the slip direction. The resolved shear stress, τ on the slip plane in the slip direction is given by* $\tau = \sigma \cos\chi \cos\lambda$ *[Bowden 1974].*

The values of critical resolved shear stress, τ_c, needed for the plastic deformation of crystals, can be determined from the Coulomb yield criterion [Keller 1966; Hinton 1968] described as:

$$\tau_c = \tau_o - k\sigma_n \tag{1.13}$$

where τ_o is the critical resolved shear stress in the absence of any normal stress on the slip plane, σ_n is the resolved stress normal to the slip plane, and *k* is a constant demonstrating the sensitivity of the shear to the normal stress. The critical resolved shear stresses for possible slip systems are well known only for few polymers [Bowden 1971; Bowden 1974; Lin 1992; Bartczak 1992b; Aboulfaraj 1995].

Yield stress is governed either by the generation and motion of crystal dislocations or by the Peierls [Peierls 1940] stress required to move them [Hosemann 1963; Predecki 1966; Peterson 1966a; Predecki 1967; Shadrake 1976; Shadrake 1979; Lin 1994]. The number of dislocations in crystal, in the range $10^5 \div 10^8$ cm^{-2}, is usually sufficient to begin the crystallographic slip, but these value is too low in comparison with the value necessary for effectively acting slip. However, the acting stresses are able to generate meaningful number of dislocations, sufficient for a continuous slipping mechanism. In the case of thin crystals, the dislocations are thermally generated, while in thick crystals a nucleation of dislocation proceeds by so-called half-loop dislocation mechanism [Kazmierczak 2005, Argon 2005]. Plastic deformation by crystallographic slip is usually governed by the

resistance to the motion of dislocations on the slip planes [Bowden 1974; Reck 1985; Galeski 1992; Lin 1994; Porter 1995].

The crystallographic slips in chain-folded crystals can proceed only along planes containing axes of macromolecular chains and folds since the covalent bonds along chain axes cannot be broken down during deformation. The easiest slip occurs along a slip plane which tend to be a close-packed plane in the structure. In case of polyethylene the slip plane must be of the (*hk0*) type and the slip direction parallel to the chain axis [001] [Young 1973]. Hence, there are only two possible crystallographic slips: chain slip (or parallel slip), i.e. slip along the chains, and transverse slip, i.e. slip perpendicular to the chains. The chain slip and transverse slip can occur simultaneously on a common slip plane [Lewis 1972; Young 1973], but the critical resolved shear stress for chain slip is lower than τ_c for any transverse slip [Bowden 1974].

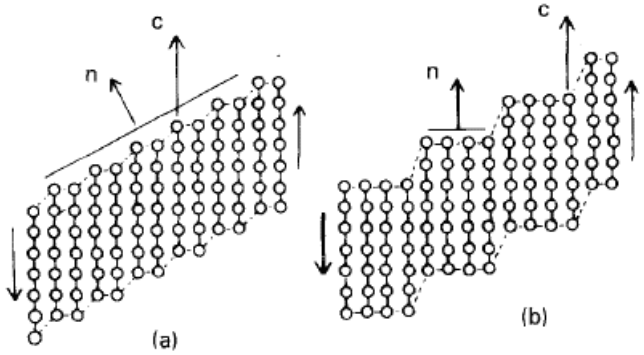

Figure 1.15. *Schematic illustration of possible types of chain slip: (a) fine slip and (b) coarse slip [Lin 1994]; n are the normals to the crystal surface and c are the chain axes.*

Chain slip is taken as the most important crystallographic deformation mechanism. In the same type of planes it can occur in two different ways: as fine or coarse slip [Bassett 1963; Shinozabi 1973; Bowden 1974; Lin 1994], which are schematically illustrated in Figure 1.15. Bowden and others [Bowden 1974; Pope 1975; Lin 1994] showed that the chain slips in polyethylene are able to recover at elevated deformation temperatures.

Fine slip consists in the slight multitude displacement of parallel planes with respect to others, which leads to a change of the angle between the molecular chain axes and the normal to the lamellar surface, i.e. tilting of chains in the crystallite. This type of chain slip is predominant mechanism of plastic deformation in polytetrafluoroethylene, PTFE under uniaxial tension or compression at room temperature and moderate strains and in oriented high density polyethylene, HDPE [Bowden 1974; Lin 1994].

In case of coarse slip the shear displacements appear only along the confined number of crystalline planes, and no chain tilting is observed during the deformation. The role of coarse slip usually increases with the total strain of the material.

From the mechanical point of view, a single slip system leads to the development of a simple shear along a single plane between two crystal parts and rotation of a crystal with respect to the stress axis [Bowden 1974], as shown in Figure 1.16. The angle, *x*, through which the crystal rotates is a simple function of the applied strain. In the case of uniaxial compression, the direction of crystal rotation is away from the compression axis (*x* increases), while in uniaxial tension, the rotation is in the direction of the tensile axis (*x* decreases).

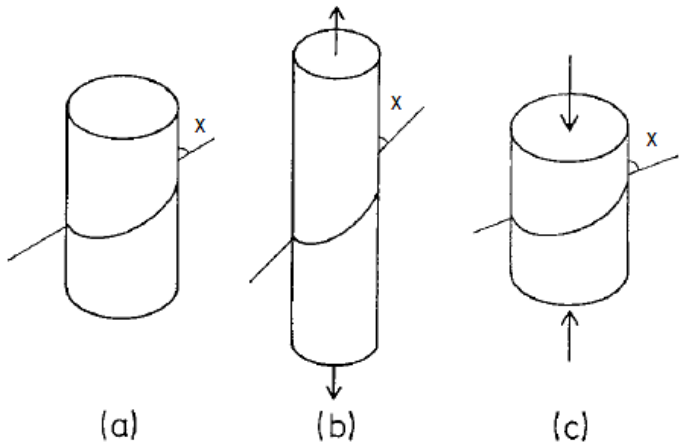

Figure 1.16. *Rotation of a crystal undergoing a single slip: (a) undeformed crystal, (b) uniaxial tension and (c) uniaxial compression [Bowden 1974].*

Five independent slip systems are required to change a shape of crystal [Kelly 1970]. Crystals in semicrystalline polymers usually possess insufficient number of independent slip systems, but under appropriate conditions the deformation of bulk-crystallized material proceeds without voiding or cracking perhaps because the amorphous regions between lamellae allow for certain amount of adjustment.

Twinning mode is allowed in polymer crystals with sufficiently low symmetries and oriented with a chain axis perpendicular to the direction of stress. In orthorhombic crystals of polyethylene twinning proceeds along (110) and (310) planes, which results in lattice rotations about the chain axis of 55^{o} and -67^{o}, respectively [Lewis 1972; Allan 1973], while twinning in polypropylene proceeds along (130) plane.

Martensitic transformation, i.e. stress-induced transformation from one crystallographic form to another, occurs only when the polymer crystal is oriented with a chain axis perpendicular to the direction of stress. These third deformation mode of

crystals was found in several polymers such as an oriented polyethylene subjected to uniaxial compression (transformation from orthorhombic to monoclinic form) [Tanaka 1962], polypropylene (transformation from γ-form to α-form), poly(L-lactic acid) with transformation from α-form to β-form [Eling 1982] and nylon 6 with α-form transforming to γ-form [Galeski 1991].

In can be concluded that plastic deformation of semicrystalline polymers requires both deformation of amorphous and crystalline phase because of their complicated hierarchical structure [Lin 1994; Galeski 2003]. Deformation of amorphous phase can be activated relatively easy [Kryszewski 1978] but it is rapidly exhausted due to different alignment of crystalline lamellae with respect to the deformation direction. Further deformation of semicrystalline polymer could be possible by initiation of plastic deformation of lamellar crystals. Plastic deformation of a polymer is initiated by crystal plasticity. Plastic yielding of semicrystalline polymers based on dislocation mechanism [Peterson 1966a; Peterson 1968; Shadrake 1974; Young 1988] was intensively studied in the past [Lin 1994; Wilhelm 2004; Kazmierczak 2005; Séguéla 2007]. It is known that the yield stress of semicrystalline polymers depends not only on crystal thickness [Brooks 2000; Séguéla 2002] but also on the degree of crystallinity and entanglement of macromolecules [O'Kane 1995; Ayoub 2011]. Bartczak *et al.* [Bartczak 2012] have shown that the molecular network characterized by the density of entanglements is the key parameter controlling deformability of the melt of ultra high molecular weight polyethylene, UHMWPE. Lower the entanglements density the higher the ultimate strain in the plain-strain compression of a molten material.

1.3.3 References

Aboulfaraj M., G'Sell C., Ulrich B., Dahoun A., **1995**. *In situ observation of the plastic deformation of polypropylene spherulites under uniaxial tension and simple shear in the scanning electron microscope*. Polymer 36, 731-742;

Allan P., Crellin E.B., Bevis M., **1973**. *Stress-induced twinning and phase transformations in polyethylene single crystals.* Philos. Mag. 27, 127-145;

Annis B.K., Strizak J., Wignall G.D., Alamo R.G., Mandelkern L., **1996**. *A small-angle neutron scattering study of the plastic deformation of linear polyethylene.*
Polymer 37, 137-140;

Argon A.S., Galeski A., Kazmierczak T., **2005**. *Rate mechanisms of plasticity in semi-crystalline polyethylene*. Polymer 46, 11798-11805;

Ayoub G., Zairi F., Frederix C., Gloaguen J.M., Nait-Abdelaziz M., Seguela R., **2011**. *Effects of crystal content on the mechanical behaviour of polyethylene under finite strains: experiments and constitutive modeling*. Int. J. Plasticity 27, 492-511;

Bartczak Z., Cohen R.E., Argon A.S., **1992a**. *Evolution of the Crystalline Texture of High-Density Polyethylene during Uniaxial Compression.* Macromolecules 25, 4692-4704;

Bartczak Z., Argon A.S., Cohen R.E., **1992b**. *Deformation Mechanisms and Plastic Resistance in Single-Crystal-Textured High-Density Polyethylene.* Macromolecules 25, 5036-5053;

Bartczak Z., Argon A.S., Cohen R.E., **1994**. *Texture evolution in large strain simple shear deformation of high density polyethylene.* Polymer 35, 3427-3441;

Bartczak Z., Galeski A., Argon A.S., Cohen R.E., **1996**. *On the plastic deformation of the amorphous component in semicrystalline polymers.* Polymer 37, 2113-2123;

Bartczak Z., Martuscelli E., **1997**. *Orientation and properties of sequentially drawn films of an isotactic polypropylene/hydrogenated oligocyclopentadiene blend.* Polymer 38, 4139-4149;

Bartczak Z., **2005**. *Influence of molecular parameters on high-strain deformation of polyethylene in the plane-strain compression. Part II. Strain recovery.* Polymer 46, 10339-10354;

Bartczak Z., Beris P.F.M., Wasilewski K., Galeski A., Lemstra P.J., **2012**. *Deformation of the Ultra-High Molecular Weight Polyethylene Melt in the Plain-Strain Compression*. J. Appl. Polym. Sci. DOI 10.1002/app.36595;

Bassett D.C., Keller A., Mitsuhashi S., **1963**. *New features in polymer crystal growth from concentrated solutions*. J. Polym. Sci. Part A 1, 763-788;

Bowden P.B., Young R.J., **1971**. *Critical Resolved Shear Stress for [001] Slip in Polyethylene.* Nature Phys. Sci. 229, 23-25;

Bowden P.B., Young R.J., **1974**. *Deformation mechanisms in crystalline polymers*. J. Mater. Sci. 9, 2034-2051;

Brooks N.W.J., Mukhtar M., **2000**. *Temperature and stems length dependence of the yield stress of polyethylene.* Polymer 41, 1475-1480;

Capaccio G., Ward I.M., **1975**. *Effect of molecular weight on the morphology and drawing behaviour of melt crystallized linear polyethylene*. Polymer, 16, 239-243;

Capaccio G., Chapman T.J., Ward I.M., **1976**. *The Drawing Behavior of Linear Polyethylene. I. Rate of Drawing as a Function of Polymer Molecular Weight and Initial Thermal Treatment*. J. Polym. Sci. Polym. Phys. Ed. 14, 1641-1658;

Cowking A., Rider J.G., Hay I.L., Keller A., **1968**. *A Study of the Orientation Effects in Polyethylene in the Light of Crystalline Texture. Part 3 On the Effect of Applied Stress on the Molecular and Textural Orientation.* J. Mater. Sci. 3, 646-654;

Davies R., Zafeiropoulos N., Schneider K., Roth S., Burghammer M., Riekel C., Kotek J., Stamm M., **2004**. *The use of synchrotron X-ray scattering coupled with in situ mechanical testing for studying deformation and structural change in isotactic polypropylene.* Colloid Polym. Sci. 282, 854-866;

Eling B., Gogolewski S., Pennings A.J., **1982**. *Biodegradable materials of poly(L-lactid acid): 1. Melt-spun and solution-spun fibers.* Polymer 23, 1587-1593;

Escaig B., G'Sel C., **1982**. *Plastic Deformation of Amorphous and Semicrystalline Materials.* Les Editeurs de Physique, Paris;

Fisher E.W., **1988**. *The conformation of polymer chains in the semicrystalline state.* Macromol. Chem. Macromol. Symp. 20-21, 277-291;

Flory P.J., Yoon D.Y., **1978**. *Molecular morphology in semicrystalline polymers.* Nature 272, 226-229;

Fu Q., Men Y., Strobl G., **2003**. *A molar mass induced transition in the yielding properties of linear polyethylene.* Polymer 44, 1941-1947;

Galeski A., Argon A.S., Cohen R.E., **1991**. *Morphology of Bulk Nylon 6 Subjected to Plane Strain Compression.* Macromolecules 24, 3953-3961;

Galeski A., Bartczak Z., Argon A.S., Cohen R.E., **1992**. *Morphological Alternations during Texture-Producing Plastic Plane Strain Compression of High-Density Polyethylene.* Macromolecules 25, 5705-5718;

Galeski A., **2003**. *Strength and toughness of crystalline polymer systems.* Prog. Polym. Sci. 28, 1643-1699;

Gent A.N., Madan. S., **1989**. *Plastic Yielding of Partially Crystalline Polymers.* J. Polym. Sci. Part B: Polym. Phys. 271, 1529-1542;

Groves G.W., Hirsch P.B., **1969**. *Interlamellar Slip in Polyethylene.* J. Mater. Sci. Lett. 4, 929-932;

Hartmann B., Lee G.F., Wong W., **1987**. *Tensile Yield in Polypropylene.* Polym. Eng. Sci. 27, 823-828;

Hinton T., Rider G.J., **1968**. *Tensile Deformation of Oriented Polyethylene.* J. Appl. Phys. 39, 4932-4938;

Hobeika S., Men Y., Strobl G., **2000**. *Temperature and Strain Rate Independence of Critical Strains in Polyethylene and Poly(ethylene-co-vinyl acetate).* Macromolecules 33, 1827-1833;

Hosemann R., **1963**. *Crystalline and Paracrystalline Order in High Polymers.* J. Appl. Phys. 34, 25-42;

Kaufman W.E., Schultz J.M., **1973**. *Lamellar and interlamellar structure in melt-crystallized polyethylene. Part 3 Effects of small deformation*. J. Mater. Sci. 8, 41-46;

Kazmierczak T., Galeski A., Argon A.S., **2005**. *Plastic deformation of polyethylene crystals as a function of crystal thickness and compression rate*. Polymer 46, 8926-8936;

Keller A., Rider J.G., **1966**. *On the Tensile Behaviour of Oriented Polyethylene.* J. Mater. Sci. 1, 389-398;

Keller A., **1968**. *Polymer crystals*. Rep. Prog. Phys. 31, 623-704;

Keller A., Pope D.P., **1971**. *Identification of Structural Processes in Deformation of Oriented Polyethylene*. J. Mater. Sci. 6, 453-578;

Kelly A., Groves G.W., **1970**. *Crystallography of crystal defects*. Longman, London;

Kennedy M.A., Peacock A.J., Mandelkern L., **1994**. *Tensile Properties of Crystalline Polymers: Linear Polyethylene.* Macromolecules 27, 5297-5310;

Kryszewski M., Pakula T., Galeski A., Milczarek P., Pluta M., **1978**. *Uber einige Ergebnisse der Untersuchung der Korrelation zwischen der Morphologie und den mechanischen Eigenschaften von kristallinen Polymeren.* Faserforschung u Textiltech. 29, 76-85;

Lewis D., Wheeler E.J., Maddams W.F., Preedy J.E., **1972**. *Comparison of twinning produced by rolling and annealing in high- and low-density polyethylene.* J. Polym. Sci. A-2 Notes 10, 369-373;

Lin L., Argon A.S., **1992**. *Deformation Resistance in Oriented Nylon 6.* Macromolecules 25, 4011-4024;

Lin L., Argon A.S., **1994**. *Structure and plastic deformation of polyethylene.* J. Mater. Sci. 29, 294-323;

Oleinik E.F., **2003**. *Plasticity of Semicrystalline Flexible-Chain Polymers at the Microscopic and Mesoscopic Levels*. Polym. Sci. Ser. *C*. 45, 17-117;

O'Kane W.J., Young R.J., Ryan A.J., **1995**. *The effect of annealing on the structure and properties of isotactic polypropylene films*. J.Macromol. Sci. Phys. B34, 427-458;

Peacock A.J., Mandelkern L., Alamo R.G., Fatou J.G., **1998**. *The influence of the deformation temperature on the tensile properties of polyethylenes.* J. Mater. Sci. 33, 2255-2268;

Pawlak A., Galeski A., **2005**. *Plastic Deformation of Crystalline Polymers: The Role of Cavitation and Crystal Plasticity.* Macromolecules 38, 9688-9697;

Pawlak A., **2007**. *Cavitation during tensile deformation of high-density polyethylene.* Polymer 48, 1397-1409;

Pawlak A., Galeski A., **2008**. *Cavitation during Tensile Deformation of Polypropylene.* Macromolecules 41, 2839-2851;

Peierls R., **1940**. *The size of dislocations.* Proc. Phys. Soc. 289, 34-37;

Peterlin A., **1969**. *Plastic deformation of polyethylene by rolling and drawing*. Kolloid Z.Z. Polym. *233*, 857-862;

Peterlin A., **1971**. *Molecular Model of Drawing Polyethylene and Polypropylene*. J. Mater. Sci. 6, 490-508;

Peterlin A., **1977**. *Drawing and annealing of fibrous material.* J. Appl. Phys. *48*, 4099-4108;

Petermann J., Schultz J.M., **1978**. *Lamellar separation during the deformation of high-density polyethylene*. J. Mater. Sci. 13, 50-54;

Peterson J.M., **1966a**. *Thermal Initiation of Screw Dislocations in Polymer Crystal Platelets.* J. Appl. Phys. 37, 4047-4051;

Peterson J.M., Lindenmeyer P.H., **1966b**. *Screw Dislocations in Anisotropic Media*. J. Appl. Phys. 37, 4051-4053;

Peterson J.M., **1968**. *Peierls Stress for Screw Disclocations in Polyethylene.* J. Appl. Phys. 39, 4920-4929;

Pope D.P., Keller A., **1975**. *Deformation of oriented polyethylene.* J. Polym. Sci. Polym. Phys. Ed. 13, 533-566;

Popli R., Mandelkern L., **1987**. *Influence of structural and morphological factors on the mechanical properties of the polyethylenes.* J. Polym. Sci. Polym. Part B: Polym. Phys. 25, 441-483;

Porter R.S., Wang L.-H., **1995**. *Uniaxial Extension and Order Development in Flexible Chain Polymers*. J. Macromol. Sci. Part C: Polym. Rev. 35, 63-115;

Predecki P., Statton W.O., **1966**. *Dislocation caused by chain ends in crystal polymers.* J. Appl. Phys. 37, 4053-4059;

Predecki P., Statton W.O., **1967**. *A Dislocation Mechanism for Deformation*

in Polyethylene. J. Appl. Phys. 38, 4140-4144;

Quynn R.G., Brody H., **1971**. *Elastic "Hard" Fibers.*
J. Macromol. Sci. Phys. B5, 721-738;

Reck E.-M., Schenk H., Wilke W., **1985**. *Investigation of the deformation and relaxation of various polyethylenes by X-ray diffraction.* Progr. Coll. Polym. Sci. 71, 154-163;

Schneider K., **2010**. *Investigation of Structural Changes in Semi-Crystalline Polymer During Deformation by Synchrotron X-Ray Scattering*.
J. Polym. Sci. Part B: Polym. Phys. 48, 1574-1586;

Séguéla R., **2002**. *Dislocation approach to the plastic deformation of semicrystalline polymers: kinetic aspects for polyethylene and polypropylene.* J. Polym. Sci. Part B: Polym. Phys. 40, 593-601;

Séguéla R., **2007**. *Plasticity of semi-crystalline polymers: crystal versus melting-recrystallization.* e-Polymers Art. No: 032, 1-20;

Shadrake L.G., Guiu F., **1974**. *Dislocation in polyethylene crystals: line energies and deformation modes.* Philos. Mag. 34, 565-581;

Shadrake L.G., Guiu F., **1976**. *Dislocations in polyethylene crystals: Line energies and deformation modes.* Philos. Mag. 34, 565-582;

Shadrake L.G., Guiu F., **1979**. *Elastic line energies and line tensions of dislocations in polyethylene crystals*. Philos. Mag. 39, 785-796;

Shinozabi D., Groves G.W., **1973**. *The plastic deformation of oriented polypropylene and polyethylene: deformation mechanisms.* J. Mater. Sci. 8, 1012-1022;

Stern C., Frick A., Weickert G., **2007**. *Relationship Between the Structure and Mechanical Properties of Polypropylene: Effects of the Molecular Weight and Shear-Induced Structure.* J. Appl. Polym. Sci. 103, 519-533;

Tagawa T., Ogura K., **1980**. *Piled-Lamellae Structure in Polyethylene Films and its Deformation.* J. Polym. Sci. Polym. Phys. Ed. 18, 971-979;

Tanaka K., Seto T., Hara T., **1962**. *Crystal structure of a new form of high-density polyethylene produced by press.* J. Phys. Soc. Jpn. 17, 873-874;

Viana J.C., **2005**. *Structural interpretation of the strain-rate, temperature and morphology dependence of the yield of injection molded semicrystalline polymers*.
Polymer 46, 11773-11785;

Wilhelm H., Paris A., Schafler E., Bernstorff S., Bonarski J., Zehetbauer M.J., **2004**. *Evidence of dislocations in melt-crystallized and plastically deformed polypropylene.*
Mater. Sci. Eng: A 387-389, 1018-1022;

Wu W., Wignall G.D., Mandelkern L., **1992**. *A SANS study of the plastic deformation mechanism in polyethylene.* Polymer 33, 4137-4140;

Young R.J., Bowden P.B., Ritchie J.M., Rider J.G., **1973**. *Deformation mechanisms in oriented high-density polyethylene.* J. Mater. Sci. 8, 23-36;

Young R.J., Bowden P.B., **1974a**. *Twinning and martensitic transformations in oriented high-density polyethylene.* Philos. Mag. 29, 1061-1073;

Young R.J., **1974b**. *A dislocation model for yield in polyethylene.* Philos. Mag. 30, 85-94;

Young R.J., **1988**. *Screw dislocation model for yield in polyethylene.*
Mater. Forum. 11, 210-216;

1.4 Scope of the thesis

Polymer nanocomposites are materials in which nanometric, usually inorganic particles are dispersed in an organic polymer matrix in order to dramatically improve the performance properties of the polymer. Polymer-polymer nanocomposites are rear and known only when ready-made nanofibers or nanodroplets are dispersed in the matrix. Previous attempts of formation of polymer nanocomposites with fibrillar inclusions by compounding were unsuccessful, because it was impossible to deform a solidified polymer inclusions during compounding, while in a molten state impossible to preserve the shape of extended threads because of capillary instabilities leading to their breakup into droplets. A new idea is to use crystalline polymer inclusions and deform them into nanofibers during compounding by shearing via second polymer being in the molten state. If the crystals of polymer inclusions will be sufficiently large, macromolecules disentangled while the deformation ratios and rates sufficiently large the crystals can be deformed to nanofibers dispersed in the polymer matrix. In consequence, a nanocomposite with nanofibrillar inclusions, containing only two polymers, can be formed after solidification of the material by cooling.

Deformation of polymer crystals to large strains is possible when the density of entanglements persisting in the amorphous phase is drastically reduced. This state can be achieved by crystallization under pressure (e.g. for polyethylene, PE, and poly(vinylidene fluoride), PVDF), crystallization from dilute solutions and crystallization during polymerization (e.g. polytetrafluoroethylene, PTFE, and ultra-high molecular weight polyethylene, UHMWPE). Hence, selection of a polymer for the studies was based on the chain disentanglement ability of the polymer forming crystals. Since, the slow polymerization of tetrafluoroethylene, TFE, at suitable carefully selected conditions (temperature, pressure), which result in much faster crystallization compared to polymerization, enables formation of separate extended-chain crystals of polytetrafluoroethylene and/or their small agglomerates. Because of reduced density of entanglements and crystals with extended chains, deformation process of PTFE by shearing is possible. Such phenomenon was observed in our laboratory few years ago when non-isothermal crystallization of thin iPP+PTFE films with free surface was studied. During mixing isotactic polypropylene with aqueous emulsion of polytetrafluoroethylene, some PTFE grains were deformed into PTFE nanofibers with lateral dimensions

200÷350 nm. These unexpected results inspired us to select polytetrafluoroethylene as crystalline polymer inclusions for further studies.

The main objective of this thesis was to generate nanofibers of polytetrafluoroethylene *in situ* during compounding solid PTFE particles with thermoplastic matrix being in a molten state. The influence of a type of polytetrafluoroethylene, polymer matrix and its viscosity, as well as processing parameters including shear rate and compounding time on the so-called fibrillation process, understood as a deformation of polymer crystals into form of nanofibers, has been studied. Other objective of the thesis was to analyze an effect of generated PTFE nanofibers on the thermal, mechanical, and rheological properties of studied materials.

The results in this thesis will lead to a development of new generation of 'all polymer' nanocomposites reinforced by polymer nanofibers with wide potential applications. Simplicity of fabrication just by shearing the dispersion in another molten polymers would play very important role in minimizing the costs, hazardous exposure and environmental impact, all being usually very high when dealing with ready made nanofillers.

Chapter 2
Experimental Section

2.1 Materials

Studies presented in the paper have been conducted for a number of compositions prepared by compounding thermoplastic polymers with virgin polytetrafluoroethylene powders. Four grades of isotactic polypropylene, low density polyethylene, high density polyethylene and atactic polystyrene were used as polymeric matrices. Three grades of polytetrafluoroethylene powders were utilized as fillers. Characteristics of thermoplastic polymers and PTFE fillers according to their manufacturers and codes used in the studies are presented below.

Polypropylene (1), i-PP (PP) having weight-average molecular weight, M_w, of 220 kg mol^{-1}, melt flow index, MFI, of 13.8 g/10min (for 230 ^{o}C, 2.16 kg according to ISO 1133 standard) and density, *d*, of 0.89 g cm^{-3}, by Polysciences Inc., USA;

Polypropylene (2), Malen-P B200 (PPB) having melt flow index, MFI, of 0.6 g/10min (for 230 ^{o}C, 2.16 kg according to ISO 1133 standard), density, *d*, of 0.91g cm^{-3}, by Basell Orlen Polyolefins, Poland;

Polypropylene (3), Hostalen H 2150 (PPH) having melt flow index, MFI, of 0.3 g/10min (for 230 ^{o}C, 2.16 kg according to ISO 1133 standard) and density, *d*, of 0.90 g cm^{-3}, by LyondellBasell, the Netherlands;

Polypropylene (4), Adstif HA840K (PPA) having melt flow index, MFI, of 3.5 g/10min (for 230 ^{o}C, 2.16 kg according to ISO 1133 standard) and density, *d*, of 0.90 g cm^{-3}, by LyondellBasell, the Netherlands;

Low density polyethylene, Lupolen 1810D (LDPE) having melt flow index, MFI, of 0.1–0.3 g/10min (for 190 ^{o}C, 2.16 kg according to ISO 1133 standard) and density, *d*, of 0.92 g cm^{-3}, by LyondellBasell, the Netherlands;

High density polyethylene, S-2203 (HDPE) having melt flow index, MFI, of 0.03 g/10min (for 190 ^{o}C, 5 kg according to ISO 1133 standard) and density, *d*, of 0.97 g cm^{-3};

Atactic polystyrene, a-PS (PS) having weight-average molecular weight, M_w, of 120-250 kg mol^{-1} and density, *d*, of 1.05 g cm^{-3}, by Polysciences, Inc., USA;

Polytetrafluoroethylene (1), Teflon PTFE 7C (7C) having average particle size of 28 μm and melting peak temperature, T_m, of 346 ^{o}C, by DuPont, USA;

Polytetrafluoroethylene (2), PTFE Microdispers-200 (m-200) having average particle size of 0.2÷0.3 μm and melting peak temperature, T_m, of 325 ^oC, by Polysciences, Inc., USA;

Polytetrafluoroethylene (3), PTFE Fluoroplast-4 Reactor Bead (F4-RB) having melting peak temperature, T_m, of 345 ^oC, by Kirowo-Chepieck, Russia.

In general, the materials studied further in the paper were prepared by compounding thermoplastic polymers with 1, 3, 5 and 7 wt.% of polytetrafluoroethylene powder at temperature higher than the softening temperature of the polymeric matrix, and at various processing protocols using Brabender internal mixer and two various co-rotating twin-screw extruders 20/40D: BTSK Buhler and EHP. Composition and codes of the materials studied further in the thesis are listed in Table 2.1.

Table 2.1. *Codes and composition of materials studied.*

Material	Thermoplastic matrix	PTFE powder	Matrix content (wt.%)	PTFE content (wt.%)
PP/m-200/3	i-PP	PTFE Microdispers-200	97	3
PP/7C/3	i-PP	Teflon PTFE 7C	97	3
PPH/m-200/3	PP Hostalen H 2150	PTFE Microdispers-200	97	3
PPH/7C/3	PP Hostalen H 2150	Teflon PTFE 7C	97	3
PPH/7C/5	PP Hostalen H 2150	Teflon PTFE 7C	95	5
PPB/7C/1	PP Hostalen H 2150	Teflon PTFE 7C	99	1
PPB/7C/3	PP Malen-P B200	Teflon PTFE 7C	97	3
PPB/7C/5	PP Malen-P B200	Teflon PTFE 7C	95	5
PPB/7C/7	PP Malen-P B200	Teflon PTFE 7C	93	7
PPB/F4-RB/3	PP Malen-P B200	PTFE Fluoroplast-4 RB	97	3
PPB/F4-RB/5	PP Malen-P B200	PTFE Fluoroplast-4 RB	95	5
PPA/7C/3	PP Adstif HA840K	Teflon PTFE 7C	97	3
HDPE/7C/3	HDPE S-2203	Teflon PTFE 7C	97	3
LDPE/7C/3	LDPE Lupolen 1810D	Teflon PTFE 7C	97	3
LDPE/7C/5	LDPE Lupolen 1810D	Teflon PTFE 7C	95	5
LDPE/7C/7	LDPE Lupolen 1810D	Teflon PTFE 7C	93	7
PS/7C/3	a-PS	Teflon PTFE 7C	97	3
PS/7C/5	a-PS	Teflon PTFE 7C	95	5
PS/7C/7	a-PS	Teflon PTFE 7C	93	7

The detailed compounding procedures of materials studied further in the thesis are described below.

(a) *Polypropylene (i-PP), high density polyethylene (HDPE S-2203) with PTFE powder (Teflon PTFE 7C and PTFE Microdispers-200):* Polytetrafluoroethylene powder was finely grounded in a homogenizer at the temperature of liquid nitrogen, then added to the polypropylene powder in the amount of 3 wt.%. The mixture of powders was compounded in the Brabender internal mixer at 200 ^{o}C and 120 rev. min^{-1} for 15 min. Neat polypropylene was processed in the similar conditions in order to apply the same thermo-mechanical history as for the materials with polytetrafluoroethylene. Compounding procedure described above was also utilized for the preparation of high density polyethylene-based materials with polytetrafluoroethylene, however the compounding temperature of 170 ^{o}C was applied in order to maintain high viscosity of the matrix during processing.

(b) *Polypropylene (PP Hostalen H 2150; PP Malen-P B200) with polytetrafluoroethylene powder (Teflon PTFE 7C; PTFE Microdispers-200 and PTFE Fluoroplast-4 RB):* Polypropylene was melted in the Brabender internal mixer. Then polytetrafluoroethylene powder was added to the molten polymer in the amount of 1, 3, 5 and 7 wt.%, respectively. The polytetrafluoroethylene powder was compounded with polypropylene at 200 ^{o}C and 120 rev. min^{-1} for 10 or 15 min. Neat polypropylene was processed at the similar conditions in order to apply the same thermo-mechanical history as for the materials with PTFE.

(c) *Low density polyethylene (LDPE Lupolen 1810D), atactic polystyrene (a-PS) with polytetrafluoroethylene powder (Teflon PTFE 7C):* Low density polyethylene was melted in the Brabender internal mixer. Then polytetrafluoroethylene powder was added to the molten polymer in the amount of 3, 5 and 7 wt.%, respectively. The PTFE powder was compounded with low density polyethylene at 170 ^{o}C and 120 rev. min^{-1} for 15 min. Neat low density polyethylene was processed at the similar conditions in order to apply the same thermo-mechanical history as for the materials with polytetrafluoroethylene. Compounding procedure described above was also utilized for the preparation of atactic polystyrene-based materials with polytetrafluoroethylene.

(d) *Polypropylene (PP Hostalen H 2150) with polytetrafluoroethylene powder (Teflon PTFE 7C):* Polypropylene pellets were covered with polytetrafluoroethylene powder in the amount of 5 wt.% and then compounded using co-rotating twin-screw extruder, type BTSK 20/40D operating at 250 rev. min^{-1}. The temperature profile of 215, 230, 230, 230 and 200 ^{o}C was applied. Neat polypropylene was

processed at the similar conditions in order to apply the same thermo-mechanical history as for the materials with polytetrafluoroethylene.

(e) *Polypropylene (PP Adstif HA840K) with polytetrafluoroethylene powder (Teflon PTFE 7C):* Polypropylene pellets were transformed to a powder form by two-step process: dissolution in hot toluene, and then precipitation in methanol. Afterwards, the dried polypropylene powder was used to produce masterbatch containing 20 wt.% of polytetrafluoroethylene in the Brabender internal mixer at 200 ^{o}C and 100 rev. min^{-1} for 10 min. The final material containing 3 wt.% of polytetrafluoroethylene was prepared by dilution of former masterbatch using co-rotating twin-screw extruder, type EHP 20/40D operating at 100 rev. min^{-1}. The temperature profile of 175, 180, 185, 190, 190, 195, 200, 200 and 200 ^{o}C was applied. Neat polypropylene was processed at the similar conditions in order to apply the thermo-mechanical history as for the material with PTFE.

Processing devices used to produce materials studied further in the thesis are described below:

(a) Brabender internal mixer consists of a mixer backstand with gear unit and a mixer bowl. It is equipped with two counter-rotating rotors (roller blades type W50 E). Volume of the mixer bowl is approx. 55 cm^3. The special shape of the rotors as well as the tight clearance between rotors and mixing chamber guarantee an intensive, high shear mixing.

(b) Co-rotating twin-screw extruder BTSK 20/40D (Buhler, Germany). The screws are 20 mm in diameter and possess a length/diameter ratio equal to 40. The segmented screw in configuration of K3 consists of 30 segments, including 8 starting segments and 6 final segments of the same size and shape. Segments from 9 to 24 (double-winded transporting segments and mixing shearing segments) perform intensive plasticization in the II zone and intensive mixing in III zone. The extruder contains five heating zones.

(c) Co-rotating twin-screw extruder EHP 20/40D (Zamak, Poland). The screws are 20 mm in diameter and possessed a length/diameter ratio equal to 40. The segmented screw consists of 17 segments, including 2 starting and 1 final segment of the same size and shape. Segments from 3 to 16 (double-winded transporting segments and mixing shearing segments) perform intensive plasticization in the II zone and intensive mixing in III zone. This extruder contains nine heating zones.

Materials prepared in Brabender internal mixer were collected in the form of billets which were further cut into smaller pieces using metal-cutting machine, while materials produced using co-rotating twin screw extruders, both BTSK and EHP, were extruded out from the die in the form of continuous strand. The strand after air cooling was cut into small pellets (granules) using pelleting machine (PROMA).

2.2 Apparatus and experimental techniques

Results presented further in the paper were obtained on the basis of a number of research methods and techniques. Measuring instruments used to characterize materials which are the subject of the paper included a scanning electron microscope (SEM), tensile, compression and impact testing machines, rotational rheometer (ARES), wide-angle X-ray diffractometer (WAXS), differential scanning calorimeter (DSC), polarized light microscope (PLM) and dynamic mechanical thermal analyzer (DMTA).

2.2.1 Scanning Electron Microscopy (SEM)

The bulk morphology of samples was studied by means of scanning electron microscopy (SEM) using a microscope JEOL JSM 5500LV. The 1 mm thick films were prepared by compression molding at 190 ^{o}C for polypropylene-based materials and 170^{o}C for both low density polyethylene, high density polyethylene, and atactic polystyrene-based materials. Afterwards, all samples were solidified between two metal blocks. In order to display the internal structure of samples, two separate methods were applied: etching of polymeric matrix and fracture of samples at temperature of liquid nitrogen. The film for etching was first cut with an ultramicrotome (Power Tome XL, Boeckeler Instruments, Inc.) equipped with a glass knife, in order to expose a flat and smooth cross-section surface. The exposed surfaces of the material were then etched for 45 days at room temperature in permanganic etchant according to the procedure proposed by Olley *et al.* [Olley, 1982]. It must be mention that PTFE is resistant to permanganic etching, only polyolefins are susceptible to etching. The purpose of such prolonged etching was to reveal large fragments of PTFE nanofibers. The etching solution was composed of potassium permanganate, $KMnO_4$ (0.7 wt.%) dissolved in a mixture of concentrated sulphuric acid, H_2SO_4 (95 %), orthophosphoric acid, H_3PO_4 (85 %) and distilled water in the volume ratio 5/4/1. To improve etching, the mixture was placed in an ultrasonic bath running periodically for short time periods during the etching process (for approximately 5 min

every 1 hour). After completion of etching, the sample was immersed into four tubes in the following order: with diluted sulphuric acid (sulphuric acid/water 2/7 vol), perhydrol, distilled water and acetone. Washing was run in the presence of ultrasounds, so as to ensure more efficient transport from/to the surface of impurities/liquids.

The cryogenic fracture was also used to display the internal surface of samples. In this method a piece of sample placed between pliers was immersed into a vessel containing a liquid nitrogen (LN2). After 60 min, the sample was fractured inside vessel and left to dry heat to room temperature.

Afterwards, exposed surfaces of samples were coated with a fine gold layer (about 20 nm) by ion sputtering (JEOL JFC-1200) and examined with SEM in a high vacuum mode at the accelerating voltage of 10 kV. Microscopic images were created using secondary electron detector (SEI).

2.2.2 Mechanical properties

Tensile Testing. Uniaxial tensile drawing of the selected materials was assessed using a testing machine (Instron 5582) with load range of 0-100 kN. The oar-shaped samples according to ISO 527-2 1BA standard were cut out from 1 mm thick films non-isothermally crystallized in the conditions analogous to those used to prepare the materials for morphology studies. The samples with the gauge length of 25 mm were applied. All measurements were performed at the room temperature. In order to characterize tensile properties of materials, two tests with different cross-head speeds were performed. For determination modulus of elasticity, *E*, an extensometer with a gauge length of 25 mm and an accuracy of 1 % was utilized. A cross-head speed of 1 mm min^{-1} which corresponds to strain rate of 4 % min^{-1} was applied. The tensile properties were measured at the cross-head speed of 5 mm min^{-1} corresponding to strain rate of 20 % min^{-1}. The modulus of elasticity and selected tensile parameters of studied materials were determined on the basis of recorded stress-strain curves.

Compression Testing. The samples of polytetrafluoroethylene were uniaxially compressed in order to determine their mechanical behavior. The 15 mm × 20 mm × 13 mm rectangular prisms were cut out from the samples prepared by: (a) sintering of polytetrafluoroethylene powder in dedicated brass mould at 290 ^{o}C and 2×10^{7} Pa for 3 h, and (b) melting at 360 ^{o}C for 3 h and subsequent non-isothermal crystallization. The compression tests were carried out using testing machine (Instron 5582), sample stabilizing

fixture and compression plates. The specimens were uniaxially compressed in a special device with initial compression rate of 0.5 mm min^{-1} at room temperature. The compressive yield stress, σ_y, was determined at the intersection of measured stress-strain curve and a straight line parallel to initial slope of the curve and offset by 2 % of strain.

Impact Testing. Izod impact measurements of selected materials were performed using instrumented impact tester (Resil 5.5, CEAST S.p.A.). The 80 mm × 10 mm × 4 mm bar-like specimens according to ISO 180/1A standard were injection molded by means of a 5 g laboratory injection molding machine (PROMA, Poland) at 4.5×10^5 Pa and 200 ^oC for polypropylene-based materials and 170 ^oC for both atactic polystyrene and low density polyethylene-based materials. Later, the notch type A with a base radius of 0.25 mm was cut into the samples in order to achieve a stress concentration as well as an increase in crack propagation rate at the front of the crack tip. Notched samples were tested in Izod configuration using pendulum hammer with nominal impact energy of 4 J and impact velocity of 3.5 m s^{-1}. Izod impact strength, U_I, was determined as an impact energy absorbed in breaking a notched specimen, referred to the original cross-sectional area of the specimen at the notch.

2.2.3 Instruments for rheological tests

Linear viscoelasticity. The small-amplitude oscillatory measurements of selected materials were executed using a strain-controlled rheometer (ARES LS2, TA Instruments) with both a torque transducer (0.02÷2000 g cm) and a normal force transducer (2–2000 g). Parallel plates with diameter of 25 mm and the gap distance kept in the range of 0.8-0.9 mm were applied. The disk-shaped samples were cut out from 1 mm thick films prepared by compression molding at 200 °C. The boundaries of the linear regime over which the storage modulus, *G'*, and loss modulus, *G''*, are independent on the strain amplitude were determined by running the strain amplitude sweeps from 0.1 to 10 % at different frequencies on each sample. The main oscillatory measurements were performed by running the frequency sweeps from 0.01 to 100 rad s^{-1} at 190 °C and 0.5 % of strain.

Steady shear. Simple shear measurements of selected materials were performed using the ARES rheometer described above. Parallel plates in diameter of 25 mm with the gap distance kept in the range of 0.8÷0.9 mm were applied. Disk-shaped samples were cut out from 1 mm thick films prepared by compression molding at 200 °C and subjected to shearing with the rate of 4 s^{-1} at various temperatures ranging from 200 to 230 ^oC until the

requested deformation was achieved. The steady shear viscosity, η_s, was measured during the rheometer runs and deformed samples were picked up for morphology investigation by scanning electron microscopy.

Extensional viscosity. Uniaxial extension tests of selected samples were performed using extensional viscosity fixture (EVF, TA Instruments) attached to the ARES rheometer as shown in Figure 2.1.

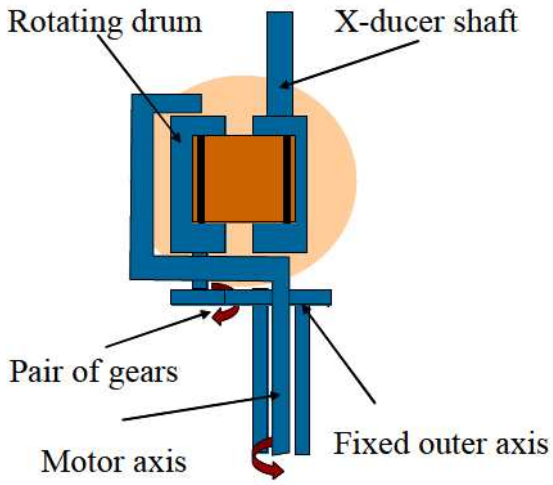

Figure 2.1. *Scheme of extensional viscosity fixture (EVF)[Franck 2010].*

The EVF consists of paired drums arranged in vertical position and parallel to each other. Between them a sample strip is positioned at middle height using two clamps. The EVF is attached to the ARES rotational rheometer, with one cylinder connected to the force transducer, and the other to the motor. In order to wind up the sample equally on both sides, the rotating cylinder moves on a circular orbit around the force measuring cylinder while rotating around its own axis at the same time, thereby stretching the sample uniaxially and under a constant Hencky rate. The force measurement is decoupled from all the moving parts and consequently friction and inertia contributions are not affecting the material response [Hodder 2005].

The 18 mm × 10 mm × 0.7 mm rectangular specimens were prepared by compression molding in dedicated mould at 200 °C for polypropylene-based materials and at 170 ^{o}C for both atactic polystyrene, low density polyethylene and high density polyethylene-based materials. Molten samples were uniaxially stretched at a constant extensional rate (0.1, 1.0, 2.0, and 5.0 s^{-1}), and 170 °C for both atactic polystyrene, low density polyethylene and high density polyethylene-based materials and at 200 °C for polypropylene-based

materials. The transient extensional viscosity, η_E^+, as a function of extensional time at a constant strain rate was determined.

Shear viscosity. Transient shear measurements of selected samples were executed using rheometer ARES described above. Cone-plate geometry with diameter of 25 mm, the cone angle of 0.1 rad and actual gap distance of 0.46 mm was applied. Disk-shaped samples were cut out from 1 mm thick films prepared by compression molding at 200 °C for polypropylene-based materials and 170 ^{o}C for high density polyethylene-based materials. Data of the transient shear viscosity, η_S^+, were collected during shearing of molten samples at the strain rate of 0.01 s^{-1} and 170 °C for high density polyethylene-based materials and 200 °C for polypropylene-based materials. Trouton ratio, T_r, was estimated as the ratio of the transient extensional viscosity to the transient shear viscosity at a total strain achieved.

2.2.4 Wide-Angle X-ray Scattering (WAXS)

The crystalline structure of materials was probed by wide-angle X-ray scattering. Computer controlled wide-angle goniometer coupled to a Philips PW3830 sealed-tube X-ray generator operating at 30 kV and 50 mA was used. The X-ray beam consisted of Cu K_α radiation Ni-filtered. The samples for WAXS measurements were prepared from 1 mm thick films non-isothermally crystallized in the conditions analogous to those used to produce the materials for morphological and mechanical studies. 2θ scans were collected both in reflection and transmission mode with a divergence angle of 0.05^{o}.

2.2.5 Differential Scanning Calorimetry (DSC)

Melting and non-isothermal crystallization of selected materials were performed by means of differential scanning calorimetry (DSC) using an indium-calibrated TA Instruments 2920 calorimeter. 1 mm thick films were prepared by compression molding in the conditions analogous to those used to produce the materials for morphology and mechanical studies. Samples of weight 6÷10 mg were heated at the rate of 10 ^{o}C min^{-1} to 220 ^{o}C, annealed for 3 min and then cooled at the rate of 10 ^{o}C min^{-1} to room temperature. The entire thermal treatment was performed under nitrogen flow.

The melting peak temperature, T_m, and crystallization peak temperature, T_c, of the samples were determined from recorded DSC thermograms as a maximum value of

endothermic and exothermic peaks, respectively. The degree of crystallinity, *C*, was estimated from the heat of melting according to a formula:

$$C = \frac{\Delta H_m}{\Delta H_m^0} \tag{2.1}$$

where ΔH_m is the measured heat of melting of the sample and ΔH_m^0 is the heat of melting of 100 % crystalline material. In this study, ΔH_m^0 of 82 J g^{-1} for polytetrafluoroethylene [Lau 1984], 293 J g^{-1} for polyethylene [Wunderlich 1977], and 177 J g^{-1} for polypropylene [Li 1999] has been assumed.

Polytetrafluoroethylene powders were characterized by DSC during heating to 400 ^oC and cooling to room temperature, followed by subsequent heating. Both the cooling and heating rate of 10 ^oC min^{-1} was applied. The entire thermal treatment was performed under nitrogen flow. The melting peak temperature, T_{m1} and T_{m2}, crystallization peak temperature, T_c, degree of crystallinity, C_1 and C_2, were calculated on the basis of DSC thermograms.

Differential scanning calorimetry was also used to study isothermal crystallization of neat isotactic polypropylene and isotactic polypropylene with polytetrafluoroethylene. 1 mm thick films were prepared by compression molding at conditions analogous to those used to produce the materials for morphology and mechanical studies. Samples of 6-10 mg were heated at the rate of 10 ^oC min^{-1} to 220 ^oC, annealed for 3 min and then cooled at the rate of 10 ^oC min^{-1} to pre-selected crystallization temperature of 128 ^oC or 145 ^oC, respectively. The entire thermal treatment was performed under nitrogen flow. Afterwards, 10 μm thin sections of selected isothermally crystallized samples were examined by polarized light microscopy (PLM). Conversion degree, $\alpha(t)$ was calculated based on DSC thermograms recorded during isothermal crystallization.

2.2.6 Polarized Light Microscopy (PLM)

Isothermal crystallization of selected materials was studied by polarized light microscopy (PLM) in quiescent state using a Linkam hot stage CSS450 mounted on a Nikon Eclipse 80i light microscope. 30 μm thick films were placed between microscope glass slides, heated to 220 ^oC, annealed for 3 min and then cooled at the rate of 30 ^oC min^{-1} to pre-selected crystallization temperature of 132 ^oC and 138 ^oC, respectively. The isothermal crystallization was monitored and recorded by a camera connected to a PC class

computer with a frame grabber card. All isothermal crystallization measurements were performed under nitrogen flow.

Additionally, thin films of selected materials were non-isothermally crystallized with free surface using a Linkam hot stage CSS450. The 70 μm thick samples were heated at the rate of 30 ^{o}C min^{-1} to 220 ^{o}C, annealed for 3 min and then cooled at the rate of 10 ^{o}C min^{-1} to room temperature. Afterwards, the non-isothermally crystallized samples were picked up for morphology investigation by SEM.

2.2.7 Dynamic Mechanical Thermal Analysis (DMTA)

Dynamic mechanical thermal measurements of selected materials were conducted using DMTA MkIII apparatus (Rheometric Scientific Inc.) in a double cantilever bending mode at the frequency of 1 Hz and heating rate of 2 °C min^{-1}, in the temperature range from -100 to 100 ^{o}C for polypropylene-based materials and -100 ^{o}C to 140 ^{o}C for atactic polystyrene-based materials. The 30 mm × 10 mm rectangular specimens were cut out from 1 mm thick films non-isothermally crystallized in the conditions analogous to those used to produce the materials for morphological, thermal and mechanical studies. The storage modulus, *E'*, and loss modulus, *E''*, as a function of temperature were recorded during DMTA runs.

Chapter 3
Results and Discussion

3.1 Nascent polytetrafluoroethylene powders

Some semicrystalline polymers like polyethylene, PE, or poly(vinylidene fluoride), PVDF, are able to crystallize in a chain-extended fashion under elevated pressure [Philips 1990]. Polytetrafluoroethylene, PTFE, can also possess either chain-folded or chain-extended crystals depending on the conditions of crystallization process. Melting of semicrystalline polymers with very high molecular weight ($M_w \geq 10^6$), like ultra high molecular weight polyethylene, UHMWPE, and polytetrafluoroethylene leads to the systems with high concentration of entanglements. Experimental observations revealed that chain-folded crystals "explode" upon melting [Barham 1991]. Once the constraints (lattice forces) are removed by melting, folded molecules expand rapidly, driven by the need to increase its entropy. Chain segments are then ejected with a high kinetic energy into the already molten surrounding and interlace with other chains rapidly leading to significant increase of the number of entanglements.

During crystallization entanglements are rejected to the amorphous phase. In the case of PTFE much less entangled system with either fully or nearly chain-extended crystals can be obtain by the crystallization during polymerization. While decreasing the polymerization temperature well below the crystallization temperature, the polymerization rate becomes lower than the crystallization rate and it is possible to reach the state when growing chains are separated from each other while crystallization proceeds simultaneously with polymerization. This results in an independent growth of monomolecular crystals - a single chain forming a single crystal. Polymer crystals grown during polymerization are called nascent or as-polymerized crystals [Wunderlich 1976].

Three different polytetrafluoroethylene powders were used in these studies. Two nascent powders: Teflon PTFE 7C (7C) and PTFE Fluoroplast-4 Reactor Bead (F4-RB) and dried aqueous dispersion of polytetrafluoroethylene: PTFE Microdispears-200 (m-200). The morphology of polytetrafluoroethylene powders was examined by scanning electron microscopy. SEM micrographs of PTFE powders with appropriate diagrams of particle

size distribution are presented in Figure 3.1. The diagrams were based on counting particles in several SEM images.

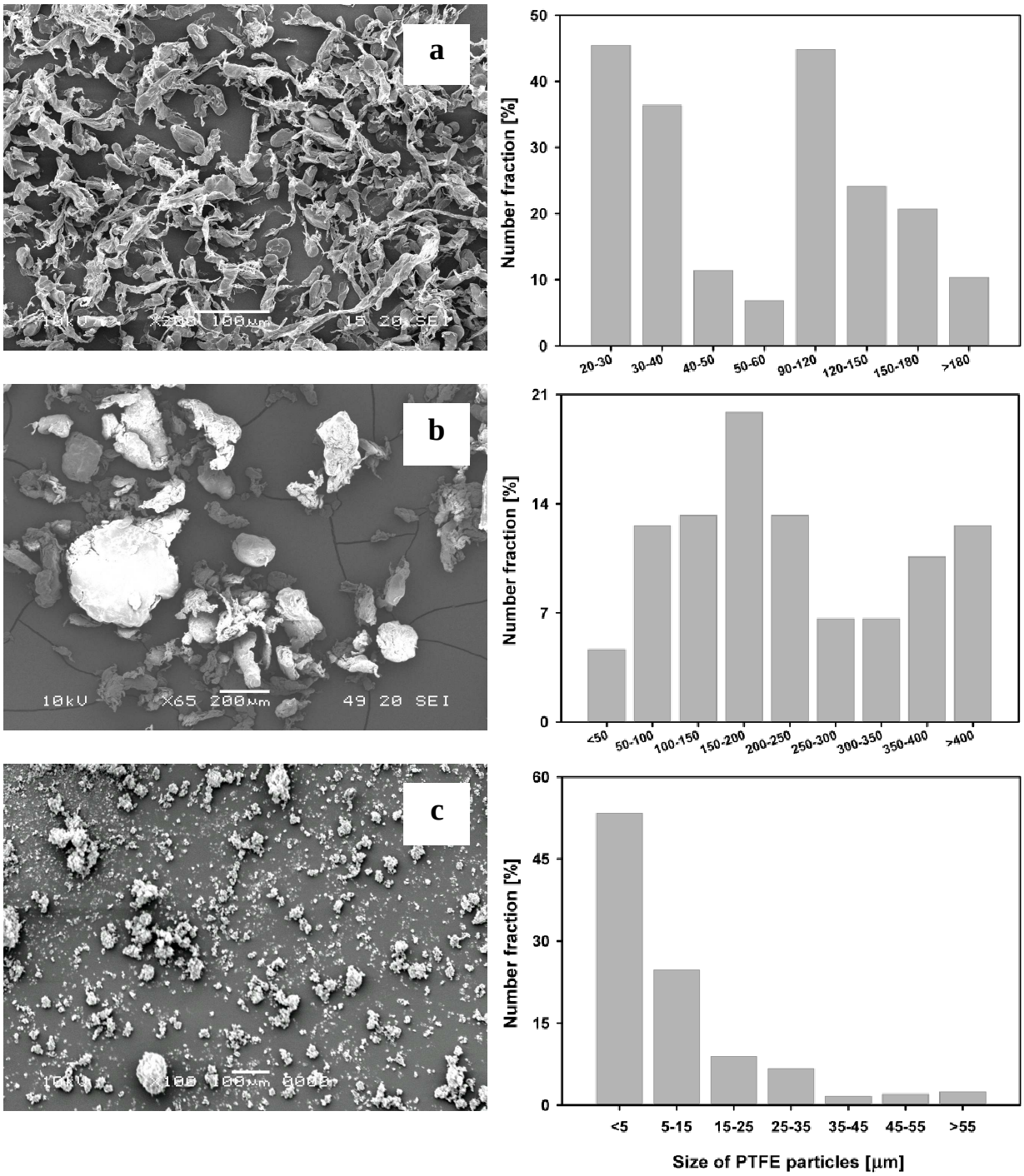

Figure 3.1. *SEM images of polytetrafluoroethylene powders studied with diagrams of PTFE particle size distribution: (a) Teflon PTFE 7C, (b) PTFE Fluoroplast-4 RB, and (c) PTFE Microdispers-200.*

Manufacturer of as-polymerized polytetrafluoroethylene 7C states that this powder consists of spherical particles with an average size of 28 μm. However, the morphology studies revealed that 7C, shown in Figure 3.1a, contains two populations of particles: a flat ellipsoidal particles with length in the range between 20 and 60 μm and a flaky fibrillar

particles having length in the range from 90 to 200 μm. This difference in morphology of polytetrafluoroethylene powder 7C arises from pretreatment of the producer (Dupont Co.) of as-polymerized powder by rolling.

Second nascent PTFE powder F4-RB contains spherical and flaky particles with different lengths ranging from 30 up to 600 μm as shown in Figure 3.1b.

The dominant population of polytetrafluoroethylene particles in m-200, prepared by drying the aqueous dispersion of PTFE are particles with sizes of 0.2-0.3 μm and aggregates of polytetrafluoroethylene smaller than 5 μm. Aggregates larger than 55 μm are also observed in Figure 3.1c.

The thermal properties of so-called virgin polytetrafluoroethylene, i.e. the polymer which has never been heated above the melting temperature after polymerization, were studied by means of differential scanning calorimetry. Figure 3.2 shows exemplary DSC thermograms of virgin, as-polymerized PTFE powder F-4 RB with melting and crystallization peaks recorded during heating, and cooling. The melting of as-polymerized PTFE is at high temperature, above equilibrium melting temperature, T_m^0, and is very strong suggesting high degree of crystallinity. T_m^0 was determined by different authors being in the range between 332 and 336 ^oC [Lau 1984; Bassett 1974; Pucciariello 1999]. Crystallization peak during cooling is at much lower temperature, the subsequent melting differs significantly from the first melting: the melting temperature is significantly lower than T_m^0. Similar behavior is exhibited by PTFE 7C. PTFE dispersion m-200 shows first melting peak at lower temperature and the peak is lower. The calorimetric data of all three studied polytetrafluoroethylene powders are collected in Table 3.1, where T_{m1}, T_{m2}, and ΔH_{m1}, ΔH_{m2} denote the melting peak temperature and the melting enthalpy during the first and the second heating, respectively, whereas T_c, denotes the crystallization peak temperature. The degrees of crystallinity, C_1 and C_2, were calculated from the eq. 2.1, on the basis of the heat required to melt the sample, ΔH_{m1} and ΔH_{m2}, respectively, assuming the heat of melting of 100 % crystalline polytetrafluoroethylene of 82 $J \cdot g^{-1}$ [Lau 1984].

Polytetrafluoroethylene powder m-200 shows the melting peak temperature, T_{m1}, lower than both T_{m2} and the equilibrium melting temperature, T_m^0. It is known that the polymer crystals with chain folding are not equilibrium crystals.

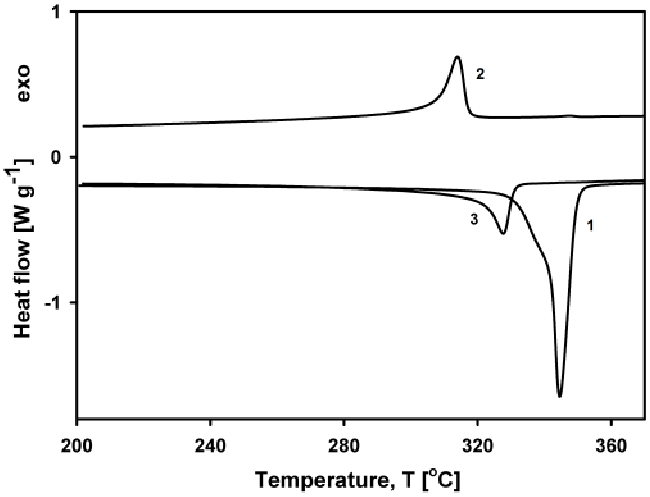

Figure 3.2. *DSC thermograms of virgin polytetrafluoroethylene powder F4-RB: (1) the first heating, (2) the first cooling, and (3) the second heating. The thermograms were shifted for clarity.*

Their melting peak temperature, T_m, determined from Gibbs-Thomson equation [Wunderlich 1980] expressed as

$$T_m = T_m^0\left(1-\frac{2\sigma_e}{\Delta H_m}\cdot\frac{1}{l}\right) \tag{3.1}$$

where σ_e is the basal surface free energy, l is the lamellae thickness, and ΔH_m is the enthalpy of fusion per unit volume of crystal, T_m is lower than the equilibrium melting temperature of infinitely thick crystal, T_m^0, by the magnitude inversely proportional to the their thickness.

Table 3.1. *Thermal properties of polytetrafluoroethylene powders used in the studies.*

PTFE	T_{m1} [°C]	T_{m2} [°C]	T_c [°C]	ΔH_{m1} [J g^{-1}]	ΔH_{m2} [J g^{-1}]	C_1 [%]	C_2 [%]
m-200	325.1	325.9	313.1	73.0	69.7	89.1	85.0
7C	345.7	327.8	315.2	77.7	39.0	94.7	47.6
F4-RB	344.6	327.6	314.0	75.8	34.7	92.4	42.3

The melting peak temperature, T_{m1}, of both virgin polytetrafluoroethylene powders: 7C and F4-RB exceeds their T_{m2}, and is above T_m^0. Such high melting peak temperature, T_{m1}, of nascent polytetrafluoroethylene was measured by others [Bassett 1974; Toda 2002; Pucciariello 2004] and interpreted as superheating of chain-extended crystals. The most stable state are crystals built from the extended polymer chains. Such thick crystals being unable to melt sufficiently quickly during heating at high heating rates, hence their interior are heated above the equilibrium melting point.

In all cases, ΔH_{m1} exceeds ΔH_{m2} indicating the high degree of crystallinity of polytetrafluoroethylene powders developed during polymerization, being in the range between 89 and 95 %.

It can be concluded on the basis of above results that polytetrafluoroethylene powder m-200 obtained by drying the aqueous dispersion of PTFE particles is composed of chain-folded crystals. While the conditions used to polymerize tetrafluoroethylene, TFE, enabled the synthesis of polytetrafluoroethylene powders (7C and F4-RB) with large crystals in chain-extended fashion without significant entanglements. It is expected that such crystals will deform easily.

3.2 Deformation of polytetrafluoroethylene crystals

Plastic deformation of semicrystalline polymers requires both deformation of amorphous and crystalline phase [Lin 1994; Galeski 2003] due to their complicated, hierarchical structure develop during crystallization from a molten state [Keller 1968]. Plastic deformation of a polymer is initiated by crystal plasticity. Bartczak *et al.* [Bartczak 2012] have shown that the density of entanglements is the key parameter controlling deformability of the melt of UHMWPE. Lower the entanglements density the higher the ultimate strain in the plain-strain compression of a molten material.

The effect of topological structure on the deformation behavior of polytetrafluoroethylene was studied by means of uniaxial compression, which is more fundamental deformation mode than tensile drawing as it avoids such phenomena as cavitation and voiding. Two methods were used to prepare samples for uniaxial compression measurements: (a) sintering of as-polymerized polytetrafluoroethylene 7C particles at 290 ^{o}C, i.e. temperature below the onset of melting of nascent PTFE 7C crystals (T_{ons} > 333.8 ^{o}C); and (b) melting of nascent polytetrafluoroethylene powder 7C at 360 ^{o}C for 3h and subsequently crystallization. Rastogi *et al.* [Rastogi 1997; Lippits 2006] have shown that a sufficiently long melting time of nascent UHMWPE larger than 10^4 s, is necessary to increase the concentration of chain entanglements.

The crystalline structure of polytetrafluoroethylene 7C as-polymerized and after sintering at 290 ^{o}C was studied by means of wide-angle X-ray scattering (WAXS). X-ray diffraction patterns of as-polymerized polytetrafluoroethylene 7C and after sintering at 290 ^{o}C are presented in Figure 3.3. Diffraction pattern for polytetrafluoroethylene 7C after sintering at 290 ^{o}C is similar to that for as-polymerized polymer. Besides the reflex from (100) crystallographic plane observed at 18.1^{o} four small reflexes are visible in the 2θ range between 30 and 45^{o}, which corresponds to (110), (200), (107) and (108) crystallographic planes, respectively. The presence of (107) and (108) peaks at temperature of 25 ^{o}C is indicative of the crystalline phase IV of polytetrafluoroethylene 7C [Bunn 1954]. Degree of crystallinity of nascent polytetrafluoroethylene 7C is 94.7 % while after sintering *C* slightly increases to 95.1 %. Applied sintering procedure enabled coalescence of particles of nascent polytetrafluoroethylene 7C without changing its topological structure.

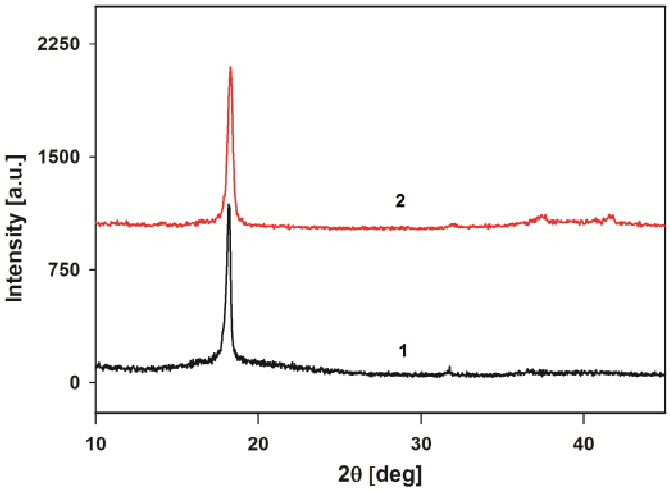

Figure 3.3. *Diffractograms 2θ for samples of polytetrafluoroethylene 7C as (1) nascent powder and (2) after sintering at 290 °C and 2×10⁷ Pa for 3 h, recorded in reflection mode at 25 °C. The WAXS diffractograms were shifted vertically for clarity.*

Melt-crystallized polytetrafluoroethylene 7C shows the melting peak temperature (331.7 °C) lower than T_m of nascent polymer which in consequence leads to drastic decrease of the degree of crystallinity by about 30 % from 94.7 % to 65.1 %. This suggests that applied method of crystallization causes formation of polytetrafluoroethylene 7C chain-folded crystals composed of many different chains and entangling of these chains in adjacent amorphous layers.

Figure 3.4 presents the true stress-compression ratio curves obtained for the samples of polytetrafluoroethylene 7C after sintering and melt-crystallization deformed by uniaxial compression. Samples were deformed with the constant compression rate of 0.5 mm min^{-1} at room temperature.

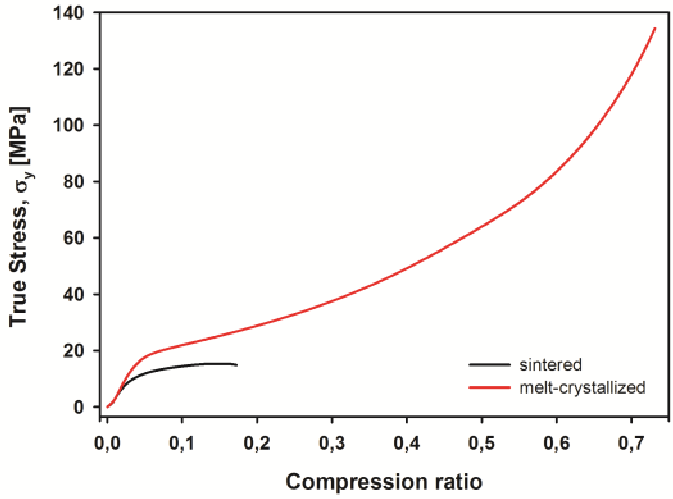

Figure 3.4. *True stress-compression ratio curves of PTFE 7C samples after sintering at 290 °C and melt-recrystallization at 360 °C deformed at room temperature with the compression rate of 0.5 mm* min^{-1}.

The compressive yield stress, σ_y, for sintered nascent PTFE 7C is only about 12.1 MPa at room temperature, while for melt-crystallized material is 19.5 MPa. Sintered polytetrafluoroethylene, deformed at room temperature, fractured early at compression ratio of 0.18, due to poor connectivity between crystals and/ or grains of the powder [see Bartczak 2012, for similar phenomena in UHMWPE sintered powder]. In contrast, melt-crystallized sample deformed to 0.72 with a distinct strain hardening stage, leading to ultimate stress of 137 MPa. The resolved shear stress , τ, acting under 45^o can be calculated according to the following equation:

$$\tau = \sigma \cos(45^o)\cos(45^o) = \sigma / 2 \tag{3.2}$$

Hence, to initiate plastic deformation of chain-extended crystals of polytetrafluoroethylene 7C embedded in viscous media (a polymeric matrix) through shearing, the resolved shear stress of only 6.05 MPa must be reached and exceeded at room temperature. Since crystal plasticity is thermally activated process, the required resolved shear stress at elevated temperature will be significantly lower. The higher the temperature the lower the shear stress for crystal plasticity.

3.3 Structure of the nanocomposites with PTFE inclusions

The materials studied further in the paper were generally prepared by compounding of polytetrafluoroethylene powders with thermoplastic polymers including isotactic polypropylene, i-PP, high density polyethylene, HDPE, low density polyethylene, LDPE, and atactic polystyrene, PS, at various processing conditions, which are described in details in Chapter 2.1. The effect of type of polytetrafluoroethylene powder and thermoplastic matrix, viscosity of matrix, shear rate and compounding time on the final morphology of the materials was intensively examined. The results of those studies are presented in the following subsections.

3.3.1 Type of polytetrafluoroethylene powder

Two nascent polytetrafluoroethylene powders (7C and F4-RB) and dried aqueous dispersion of PTFE particles (m-200) were compounded with isotactic polypropylene. The final morphology of prepared materials was examined by scanning electron microscopy. Figures 3.5a-c presents SEM images of cryogenic fractured samples of polypropylene-based materials containing 3 wt.% of PTFE m-200, 7C and F4-RB, respectively. In the case of m-200 used as a filler, aggregates of PTFE particles having longitudinal sizes of 3÷10 μm dispersed in polypropylene matrix are visible (Figure 3.5a). In contrast, when using nascent polytetrafluoroethylene 7C powder, the final morphology of PPB/7C/3 considerably differs from PP/m-200/3. During compounding nascent 7C powder with isotactic polypropylene, particles of polytetrafluoethylene are subjected to sufficient shearing and can be readily deformed and transformed without a melting step into nanofibers with transverse sizes ranging from 30 to 580 nm (Figure 3.5b). Similar fibrillar inclusions with transverse sizes in the range from 60 to 650 nm are observed in the cryogenic fractured surface of PPB/F4-RB/3 nanocomposite (Figure 3.5c).

Formation of nanofibers during shearing of grains of polytetrafluoroethylene emulsions was noticed in the past [Yang 2005]. Only few authors observed [Van der Meer 2005; Masirek 2007; Bernland 2009] that polytetrafluoroethylene powder added to thermoplastic polymer including isotactic polypropylene, poly(methylene oxide), POM, and high density polyethylene can transform to a network of fibers, in the form of bunches and bundles. Those studies aimed at optimizing the nucleation of crystallization of PP, POM and PE by PTFE. But untill now, no one has determined the critical conditions for

fibrillation of polytetrafluoroethylene and the mechanism responsible for deformation of PTFE crystals into form of nanofibers.

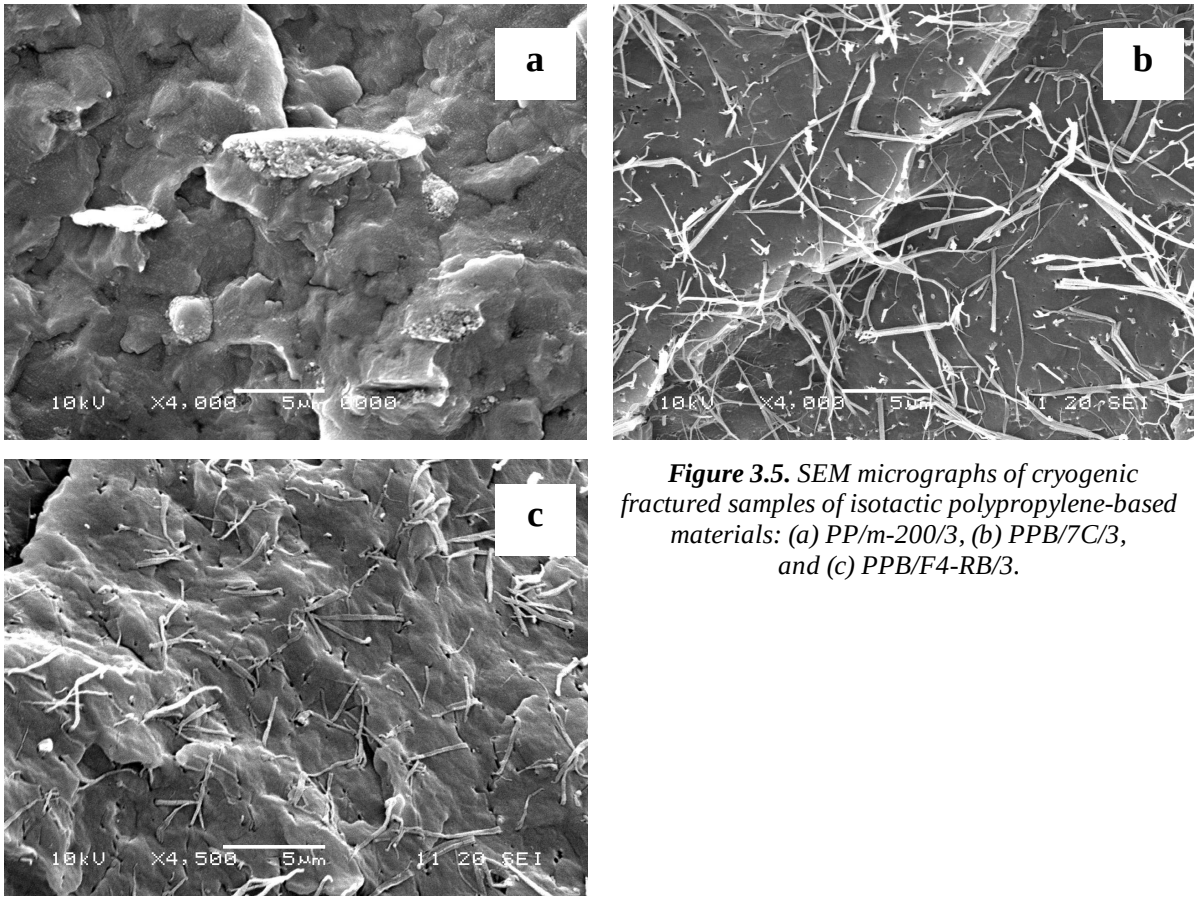

Figure 3.5. *SEM micrographs of cryogenic fractured samples of isotactic polypropylene-based materials: (a) PP/m-200/3, (b) PPB/7C/3, and (c) PPB/F4-RB/3.*

In contrast to polytetrafluoroethylene m-200 with melting peak temperature of 325.1 ^{o}C, particles of nascent PTFE powders: 7C and F4-RB exhibiting T_m of 345.7 ^{o}C and 344.6 ^{o}C respectively, can undergo easy fibrillation by plastic deformation of PTFE chain extended crystals, directly during compounding with thermoplastic polymers, leading to polymer nanocomposites with fibrillar nanoinclusions of PTFE. This phenomenon was observed only for PTFE whose crystals are characterized by high melting temperature, in this case exceeding the equilibrium melting peak temperature of polytetrafluoroethylene crystals (T_m^0=332÷336 ^{o}C).

The structure of polypropylene-based nanocomposite with polytetrafluoroethylene nanofibers was also examined by X-ray diffraction. Figure 3.6 presents wide-angle X-ray (WAXS) diffractograms of neat isotactic polypropylene, PPB, and its nanocomposite with 5 wt.% of PTFE 7C nanofibers recorded in the reflection mode in 2θ range from 10 to 30^{o}.

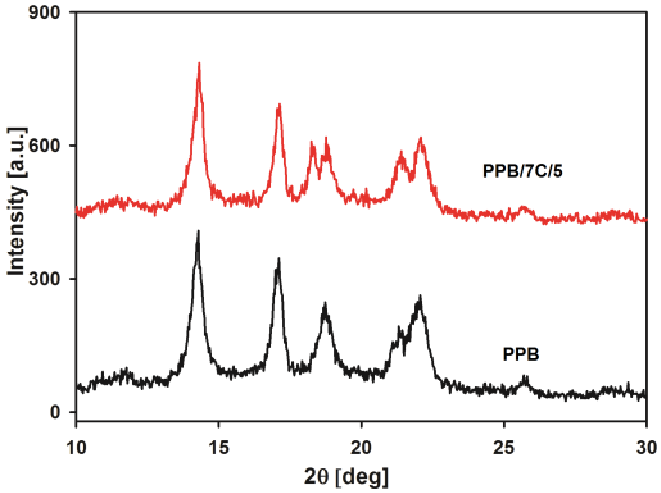

Figure 3.6. *Diffractograms 2θ of neat isotactic polypropylene, PPB, and its nanocomposite with 5 wt.% of PTFE 7C nanofibers recorded in the reflection mode at 25 °C. Curves have been shifted along the vertical axis for better visualization.*

Neat isotactic polypropylene, PPB, crystallized in its usual α monoclinic form confirmed by five crystallographic peaks of (110), (040), (130), (111) and (041) planes. In case of PPB/7C/5 nanocomposite, beside crystallographic planes corresponding α-form of PPB, additional shoulder on right side of the peak (130) which corresponds to (100) plane of polytetrafluoroethylene at 18.1°.

Polytetrafluoroethylene 7C have been chosen for further studies since the deformation of PTFE 7C particles via shearing in a viscous polymer matrix leads to obtain the thinnest polytetrafluoroethylene nanofibers.

3.3.2 Thermoplastic matrix and its viscosity

Polytetrafluoroethylene nanofibers can be generated directly during compounding thermoplastic polymers including isotactic polypropylene, low density polyethylene, high density polyethylene and atactic polystyrene with nascent PTFE powders having $T_m > T_m^0$. However transverse sizes and aspect ratios of generated polytetrafluoroethylene nanofibers depend not only on the type of PTFE but also thermoplastic matrix and its viscosity, shear rate and compounding time. The last two parameters will be discussed in next subsection.

If thermoplastic matrix is a low viscosity polymer like isotactic polypropylene, PP, having MFI of 13.8 g/10min, only a part of PTFE 7C particles are fibrillated under shearing and transform into nanofibers as illustrated in Figure 3.7a, which presents SEM images of cryogenic fractured samples of the nanocomposites containing 3 wt.% of nascent PTFE 7C.

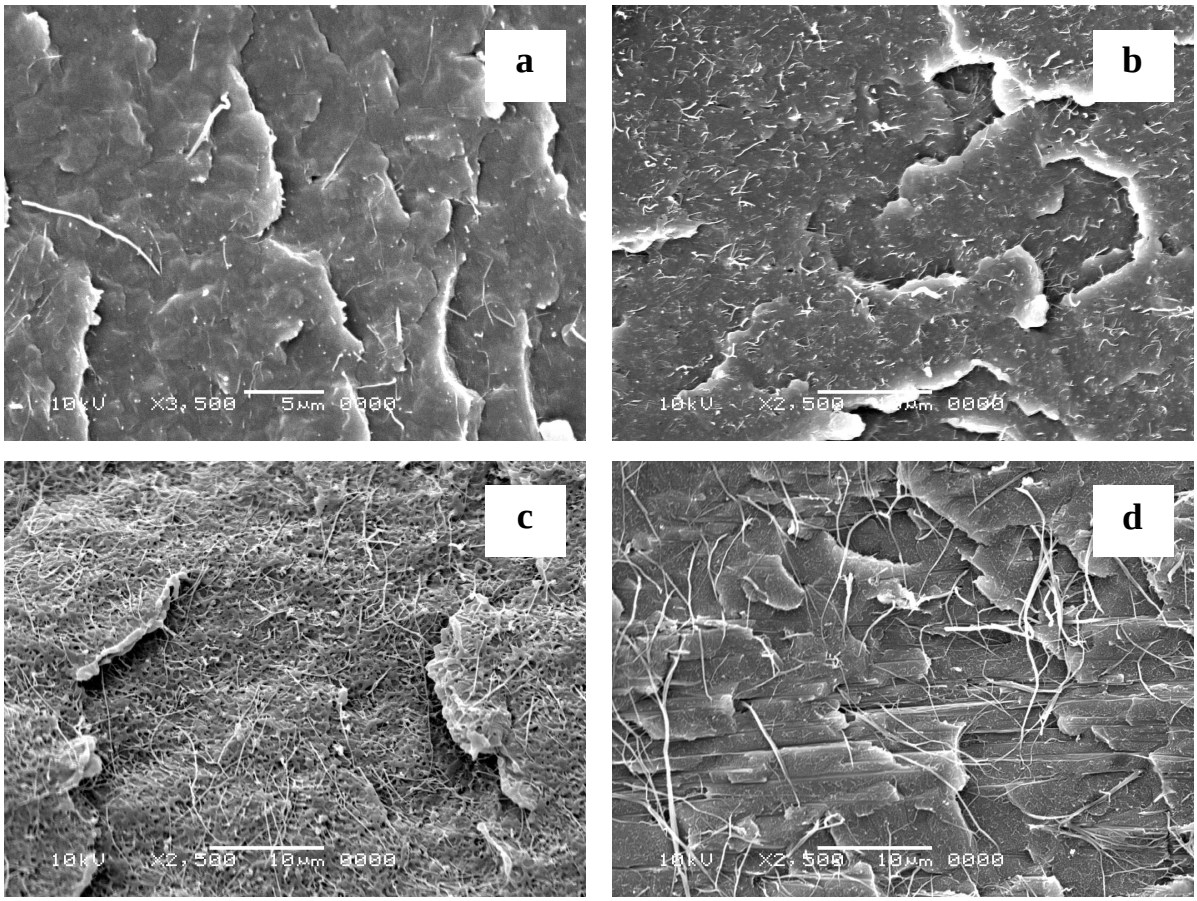

Figure 3.7. *SEM microphotographs of cryogenic fractured samples of the nanocomposites with nascent polytetrafluoroethylene 7C:(a) PP/7C/3, (b) LDPE/7C/7, (c) HDPE/7C/3 and (d) PS/7C/7.*

Changing thermoplastic matrix to more viscous one, e.g. from low viscosity polypropylene, PP, to low density polyethylene, LDPE, with melt flow index of 0.1÷0.3 g/10min or high density polyethylene, HDPE, having MFI of 0.03 g/10min enables fibrillation practically of all particles of nascent PTFE 7C powder leading to formation of polytetrafluoroethylene nanofibers (Figure 3.7b) with transverse sizes between 30 and 110 nm (Figure 3.7c) homogeneously dispersed in polyethylene matrix. In the case of using atactic polystyrene, PS, as matrix, generated PTFE 7C nanofibers are thicker (50÷230 nm) than those for HDPE (Figure 3.7d).

Structure of the nanocomposites with PTFE 7C nanofibers was also studied by wide angle X-ray diffraction. An exemplary WAXS diffractograms of neat LDPE and its nanocomposite with 3 wt.% of PTFE 7C nanofibers recorded in the reflection mode in the 2θ range between 10 and 40^{o} are shown in Figure 3.8.

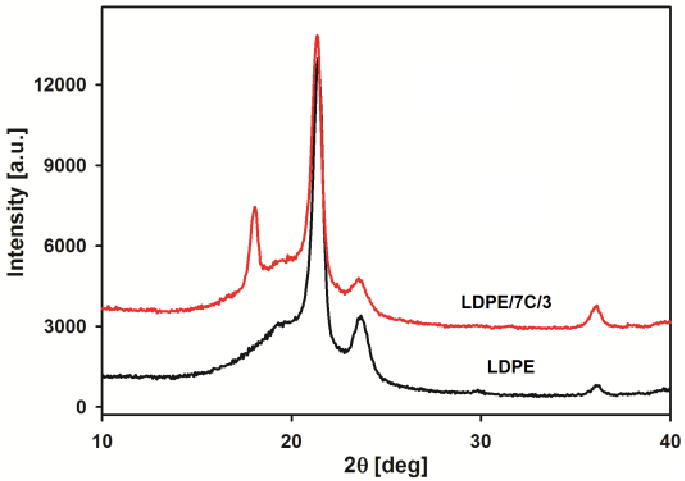

Figure 3.8. *Diffractograms 2θ of low density polyethylene, LDPE, and its nanocomposite with 3 wt.% of PTFE 7C nanofibers recorded in the reflection mode at 25 °C. Curves have been shifted along the vertical axis for better visualization.*

Neat low density polyethylene crystallized in its usual orthorhombic form which is confirmed by the presence of three crystallographic peaks of (110), (200) and (020) planes. In the case of LDPE/7C/3 nanocomposite, besides planes corresponding to LDPE, additional peak at 18.1° corresponding to (100) plane of polytetrafluoroethylene is observed.

3.3.3 Shear rate and compounding time

The effect of shearing on the final morphology of polypropylene-based nanocomposites with nascent polytetrafluoroethylene powder was studied by means of steady shear experiments. Molten samples of isotactic polypropylene, PPB, containing 3 wt.% of PTFE 7C particles were subjected to shearing with the rate of 4 s^{-1} and the range of temperatures 200÷230 ^{o}C until the requested deformation of the matrix was achieved. The dependence of steady shear viscosity, η_s, against strain, ε, is shown in Figure 3.9. The samples after shear experiments were picked up for morphology investigations by scanning electron microscopy. SEM images of cryogenic fractured samples of PPB/7C/3 nanocomposite, deformed to $\varepsilon = 10$ and $\varepsilon = 5000$, are illustrated in Figure 3.10. The continuous drop of steady shear viscosity for neat isotactic polypropylene, PPB, under shearing is observed. This is a consequence of the PTFE nanofibers and polypropylene chains orientation in the direction of shearing. In the case of PPB/7C/3 nanocomposite, after initial drop of η_s with increasing deformation, the η_s curves are leveling off.

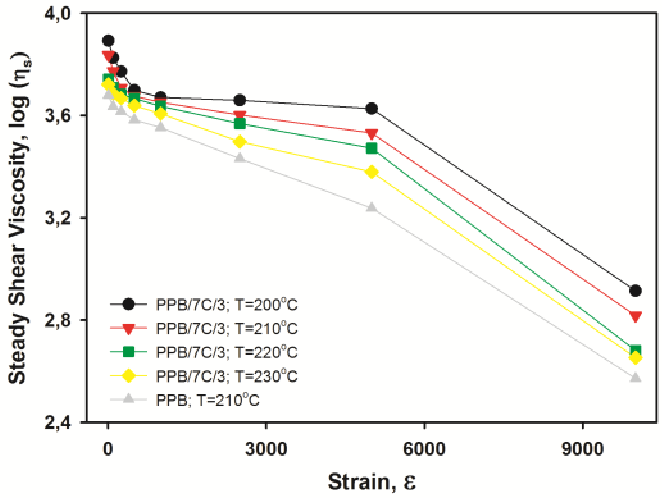

***Figure 3.9**. Logarithm of steady shear viscosity, η_s, as a function of strain, ε, for neat isotactic polypropylene, PPB, and its nanocomposite with 3 wt.% of PTFE 7C. Shear rate of 4 s^{-1} was applied.*

As it follows from morphology investigation (Figure 3.10), in the range of strains up to 4000-5000 a strong deformation of polytetrafluoroethylene 7C particles occurs leading to formation of individual nanofibers. The rate and yield of nanofibers formation is larger for lower temperatures. For the range of temperatures between 200 and 230 ^{o}C and viscosity range as characteristic for the grade of polypropylene, the deformation above 5000 results in the drop of steady shear viscosity accompanied by the orientation of PTFE 7C nanofibers and their occasional fracture.

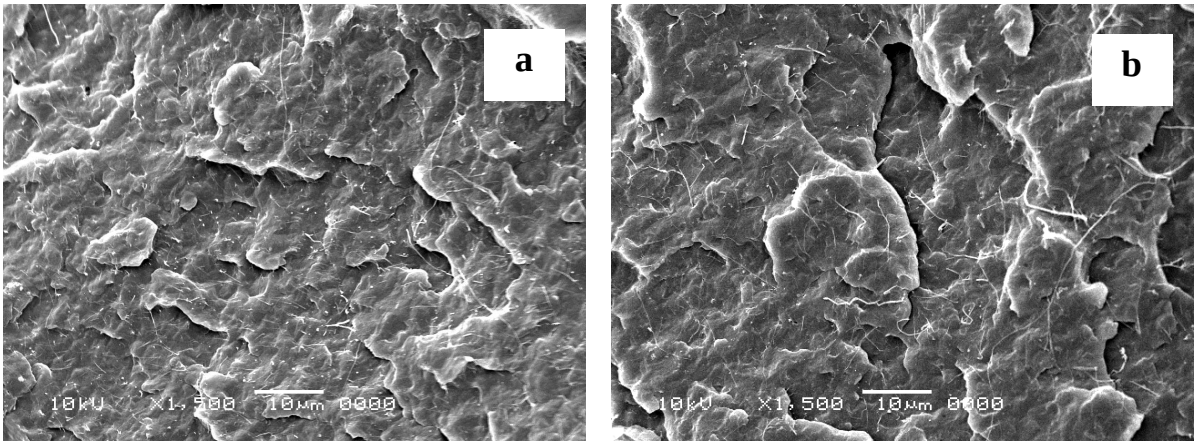

Figure 3.10. *SEM microphotographs of cryogenic fractured samples of PPB/7C/3 nanocomposite after shearing at 200 ^oC and 4 s^{-1} to a given level of deformation: (a) ε = 10 and (b) ε = 5000. Samples were fractured parallel to discs radius.*

Changing the shear rate within the same compounding device and/or changing the device, it is possible to affect strongly the final morphology of the polypropylene-based nanocomposites with nascent polytetrafluoroethylene powders. Figure 3.11 presents SEM microphotographs of cryogenic fractured samples of isotactic polypropylene-based nanocomposites with 5 wt. % of PTFE 7C prepared in two different compounding devices: internal mixer and corrotating twin-screw extruder, at the range of 120÷250 rev. min^{-1}.

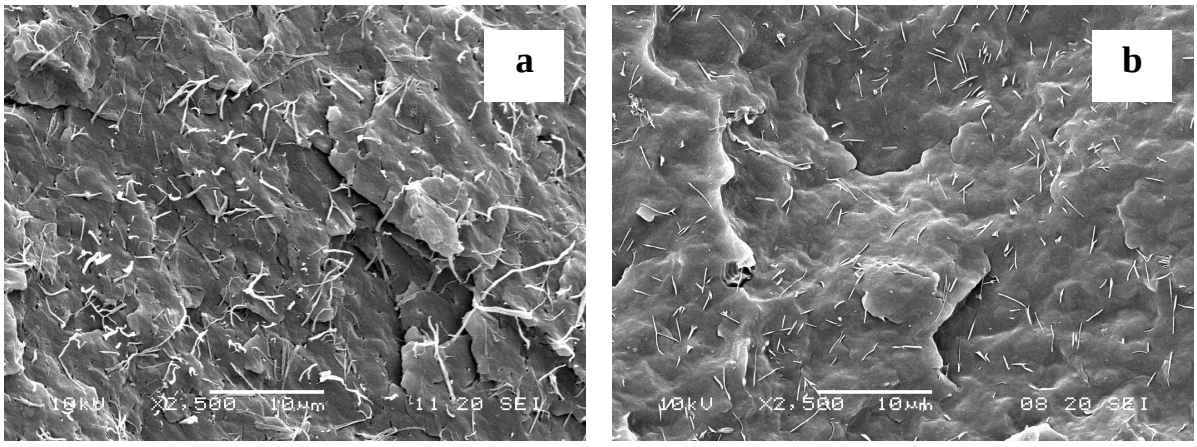

Figure 3.11. *SEM images of cryogenic fractured samples of isotactic polypropylene-based nanocomposites with 5 wt.% of PTFE 7C: (a) PPB/7C/5, 120 rev. min^{-1}, Brabender internal mixer type W50E; and (b) PPH/7C/5, 250 rev. min^{-1}, co-rotating twin-screw extruder type BTSK 20/40D.*

Flows developing in an internal mixer are extremely complex. Both shear flow and extensional flow are pronounces, and only simplified assumption that flows are isothermal, incompressible and creeping allows to derive a formula for average shear rate. Shear rates acting in chamber of internal mixer can be classified as follows: (i) shear rates are high between rotor blade crest and chamber wall, (ii) shear rates are in a transition range in the flanks and (iii) shear rates are low between rotor blade root and chamber wall. The local

average shear rates as a function of the local flight width can be calculated from the following equations [Manas-Zloczower 1994]:

$$\dot{\gamma}_{chamber} = \frac{\pi N_c D_c}{H} \tag{3.3}$$

where N_c is the rotor speed, D_c is the diameter of internal mixer chamber, and H is the rotor clearance. In contrast, the shear rate over the flight in corrotating twin-screw extruder can be determined from the following equation [Manas-Zloczower 1994]:

$$\dot{\gamma}_{flight} = \frac{\pi N_s D_s}{60\delta} \tag{3.4}$$

where N_s is the screw speed, D_s is the screw diameter, and δ is the flight clearance.

The average shear rate of 1154 s^{-1} obtained at the chamber wall in Brabender internal mixer type W50E operating at 120 rev. min^{-1}, allows to deform PTFE 7C particles and transform them into nanofibers, however generated $\dot{\gamma}_{chamber}$ is insufficient to obtain the nanofibers with very high deformation ratios. Preparation of samples for observation in SEM requires fracture of frozen material. During fracture further limited deformation of PTFE 7C nanofibers occurs, polytetrafluoroethylene 7C nanofibers are drawn out from the polypropylene matrix and are observed on the fractured surface of PPB/7C/5 nanocomposite as dangling short fiber ends (Figure 3.11a). Changing the compounding device to co-rotating twin-screw extruder type BTSK 20/40D operating at 250 rev. min^{-1} and the average shear rate of 1309 s^{-1}, thinner and stronger PTFE 7C nanofibers are generated, since only their ends are visible on the surface of cryogenic fractured PPH/7C/5 (Figure 3.11b).

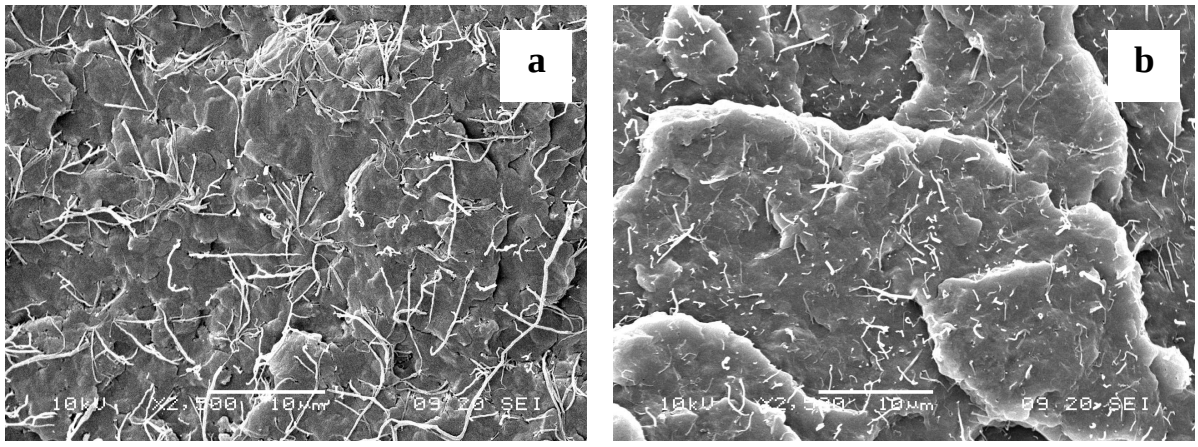

Figure 3.12. *SEM image of cryogenic fractured surface of PPB/7C/5 nanocomposite prepared in Brabender internal mixer type W50E operating at 120 rev. min^{-1} and different time of compounding: (a) 10 min and (b) 15 min.*

Additionally, the time of compounding is an important parameter affecting the final morphology of isotactic polypropylene-based nanocomposites with nascent PTFE 7C powder. Figure 3.12 presents surfaces of cryogenic fractured PPB nanocomposite containing 5 wt.% of PTFE 7C, which was prepared at different time of compounding. Longer the time of compounding larger the deformation of PTFE particles at constant shear rate leading to thinner and stronger polytetrafluoroethylene nanofibers.

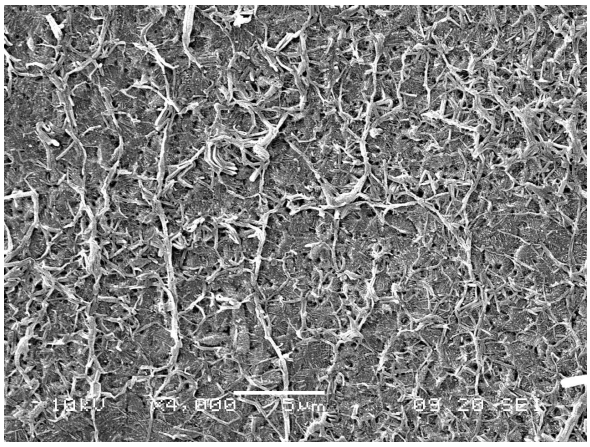

Figure 3.13. *SEM microphotograph of PPB/7C/5 nanocomposite after 45-day etching of thin layer of polypropylene. Material was produced by compounding for 15 min in Brabender internal mixer type W50E operating at 120 rev. min^{-1}.*

Figure 3.13 shows SEM image of the free surface of PPB/7C/5 nanocomposite after 45-day etching of thin layer polypropylene. It is shown that during compounding nascent polytetrafluoroethylene 7C powder with isotactic polypropylene at high shear rate (e.g. 120 rev. min^{-1}), sufficiently long compounding time (e.g. 15 min) enables generation of the entangled network of polytetrafluoroethylene nanofibers.

3.4 Thermal properties of the nanocomposites with PTFE inclusions

Semicrystalline polymers can be modified by means of nucleating agents. In general, presence of a nucleating agent accelerates the crystallization, diminishes the sizes of spherulites and in case of polyolefins can markedly elevate the crystallization temperature, which enables to shorten manufacture of a product. Polytetrafluoroethylene in the form of particles, fibers and films is known to nucleate the crystallization of several semicrystalline polymers, i.e. isotactic polypropylene, i-PP, polyoxymethylene, POM, and induce their transcrystalline morphology [Fitchmun 1970; Wittman 1991; Wang 1996; Wang 1999; Gadzinowska 2003; Van der Meer 2005; Bernland 2009; Masirek 2010].

In this thesis the influence of polytetrafluoroethylene on the crystallization behavior of various grades of isotactic polypropylene was studied both at non-isothermal and isothermal conditions. An exemplary DSC cooling thermograms of neat isotactic polypropylene, PPH, its composite containing 3 wt.% of PTFE particles (PPH/m-200/3) and its nanocomposite with 3 wt.% of PTFE nanofibers (PPH/7C/3) are shown in Figure 3.14.

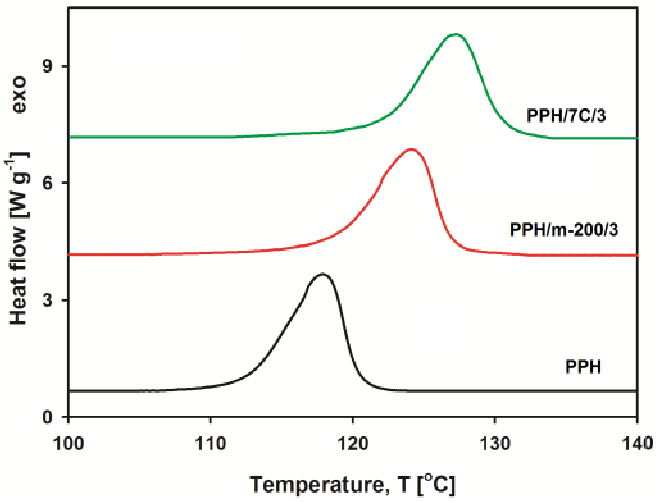

Figure 3.14. *DSC cooling thermograms of neat isotactic polypropylene and PPH containing 3 wt.% of polytetrafluoroethylene in the form of particles (m-200) and nanofibers (7C). Cooling rate of 10 °C min^{-1} was applied. The thermograms have been shifted vertically for clarity.*

The calorimetric data for all studied materials are collected in Table 3.2, where T_m and ΔH_m denote the melting peak temperature and melting enthalpy during heating, respectively, whereas T_c denotes the crystallization peak temperature. Degree of crystallinity, C, was calculated from ΔH_m assuming the heat of fusion for 100 % crystalline polypropylene of 177 J g^{-1} [Li 1999].

Table 3.2. *Thermal properties of neat isotactic polypropylene and polypropylene with various polytetrafluoroethylene powders.*

Material	T_m [°C]	ΔH_m [J g^{-1}]	T_c [°C]	C [%]
PP	161.8	92.12	109.3	52.0
PP/m-200/3	162.1	89.23	126.1	50.4
PP/7C/3	163.6	91.00	127.5	51.4
PPH	162.3	91.07	117.9	51.5
PPH/m-200/3	162.3	88.36	124.1	49.9
PPH/7C/3	162.2	89.29	127.3	50.4
PPB	163.1	91.45	116.6	51.7
PPB/7C/3	163.3	88.48	127.4	50.0
PPB/7C/5	163.7	88.05	128.0	49.7
PPB/7C/7	162.8	86.61	127.7	48.9
PPB/F4-RB/5	162.4	89.86	127.8	50.8

It appears that all three types of studied polytetrafluoroethylene powders (m-200, 7C and F4-RB) increase the crystallization peak temperature of isotactic polypropylene. Neat isotactic polypropylene, PPH, exhibits the crystallization peak temperature of 117.8 °C. Addition of 3 wt.% of PTFE m-200 increases T_c of PPH by 6.3 °C while 3 wt.% of PTFE 7C in the form of nanofibers by 9.5 °C. In the case of other grade of isotactic polypropylene, i.e. PP, showing T_c of 109.3 °C, the presence of polytetrafluoroethylene 7C increases the crystallization peak temperature of PP even by 18.2 °C. Masirek *et al.* observed [Masirek 2010] that the maximum values of the crystallization peak temperature of isotactic polypropylene are obtained when 0.2 wt.% of polytetrafluoroethylene particles are dispersed in the matrix. Further increase of PTFE content does not affect T_c. During the subsequent heating the melting temperature, T_m, of all isotactic polypropylenes was around 162÷163 °C. The enthalpy of melting, ΔH_m, of isotactic polypropylene for all studied materials was within the range of 88÷92 J g^{-1}, which corresponds to the degree of crystallinity of 48÷52 %.

Polytetrafluoroethylene accelerates the crystallization of isotactic polypropylene simultaneously increasing the crystallization peak temperature, nearly not affecting degree of crystallinity, but affecting dramatically the spherulitic pattern. Figure 3.15 compares the structure of neat PPB and PPB/7C/5 nanocomposite formed during isothermal crystallization at temperature of 132 °C and 138 °C, respectively. Two different temperatures of isothermal crystallization were applied. The nanocomposite crystallized so fast at 132 °C that it was impossible to obtain isothermal conditions, while at 138 °C the

time to crystallize neat polypropylene was too long. Large spherulites are visible in the thin film of neat isotactic polypropylene, PPB, whereas very small grains of PPB/7C/5 are hardly discernible in the PLM microphotograph.

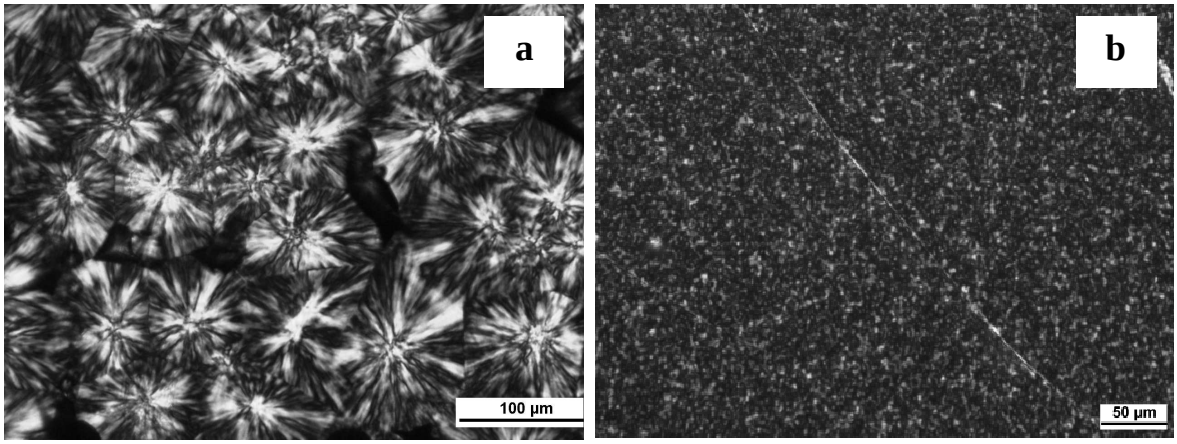

Figure 3.15. *PLM images of thin sections of isothermally crystallized films: (a) neat PPB at 132 ^{o}C, and (b) PPB/7C/5 at 138 ^{o}C.*

Figure 3.16 presents SEM microphotographs of free surfaces of 30 µm films of neat isotactic polypropylene, PPB, and its nanocomposite with 5 wt.% of PTFE 7C nanofibers crystallized in a hot stage during cooling at the rate of 10 ^{o}C min^{-1}.

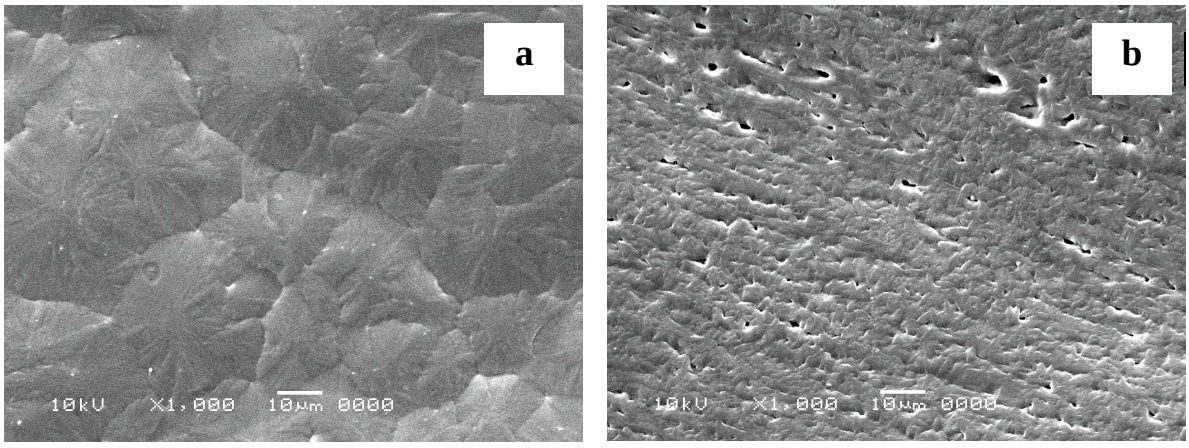

Figure 3.16. *SEM images of free surfaces of samples non-isothermally crystallized at the rate of 10 ^{o}C min^{-1}: (a) PPB and (b) PPB/7C/5.*

In PPB/7C/5 nanocomposite, instead of spherulites typical for neat isotactic polypropylene, PPB, with an average spherulite radius, R_{av}, of 32 µm, a different type of polycrystalline aggregates appears. Spherulitic nucleation of isotactic polypropylene on the surface on polytetrafluoroethylene nanofibers leads to transcrystalline layer development at the PTFE fiber/PP matrix interface. Similar phenomenon was observed earlier by Wang [Wang 1996]. It is known that in fiber-reinforced systems, where fibers are dispersed within a

polymer matrix in a more or less random way, the space inhabited by fibers is not accessible for crystallization [Piorkowska 2006]. Spherulites might be nucleated on fiber surfaces beside those nucleated in polymer bulk. The overall kinetics of crystallization in such systems was intensively studied in the literature [Mehl 1993a; Mehl 1993b; Krause 1994; Benard 1998; Piorkowska 2001]. In those papers the influence of nanofibers on the isothermal crystallization kinetics was studied on the basis of the Evans-Avrami theory [Avrami 1939; Avrami 1940; Avrami 1941]. Isothermal crystallization with the instantaneous or spontaneous nucleation can be described by following Avrami equation:

$$\sigma(t) = 1 - \exp\left(-kt^n\right) \tag{3.5}$$

where $\alpha(t)$ is the conversion degree, *k* is the parameter depending on the nucleation rate and growth rate, *n* assumes values 2, 3, or 4 depending on the type of nucleation and the dimensionality of the process. The Avrami plot of the isothermal experimental data, $\ln\left\{-\ln\left[1-\alpha(t)\right]\right\}$ vs. $\ln t$ should be linear and from the slope of that plot the exponent value, *n*, can be determined.

In this thesis a similar procedure was applied for polypropylene and polypropylene nanocomposite with PTFE nanofibers. Figure 3.17 presents the Avrami plots for neat polypropylene, PPB, and its nanocomposite with 5 wt.% of polytetrafluoroethylene 7C nanofibers. Conversion degree, $\alpha(t)$, was calculated on the basis of DSC thermograms recorded during isothermal crystallization. Two different temperatures (128 ^{o}C for neat PPB and 145 ^{o}C for PPB/7C/5) for this experiment were applied on the basis of the same problems as for isothermally crystallized samples presented in Figure 3.15.

In the case of neat isotactic polypropylene, PPB, isothermally crystallized at 128 ^{o}C, the Avrami analysis of data for *α(t)* in the range from 0.05 to 0.95 yields, the exponent value, *n*, of 2.97 (~3) indicates 3D (3-dimensional) crystallization beginning with instantaneous nucleation. This is consistent with straight interspherulitic boundaries found in thin sections of neat PPB film (Figure 3.15). In contrast, the exponent value, *n*, of 2.02 (~2) for PPB/7C/5 nanocomposite isothermally crystallized at 145 ^{o}C indicates 2D (2-dimensional) crystallization of isotactic polypropylene with its very dense instantaneous nucleation on the surfaces of polytetrafluoroethylene 7C nanofibers.

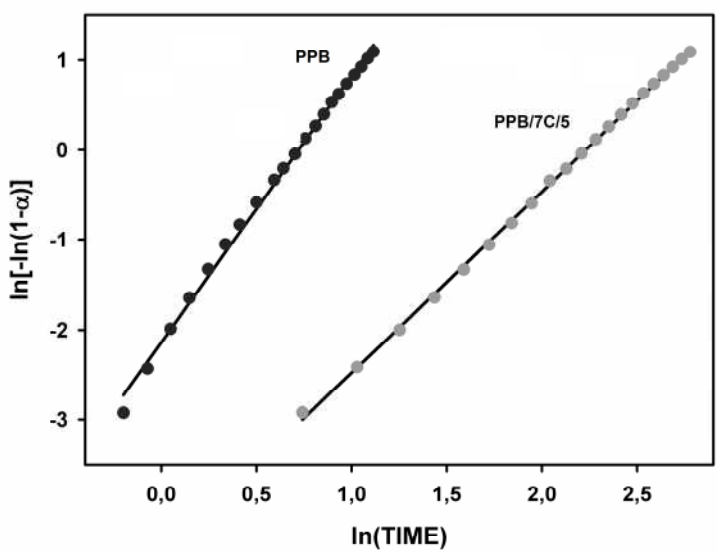

Figure 3.17. *Avrami plots for neat isotactic polypropylene, PPB, and its nanocomposite with 5 wt.% of PTFE 7C nanofibers isothermally crystallized in a DSC at 128 ^{o}C and 145 ^{o}C, respectively: symbols - experimental data, lines – linear regression; α(t) from the range of 0.05 to 0.95.*

It can be concluded that polytetrafluoroethylene nanofibers accelerate the crystallization of isotactic polypropylene with simultaneous elevation of its crystallization temperature, change the shape and diminish the size of growing spherulites. Presence of PTFE nanofibers in the PPB matrix affect the kinetics of isothermal crystallization changing the dimensionally of the crystallization process from 3-dimensional to 2-dimensional.

3.5 Mechanical properties of the nanocomposites with PTFE inclusions

The mechanical properties of polymeric materials often play a key role for their applications. To describe mechanical behavior of the polymeric materials in solid state uniaxial tensile drawing measurements was applied. All sample materials were subjected to uniaxial drawing. An exemplary engineering stress-engineering strain curves for high density polyethylene, HDPE, and its nanocomposite containing 3 wt.% of PTFE 7C nanofibers are presented in Figure 3.18. It is seen that nanocomposite becomes brittle with low elongation at break but slightly stronger. Other system with polytetrafluoroethylene m-200 nonfibrous particles behaves differently: both neat isotactic polypropylene, PPH, and its composite with 3 wt.% of polytetrafluoroethylene m-200 particles exhibit similar yield behavior, however only slight decrease of stress at break, σ_b, and elongation at break, ε_b, by 4.2 MPa and 108 % for PPH/m-200/3, respectively, are observed in comparison with neat PPH. Selected tensile parameters, modulus of elasticity, E, and degree of crystallinity, C, for all systems studied are collected in Table 3.3.

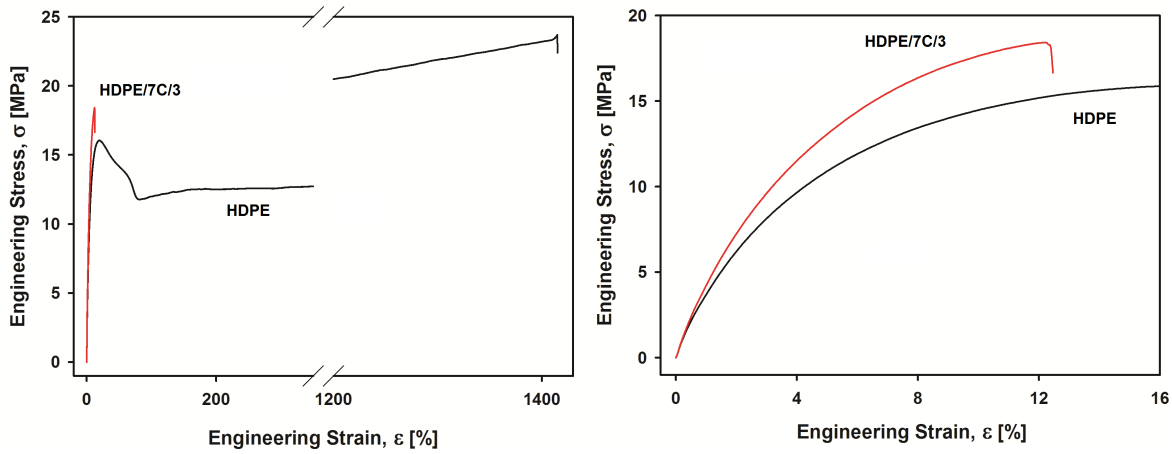

Figure 3.18. *Engineering stress-engineering strain, curves for neat HDPE and HDPE/7C/3 nanocomposite. The right plot is a magnification of curves beginning in the left plot.*

The modulus of elasticity, E, for PPH/m-200/3 increases by 10 % probably only due to the effect of filling polypropylene with PTFE m-200 particles since the degree of crystallinity, C, practically is unchanged. It is known that the presence of polytetrafluoroethylene particles does not affect the mechanical properties of isotactic polypropylene except for the slight increase of the modulus of elasticity [Masirek 2010]. Much different situation is observed in the case of PPH-based nanocomposite containing 3 wt.% of PTFE 7C nanofibers. The sample of PPH/7C/3 fractures immediately after reaching the yield point. Presence of PTFE 7C nanofibers drastically changes mechanical behavior of this nanocomposite causing the increase of yield stress, σ_s, by 3.3 MPa and dramatic decrease

of elongation at break, ε_b, to 17.3 %. This type of stress-strain behavior is also observed for other studied materials containing 3 wt. % of polytetrafluoroethylene 7C nanofibers i.e., PP/7C/3 and HDPE/7C/3, however later sample fractures even before reaching the yield point. It is known that the crystallization of isotactic polypropylene is nucleated by polytetrafluoroethylene fibers [Wang 1996; Wang 1999] and even more by nanofibers (see Chapter 3.4). This ability leads to the increase of the degree of crystallinity, *C*, even by 5 % (e.g. for PPH/7C/3) which in consequence contribute to obtain higher modulus of elasticity, *E*, for the isotactic polypropylene–based nanocomposites even by 35 % (e.g. for PP/7C/3).

Table 3.3. *Selected tensile parameters, modulus of elasticity and degree of crystallinity of tensile samples for selected neat thermoplastic polymers and the materials with polytetrafluoroethylene powder.*

Material	**Yield stress, σ_s [MPa]**	**Stress at break, σ_b [MPa]**	**Elongation at break, ε_b [%]**	**Modulus of elasticity, *E* [GPa]**	**Degree of Crystallinity, *C* [%]**
PPH	29.57	36.52	1576	1.19	42.0
PPH/m-200/3	29.74	32.35	1468	1.31	43.4
PPH/7C/3	32.90	32.62	17.3	1.37	47.3
PP	29.32	33.71	1889	1.25	46.4
PP/7C/3	31.95	31.34	17.1	1.68	51.8
HDPE	16.22	23.66	1415	0.89	58.5
HDPE/7C/3	-	19.90	34.5	0.90	62.0

Semicrystalline polymers including high density polyethylene, HDPE, and isotactic polypropylene, i-PP, exhibit attractive strength and ductility under moderate rates of deformation and at room temperature. Those features enable to use such polymers as engineering materials, however they become brittle at low temperature or high strain rates and can undergo a sharp ductile-to-brittle transition. Because of this disadvantageous behavior the toughening of semicrystalline engineering thermoplastics was intensively studied by many authors [Wu 1990; Wu 1992; Arends 1996; Martuscelli 1996; Walter 1997; Perkins 1999; Bartczak 1999a; Bartczak 1999b; Argon 2003; Lin 2010]. The toughness is a measure of ability of a material to absorb the energy up to fracture [Callister 2007]. Intrinsic properties of a polymer and in consequence its toughness can be changed by means of chemical modification. Apart from this method, two another routes can be used to improve the toughness of polymeric materials. One way is to increase the brittle strength of polymeric material by reinforcing with long, high strength fibers [Kim 1991]. Second way is to reduce the overall plastic resistance of the polymeric material directly or

indirectly by incorporation of fine particles [Bartczak 1999a; Bartczak 1999b; Argon 2003; Lin 2010]. For dynamic loading conditions (i.e. at high strain rates) and when a notch (or point of stress concentration) is present, so-called notch toughness is assessed by using an impact test. In the case of notched Izod impact experiments the Izod impact strength, U_I, [Wu 1992] is defined as a breaking energy per unit of specimen thickness at the breaking point.

The influence of polytetrafluoroethylene nanofibers on the impact properties of thermoplastic polymers including isotactic polypropylene, PPB, atactic polystyrene, PS, and low density polyethylene, LDPE was examined. Figure 3.19 presents the Izod impact strength of atactic polystyrene and the series of its nanocomposites with 1, 3, 5 and 7 wt.% of PTFE 7C nanofibers, measured at room temperature. The results of U_I also for other studied materials are collected in Table 3.4.

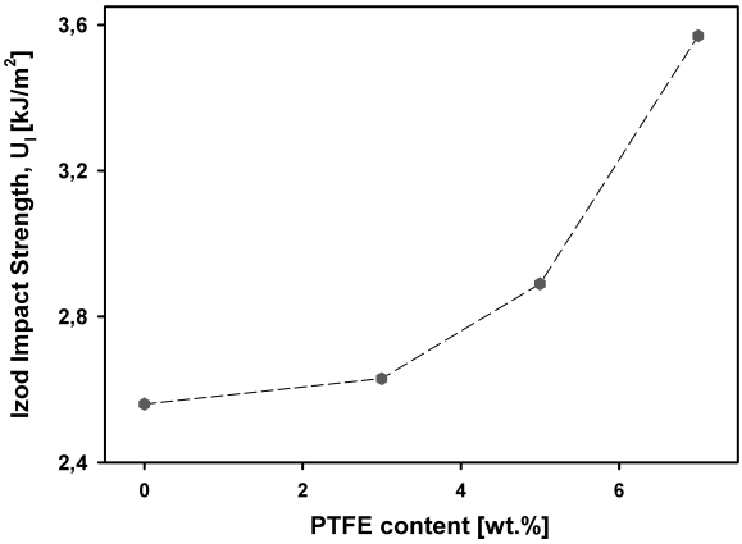

Figure 3.19. *Izod impact strength, U_I, for neat atactic polystyrene, PS, and its nanocomposites as a function of content of PTFE 7C nanofibers.*

It can be seen that the Izod impact strength of atactic polystyrene continuously increases with increasing content of polytetrafluoroethylene 7C nanofibers by 40 % for the nanocomposite containing 7 wt.% of PTFE 7C nanofibers.

The case of nanofibers-filled isotactic polypropylene, PPB, seems to be more complicated as compared to atactic polystyrene, PS. The highest value of U_I (6.27 kJ m^{-2}) is obtained for PPB containing only 1 wt.% of polytetrafluoroethylene 7C nanofibers, higher of about 58 % in comparison with PPB matrix. Concentration of polytetrafluoroethylene nanofibers higher than 1 wt.% leads to a slight decrease of Izod impact strength but obtained values of U_I are still higher as compared to neat matrix. Polytetrafluoroethylene 7C nanofibers also

affect the impact properties of low density polyethylene-based materials. Izod impact strength of low density polyethylene containing 3 or 5 wt.% of PTFE 7C nanofibers is higher by only 8 % in comparison with neat LDPE matrix.

Table 3.4. *Izod impact strength of neat polypropylene, PPB, and low density polyethylene, LDPE, and the series of their nanocomposites with PTFE 7C nanofibers.*

Material	**Izod impact strength, U_I [kJ m^{-2}]**
PPB	3.96
PPB/7C/1	6.27
PPB/7C/3	6.04
PPB/7C/5	5.54
PPB/7C/7	5.13
LDPE	39.04
LDPE/7C/3	42.17
LDPE/7C/5	42.10
LDPE/7C/7	29.67

Higher content of polytetrafluoroethylene nanofibers (i.e. 7 wt.%) causes drastic decrease of U_I by 25 % as compared to neat low density polyethylene. Since there was no intention to orient the polytetrafluoroethylene 7C nanofibers neither during compounding nor preparation of the specimens for impact testing, it is assumed that PTFE 7C nanofibers are randomly dispersed in thermoplastic matrix. So, only those straight polytetrafluoroethylene 7C nanofibers oriented perpendicular to the impact direction contribute to the increase of the Izod impact strength of the thermoplastic matrix. PTFE nanofibers which are parallel to the impact direction do not affect the toughness, but they cause a growth of e.g., polypropylene crystals perpendicular to their surface and such crystals can affect the toughness. At higher concentrations of PTFE 7C, the network of entangled polytetrafluoroethylene nanofibers produced during compounding is probably partially responsible for decrease of the Izod impact strength of both thermoplastic polymers studied.

The dynamic mechanical response of polymeric materials, typically in the terms of storage modulus, *E'*, and loss modulus, *E''*, as a function of temperature can be measured by means of the dynamic mechanical thermal analysis (DMTA). The effect of polytetrafluoroethylene 7C nanofibers on the dynamic mechanical behavior of isotactic polypropylene, PPB, and atactic polystyrene, PS, was investigated. Figure 3.20 presents the temperature-dependence of storage modulus, *E'*, for neat PPB, and its nanocomposite with 3, 5, and 7 wt.% of polytetrafluoroethylene 7C nanofibers.

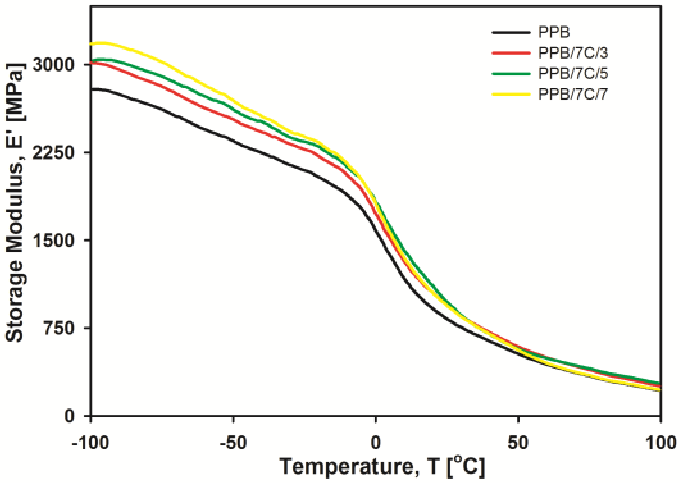

Figure 3.20. *Storage modulus, E', as a function of temperature for neat PPB and its nanocomposite with 3, 5, and 7 wt.% of polytetrafluoroethylene 7C nanofibers.*

It can be observed that the presence of 3 wt.% of PTFE 7C nanofibers causes the increase of storage modulus, *E'*, of isotactic polypropylene, PPB. The stiffness of PPB/7C/3 nanocomposite increases with decreasing temperature and is much more pronounced at temperatures below 0 °C which is attributed to the glass transition temperature, T_g, of amorphous polypropylene [ATHAS Data Bank, http://athas.prz.edu.pl].

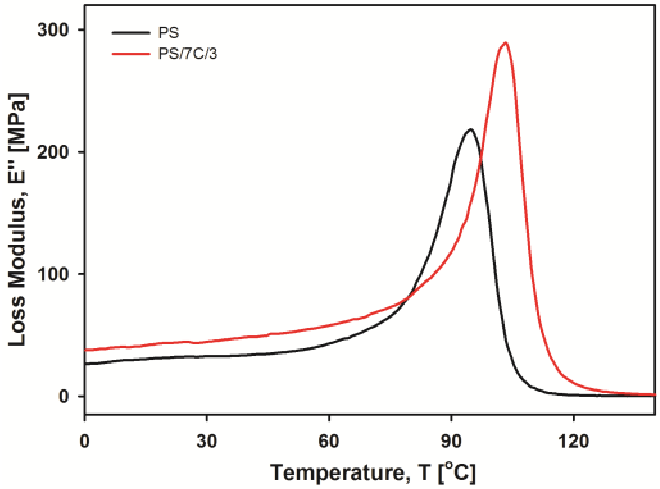

Figure 3.21. *Temperature dependence of loss modulus, E'', for neat atactic polystyrene, PS, and its nanocomposite containing 3 wt.% of PTFE 7C nanofibers.*

The glass transition temperature, T_g, can be defined as the temperature corresponding to the maximum of peak in the *E''(T)* plot. The PPB-based nanocomposites show glass transition at about 2.0 °C, the same as T_g observed for neat isotactic polypropylene, PPB. In contrast, for polystyrene an addition of 3 wt.% of PTFE 7C nanofibers dispersed in the matrix of atactic polystyrene, PS, causes a shift of the loss modulus maximum to higher temperatures, as shown in Figure 3.21. In consequence, T_g of PS increases by 9 °C from 94.5 °C to 103.6 °C. No further increase of the glass transition temperature of atactic

polystyrene is observed for the PS-based nanocomposites with higher contents of polytetrafluoroethylene 7C nanofibers.

3.6 Rheological properties of the nanocomposites with PTFE inclusions

Polymeric materials, e.g. homogeneous polymers, immiscible polymer blends, particulate- or fiber-reinforced polymers exhibit its own unique rheological characteristics. Hence, successful processing of such materials requires a good understanding of their viscoelastic behavior both in the shear and extensional flow [Han 2007]. The viscoelastic properties of polymers depend on their chemical structure [Fetters 1994], molecular weight [Fuchs 1996], molecular weight distribution [Lovell 1961], degree of branching [Berry 1968], temperature, frequency, and also the stress to which a polymer is subjected [Mittal 2010]. In the case of micro- and nanocomposite systems produced by compounding homogenous polymers with other materials, e.g. fillers, the rheological behavior depends also on the filler shape and size, filler concentration, and the extent of any interactions among the filler particles and filler-polymer matrix [Léopoldès 2004; Chabert 2004; Raos 2006; Osman 2006; Nazockdast 2008; Haghtalab 2011]. The effect of polytetrafluoroethylene nanofibers on the viscoelastic properties of the molten nanocomposites based on isotactic polypropylene, i-PP, low density polyethylene, LDPE, high density polyethylene, HPDE, and atactic polystyrene, a-PS, was intensively examined.

3.6.1 Oscillatory shear flow

In oscillatory shear flow, the molten polymer is subjected to the small-amplitude sinusoidal strain with an angular frequency, ω, and the dynamic storage and loss moduli, G' and G'', are measured. G' represents the amount of energy stored per unit volume of the molten polymer, while G'' represents the amount of energy dissipated per unit volume of the molten polymer [Dealy 2006]. Figure 3.22 presents the storage and loss moduli, G' and G'', as a function of angular frequency, ω, for isotactic polypropylene, PPB, and its nanocomposite with 5 wt.% of PTFE 7C nanofibers.

Both G' and G'' increase with increasing ω and in low frequency regime the loss modulus is larger than the storage modulus, demonstrating the viscous nature of isotactic polypropylene (note the log-log scales in Figure 3.22). However, the slope of G'' is smaller than that of G', so that with increasing frequency the two curves cross each other ($G' = G''$) at so-called cross-over frequency, ω_c. This characteristic frequency marks a transition from viscous ($G'' > G'$) to rubbery ($G' > G''$) response. It is known that at low frequency ranges, both moduli are very sensitive to the molecular structure of polymeric

material, especially the size, shape and concentration of dispersed phase [Osman 2006; Nazockdast 2008; Haghtalab 2011].

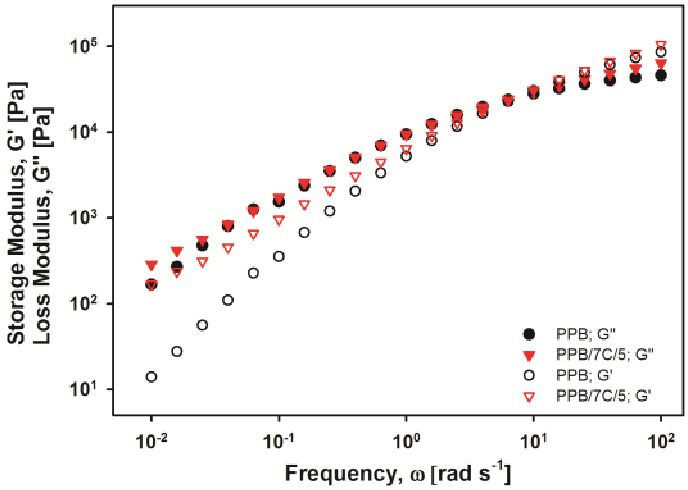

Figure 3.22. *Storage modulus, G', and loss modulus, G'', as a function of angular frequency, ω, at 190 °C for neat polypropylene, PPB, and its nanocomposite with 5 wt.% of PTFE 7C.*

Incorporation of nanoinclusions to a polymer matrix should enhance both the storage modulus and the loss modulus due to its huge specific surface area [Osman 2005]. PPB/7C/5 nanocomposite shows significantly different behavior than neat isotactic polypropylene. PTFE 7C nanofibers cause the increase in *G'* and *G''* over the low- and high frequency range but in the low frequency region the increase in the storage modulus is more pronounced than in loss modulus. Polytetrafluoroethylene 7C nanofibers act as a confinement of polypropylene chains. Such confinement effect leads to an alternation of the relaxation dynamics of isotactic polypropylene chains and in consequence dramatically changes its viscoelastic behavior.

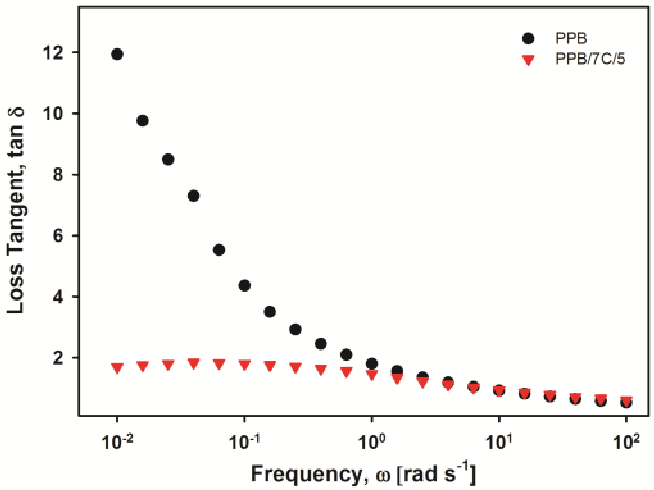

Figure 3.23. *Loss factor, tan δ, as a function of angular frequency, ω, at 190 °C for neat isotactic polypropylene, PPB, and its nanocomposite with 5 wt.% of PTFE 7C nanofibers.*

The loss factor, *tan δ* (=*G''*/*G'*), for neat isotactic polypropylene, PPB, and PPB/7C/5 nanocomposite measured in small-amplitude oscillatory shear is given in Figure 3.23 as a function of angular frequency, ω. For neat PPB, *tan δ* is high and decays very fast with increasing ω to reach a value of 0.5, while for the nanocomposite containing 5 wt.% of PTFE 7C nanofibers, the *tan δ* curve becomes almost flat i.e., shows a very broad peak, reflecting development of the physical entangled network of polytetrafluoroethylene 7C nanofibers which affect the moduli. It appears that PTFE 7C nanofibers cause an increase in *G'* (storage of elastic energy) more than in *G''* (viscous dissipation of that energy) of studied nanocomposites.

3.6.2 Uniaxial extensional flow

Transient extensional viscosity, η_E^+, characterizes a resistance of a fluid to extensional deformation. Uniaxial extension measurements of molten polymeric materials are based on the original Meissner concept [Meissner 1985]. ARES-EVF design enables to deform the sample at a constant strain rate, $\dot{\varepsilon}$, called Hencky rate by extending the sample symmetrically from the sample center with a constant velocity by rotating clamps. The measurements of transient extensional viscosity are most often used to identify propensity of polymeric materials to strain hardening, i.e. how quickly η_E^+ rises above linear viscoelastic response (LVE) with increasing total strain, $\varepsilon \ \left(= t\dot{\varepsilon}\right)$ and strain rate, $\dot{\varepsilon}$ [Takahashi 1993]. Strain hardening induces a so-called self-healing effect which supports a homogenous deformation of the polymer melt. Thus, polymers exhibiting strain hardening in extensional flows play an important role in many industrial processes including fiber spinning, film blowing, blow molding, thermoforming [Yamaguchi 2002], and foaming [Spitael 2004]. The molecular structure, especially long-chain branching strongly influences η_E^+. Hence, the uniaxial extension of the molten polymeric materials also provides a powerful tool for polymer characterization [Münstedt 1998].

The effect of polytetrafluoroethylene 7C nanofibers on the extensional behavior of various thermoplastic polymers in the molten state was examined using extensional viscosity fixture (EVF) attached to the ARES rheometer. Figure 3.24 presents curves of the time-dependent transient extensional viscosity for neat isotactic polypropylene, PPB, and its nanocomposites containing 3, 5 and 7 wt.% of PTFE 7C nanofibers, recorded during uniaxial extension at the strain rate of 2.5 s^{-1} and 200 ^{o}C. The solid line presents the curve

that was obtained by multiplying by a factor 3 the transient shear viscosity, η_S^+, of neat PPB measured at low strain rate of 0.01 s^{-1}.

In the case of viscosity, simple correlations between viscous and elastic properties in shear and extensional flow only exist in the linear regime, i.e. at low strain rates or small strains [Ferry 1970]. This relationship is known as the Trouton ratio, T_r, expressed as

$$T_r = \frac{\eta_E^+}{\eta_S^+} \tag{3.6}$$

In the linear regime the transient extensional viscosity becomes simply three times the transient shear viscosity.

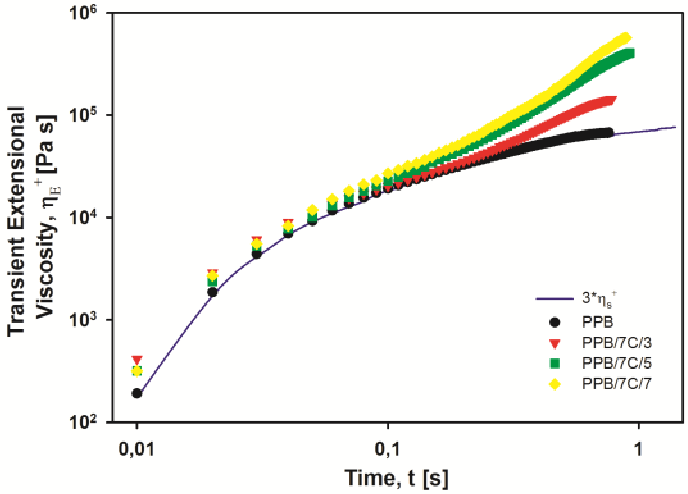

Figure 3.24. *Transient extensional viscosity, η_E^+, as a function of extensional time, t, measured at 2.5 s^{-1} and 200 °C for neat isotactic polypropylene, PPB, and its nanocomposites with 3, 5, and 7 wt.% of PTFE 7C nanofibers. Solid line presents the curve obtained by multiplying by a factor 3 - the transient shear viscosity, η_S^+, at 0.01 s^{-1}.*

During uniaxial extension the molten isotactic polypropylene, PPB, does not exhibit any indication of strain hardening. Both time-dependent η_E^+ and η_S^+ curves for neat PPB practically superimpose. This behavior is well known for linear polyolefins [Münstedt 1981; Gabriel 2003]. Transient extensional viscosity in LVE region for linear polymers is 3÷4 times of the transient shear viscosity [Macosko 1994]. This relationship was experimentally verified for various polymers including polypropylene [Auhl 2004], polyethylene [Meissner 1972; Laun 1978; Münstedt 1998] and polystyrene [Münstedt 1975]. PPB-based nanocomposites containing PTFE 7C nanofibers show a totally different time-dependence of the transient extensional viscosity in contrast to neat isotactic polypropylene. PPB/7C/3 nanocomposite shows a significant strain hardening beginning at the total strain, $\varepsilon = 1.23$. The onset of this process begins earlier with increasing content of polytetrafluoroethylene 7C nanofibers, at $\varepsilon = 0.64$ and $\varepsilon = 0.53$ for PPB/7C/5 and

PPB/7C/7, respectively. Also the magnitude of η_E^+ deviation from linear viscoelastic response arises with increasing content of PTFE 7C nanofibers.

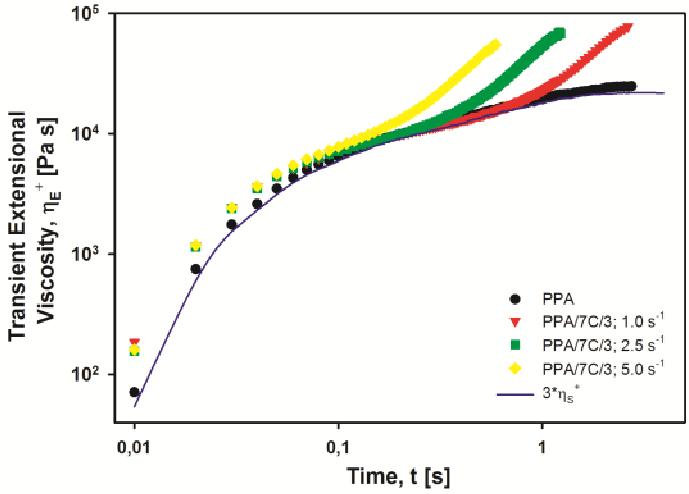

Figure 3.25. *Transient extensional viscosity, η_E^+, as a function of extensional time, t, measured at various strain rates (1.0, 2.5, 5.0 s^{-1}) and 200 °C for neat isotactic polypropylene PPA and PPA/7C/3 nanocomposite. Solid line represents the curve obtained by multiplying by a factor 3 - the transient shear viscosity, η_S^+, at 0.01 s^{-1}.*

Similar rheological behavior to neat PPB is observed for other linear polymers: isotactic polypropylene, PPA, and high density polyethylene, HDPE, as illustrated in Figure 3.25 and Figure 3.26, respectively. Both linear polyolefins: PPA and HDPE exhibit LVE response during uniaxial extension at all strain rates applied, while their nanocomposites with 3 wt.% of PTFE 7C nanofibers show significant strain hardening.

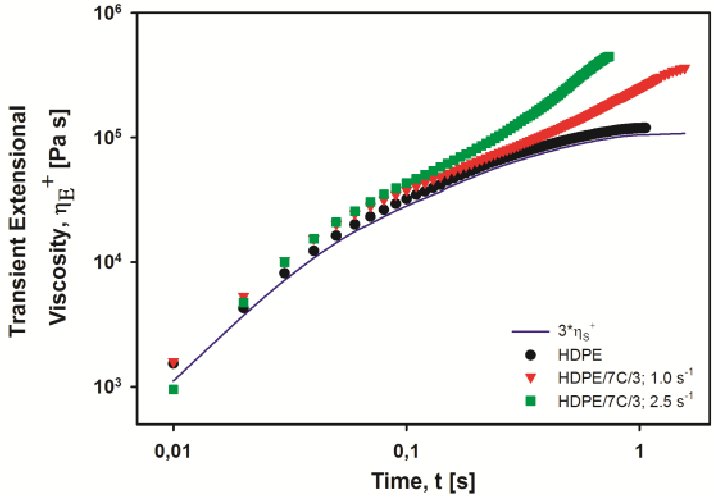

Figure 3.26. *Transient extensional viscosity, η_E^+, as a function of extensional time, t, measured at various strain rates (1.0, 2.5 s^{-1}) and 170 °C for neat HDPE and HDPE/7C/3 nanocomposite. Solid line represents the curve obtained by multiplying by a factor 3 - the transient shear viscosity, η_S^+, at 0.01 s^{-1}.*

Figure 3.27 illustrates the transient extensional viscosity of low density polyethylene, LDPE, and its nanocomposite containing 3, 5 and 7 wt.% of PTFE 7C nanofibers. In

comparison with linear polymers, LDPE exhibits pronounced strain hardening in extensional flow due to presence of long-chain branches [Laun 1978; Wagner 2000]. Hence, the influence of PTFE 7C nanofibers on its viscoelastic behavior is more difficult to observe directly from the transient extensional viscosity-time dependence. However, it can be seen that the non-linear viscoelastic response of the LDPE-based nanocomposites slightly increases with increasing content of polytetrafluoroethylene 7C nanofibers.

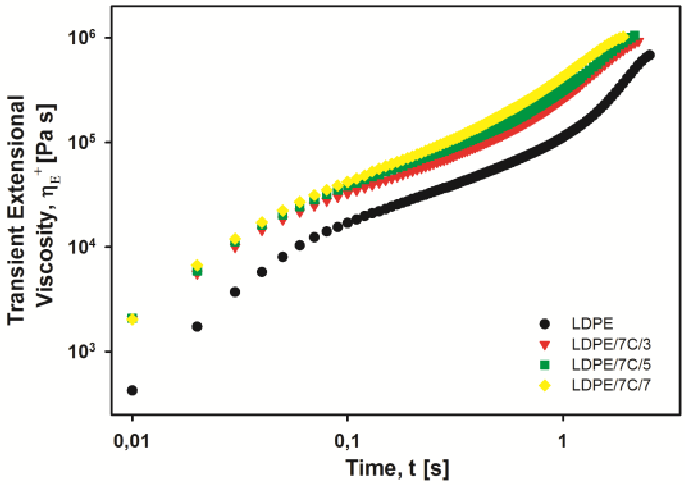

Figure 3.27. *Transient extensional viscosity, η_E^+, as a function of extensional time, t, measured at 1.0 s^{-1} and 170 ^oC for neat LDPE and its nanocomposite with 3, 5 and 7 wt.% of PTFE 7C nanofibers.*

Presence of 3 wt.% of PTFE 7C nanofibers causes a significant increase of the viscosity of LDPE/7C/3 nanocomposite in comparison with neat LDPE (note the log-log scale in Figure 3.27). Similar behaviour is also observed for atactic polystyrene-based nanocomposites with PTFE 7C nanofibers, as shown in Figure 3.28, but subsequent increase of the viscosity is observed with increasing content of polytetrafluoroethylene 7C nanofibers.

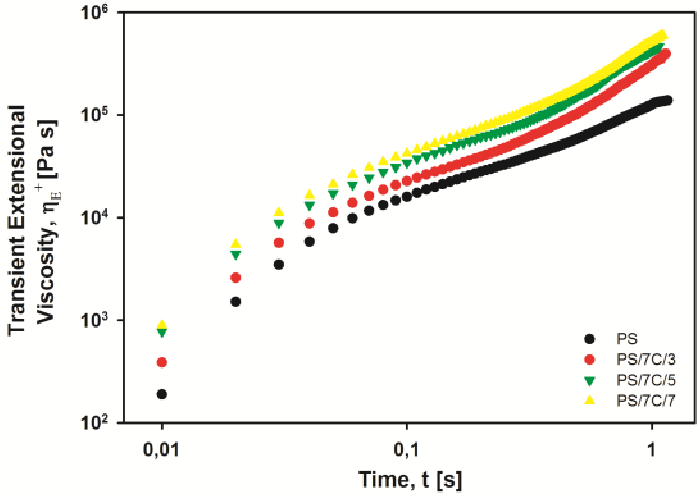

Figure 3.28. *Transient extensional viscosity, η_E^+, as a function of extensional time, t measured at 1.0 s^{-1} and 170 ^oC for neat PS and its nanocomposite with 3, 5 and 7 wt.% of PTFE 7C nanofibers.*

The Trouton ratio, expressed by eq. 3.6, is useful parameter to obtain more quantitative estimation of the strain hardening effect [Kasehagen 1998]. Table 3.5 presents the Trouton ratio determined at a given total strain and strain rate for linear thermoplastic polymers: two grades of isotactic polypropylene, high density polyethylene and their nanocomposites with PTFE 7C. Neat linear polymers including PPB, PPA and HDPE exhibit no strain hardening. Hence, obtained values of Trouton ratio are in the range from 3.22 (for HDPE) to 3.47 (for PPA) since they show linear viscoelastic response during uniaxial extensional deformation. Those T_r values are strain-rate independent. It can be seen that Trouton ratio for linear isotactic polypropylene, PPB, drastically increases with increasing content of PTFE 7C nanofibers and reaches the large value of 21.59 for PPB/7C/7 at 1.0 s^{-1}.

Table 3.5. *Trouton ratio for neat isotactic polypropylene, high density polyethylene and their nanocomposites with PTFE 7C nanofibers, uniaxially extended at 1.0, 2.5, and 5.0 s^{-1}. T_r was determined at the total strain of 1.56 for HDPE, 3.01 for PPA, and 2.65 for PPB, respectively.*

	Strain rate, $\dot{\varepsilon}$ [s^{-1}]		
	1.0	2.5	5.0
Material	**Trouton ratio, T_r**		
PPB	3.34	3.34	3.34
PPB/7C/3	8.71	6.35	5.14
PPB/7C/5	13.44	10.82	9.63
PPB/7C/7	21.59	16.57	13.41
PPA	3.47	3.47	3.47
PPA/7C/3	10.55	9.71	8.92
HDPE	3.22	3.22	-
HDPE/7C/3	9.49	9.27	-

It can also be seen that values of Trouton ratio obtained for PPB-based nanocomposites with polytetrafluoroethylene 7C nanofibers at various strain rates, $\dot{\varepsilon}$, are different. The higher the strain rate the lower T_r. This effect is more pronounced with increasing content of PTFE 7C. It appears that polytetrafluoroethylene 7C nanofibers, generated during compounding, yield to orientation and/or further deformation during uniaxial extension. Similar rheological behavior is observed for low density polyethylene- and high density polyethylene-based nanocomposites with 3 wt. % of PTFE 7C nanofibers. Trouton ratios of those nanocomposites are few times higher than T_r for neat polymers. Ultimate Trouton ratio obtained at a given level of Hencky strain depends on the type of nanocomposite studied (especially the method of its fabrication). If polytetrafluoroethylene 7C nanofibers

obtained during compounding are thinner, stronger and less deformable under extension, like in case of HDPE/7C/3 nanocomposite, Trouton ratio practically is strain-rate independent.

Another important parameter which can help to determine the influence of polytetrafluoroethylene 7C nanofibers on the rheological behavior of studied thermoplastic polymers is the melt strength. The strength of a molten polymer is a measure of its resistance to extensional deformation and in the case of uniaxial extension with a constant strain rate is defined as maximum extensional force generated during test. Melt strength is important in melt processing operations where stretching and/or drawing is involved including thermoforming, fiber extrusion, film extrusion, extrusion coating, blow molding, film blowing and melt spinning [Ghijsels 1990; Ghijsels 1994; Lau 1998]. The melt strength of neat thermoplastic polymers, i.e. PPB, PPA, LDPE, HDPE and PS, and their nanocomposites with PTFE 7C nanofibers are collected in Table 3.6.

Table 3.6. *Melt strength of neat thermoplastic polymers and nanocomposites with PTFE 7C nanofibers obtained at various strain rates (0.1, 1.0, 2.5 and 5.0 s^{-1}), and 170 ^{o}C (for LDPE, HDPE and PS-based materials) and 200 ^{o}C (for PPB and PPA-based materials).*

Material	**Melt strength [mN] at 0.1 s^{-1}**	**Melt strength [mN] at 1.0 s^{-1}**	**Melt strength [mN] at 2.5 s^{-1}**	**Melt strength [mN] at 5.0 s^{-1}**
PPB	67	276	409	453
PPB/7C/3	177	366	511	562
PPB/7C/5	244	681	958	1057
PPB/7C/7	283	715	1060	1384
PPA	-	78	126	170
PPA/7C/3	-	95	139	177
LDPE	113	391	-	-
LDPE/7C/3	286	711	-	-
LDPE/7C/5	379	965	-	-
LDPE/7C/7	617	1304	-	-
HDPE	-	465	647	825
HDPE/7C/3	-	1143	2038	2363
PS	-	211	335	495
PS/7C/3	-	414	659	743
PS/7C/5	-	629	754	1161
PS/7C/7	-	767	1008	1339

The strength in molten state of all materials increases simultaneously with increasing strain rate and content of PTFE 7C nanofibers. But its magnitude strongly depends also on the final structure of prepared nanocomposites, mainly the type and the viscosity of

thermoplastic matrix used, the transverse and longitudinal sizes of generated polytetrafluoroethylene 7C nanofibers and in consequence the magnitude of obtained entanglements between PTFE 7C nanofibers. The strongest influence of PTFE 7C nanofibers on the melt strength is observed for high density polyethylene. Only 3 wt.% of PTFE 7C nanofibers are sufficient to cause the increase in the melt strength of HDPE/7C/3 by 2.4÷3.1 times as compared to neat high density polyethylene, whereas similar values for PPB, LDPE and PS-based nanocomposites are obtain not below the content of 7 wt.% of PTFE 7C nanofibers. PPA/7C/3 nanocomposite seems to be a special case since the presence of PTFE 7C nanofibers practically do not affect its melt strength. Detailed analysis of this nanocomposite structure reveals that applied compounding protocol enabled generation of much thinner PTFE 7C nanofibers (transverse sizes of 10÷30 nm) than those obtained for other polymeric matrices (e.g., 30÷580 nm for PPB/7C/3; and 50÷230 nm for PS/7C/7). In consequence, the network built from such thin PTFE 7C nanofibers possesses either lower entanglements density or disentangling/breaking of such PTFE 7C nanofibers is much easier than in other nanocomposites.

3.7 Conclusions

Crystalline polymer inclusions (polytetrafluoroethylene) can be deformed into nanofibers during compounding by shearing via second polymer being in the molten state provided that crystalline inclusions are formed from disentangled macromolecules. In consequence, a nanocomposite with nanofibrillar inclusions, containing only two polymers, can be formed after solidification of the matrix material. Such 'all polymer' nanocomposite exhibits a series of enhanced thermal, mechanical and rheological properties as direct or indirect effects of polytetrafluoroethylene nanofibers dispersed in the polymer matrix.

To summarize, the PhD thesis allowed to formulate the following important conclusions:

1. Solid inclusions of polytetrafluoroethylene can be deformed into nanofibers by shearing via second molten polymer during compounding on the following conditions:
    (a) Polytetrafluoroethylene powder should be in the form of large crystals in chain-extended fashion without significant entanglements of macromolecules, melting temperature of such crystals must be close to or higher than equilibrium melting temperature being in the range 332÷336 ^{o}C;
    (b) The advantage of deformation of solid particles over molten inclusions is that solid fibers do not undergo capillary instabilities and they do not disintegrate into smaller droplets;
    (c) To initiate the plastic deformation by shearing of chain-extended crystals of polytetrafluoroethylene embedded in a polymer matrix at room temperature, the resolved shear stress of only 6 MPa must be reached and exceeded. The resolved shear stress for crystal shearing is significantly lower at elevated temperature because crystal plasticity is thermally activated phenomenon;
    (d) Sufficiently large deformation ratios and shear rates, and suitably long compounding time must be applied to generate thinner and stronger polytetrafluoroethylene nanofibers;

2. Formation of PTFE nanofibers was observed in all molten polymers used as a matrix, provided that a sufficient shear stress was imposed on the composite.

Various polypropylene, polyethylenes of low and high densities and polystyrene were employed in the studies.

3. Polytetrafluoroethylene nanofibers accelerate the crystallization of isotactic polypropylene with simultaneous elevation of its crystallization temperature. They cause the diminution of the spherulites sizes and change the dimensionally of the crystallization process from 3-D to 2-D, spherulites of isotactic polypropylene grow perpendicular to the nanofibers surfaces.

4. Presence of polytetrafluoroethylene nanofibers drastically changes the mechanical behavior of studied materials causing:
   (a) increase in the yield stress and dramatic decrease of the elongation at break;
   (b) increase in the Izod impact strength;
   (c) increase in the stiffness of isotactic polypropylene;
   (d) increase in the glass transition temperature of polystyrene.

5. Presence of polytetrafluoroethylene nanofibers dramatically changes the rheological behavior of studied materials causing:
   (a) alternation of the relaxation dynamics of isotactic polypropylene chains and in consequence increase in the storage modulus more than in loss modulus;
   (b) significant strain hardening of molten linear polymers like isotactic polypropylene and high density polyethylene that exhibit no strain hardening themselves. Trouton ratios of those nanocomposites are few times higher as compared to neat polymers.
   (c) Increase in the melt strength of other nanocomposites as compared to neat polymers.

6. The expected applications of such nanocomposites can be found in such area where high melt strength is required such as: foaming, fiber spinning, film blowing, film extrusion, film drawing and biaxial film drawing.

3.8 References

Argon A.S., Cohen R.E., **2003**. *Toughenability of polymers*. Polymer 44, 6013-6032;

Arends C.B., **1996**. *Polymer toughening*. Marcel Dekker, New York;

ATHAS Data Bank, (the Advanced Thermal Analysis System); http://athas.prz.edu.pl;

Auhl D., Stange J., Münstedt H., Krause B., Voigt D., Lederer A., Lappan U., **2004**. *Rheological properties of electron beam irradiated polypropylenes.* Macromolecules 37, 9465-9472;

Avrami M., **1939**. *Kinetics of phase change. I. General theory*. J. Chem. Phys. 7, 1103-1112;

Avrami M., **1940**. *Kinetics of phase change. II. Transformation-time relations for random distribution of nuclei*. J. Chem. Phys. 8, 212-224;

Avrami M., **1941**. *Kinetics of phase change. III. Granulation, phase change and microstructure.* J. Chem. Phys. 9, 177-184;

Barham P.J., Sadler D.M., **1991**. *A neutron scattering study of the melting behaviour of polyethylene single mats.* Polymer 32, 393-395;

Bartczak Z., Argon A.S., Cohen R.E., Weinberg M., **1999a**. *Toughness mechanism in semi-crystalline polymer blends: I. High-density polyethylene toughened with rubbers.* Polymer 40, 2331-2346;

Bartczak Z., Argon A.S., Cohen R.E., Weinberg M., **1999b**. *Toughness mechanism in semi-crystalline polymer blends: II. High-density polyethylene toughened with calcium carbonate filler particles*. Polymer 40, 2347-2365;

Bartczak Z., Beris P.F.M., Wasilewski K., Galeski A., Lemstra P.J., **2012**. *Deformation of the Ultra-High Molecular Weight Polyethylene Melt in the Plain-Strain Compression*. J. Appl. Polym. Sci. DOI 10.1002/app.36595;

Bassett D.C., Davitt R., **1974**. *On crystallization phenomena in polytetrafluoroethylene.* Polymer 15, 721-728;

Benard A., Advani S.G., **1998**. *An analytical model for spherulitic growth in fiber-reinforced polymers.* J. Appl. Polym. Sci. 70, 1677-1787;

Bernland K., Smith P., **2009**. *Nucleating Polymer Crystallization with Poly(tetrafluoroethylene) Nanofibrils.* J. Appl. Polym. Sci. 114, 281-287;

Berry G.C., Fox T.G., **1968**. *The viscosity of polymers and their concentrated solutions.* Adv. Polym. Sci. 5, 261-357;

Bunn C.W., Howells E.R., **1954**. *Structures of molecules and crystals of fluorocarbons.* Nature 274, 549-551;
Callister W.D. Jr., Rethwisch R.G., **2007**. *Fundamentals of Material Science and Engineering. An Integrated Approach*. Third ed., John Wiley & Sons, Inc.;
Chabert E., Dendievel R., Gauthier C., Cavaille J.-Y., **2004**. *Predictions of the elastic response of polymer based nanocomposites: a mean field approach and a discrete simulation.* Comp. Sci. Tech. 64, 309-316;
Dealy J.M., Larson R.G., **2006**. *Structure and Rheology of Molten Polymers. From structure to flow behavior and back again*. Carl Hanser Verlag, Munich;
Ferry J.D., **1970**. *Viscoelastic properties of polymers*.
John Wiley & Sons, Inc., New York;
Fetters L.J., Lohse D.J., Richter D., Witten T.A., Zirkel A., **1994**. *Connection between Polymer Molecular Weight, Density, Chain Dimensions, and Melt Viscoelastic Properties*. Macromolecules 27, 4639-4647;
Fitchmun D.R., Newman S., **1970**. *Surface Crystallization of Polypropylene.*
J. Polym. Sci. Part A-2 8, 1545-1564;
Franck A., **2010**. *The ARES-EVF: Option for Measuring Extensional Viscosity of Polymer Melts*. TA Instruments, Germany, PN002;
Fuchs K., Friedrich Chr., Weese J., **1996**. *Viscoelastic Properties of Narrow-Distribution Poly(methyl methacrylates).* Macromolecules 29, 5893-5901;
Gabriel C., Münstedt H., **2003**. *Strain hardening of various poyolefins in uniaxial elongational flow.* J. Rheol. 47, 619-630;
Gadzinowska K., Piorkowska E., **2003**. *Influence of sample thickness and surface nucleation on i-PP crystallization kinetics in DSC measurements*. Polimery 48, 790-799;
Galeski A., **2003**. *Strength and toughness of crystalline polymer systems.*
Prog. Polym. Sci. 28, 1643-1699;
Ghijsels A., Ente J.J.S.M., Raadsen J., **1990**. *Melt strength behavior of PE and its relation to bubble stability in film blowing*. Intern. Polym. Process. 5, 284-286;
Ghijsels A., De Clippeleir J., **1994**. *Melt strength behaviour of polypropylenes*.
Intern. Polym. Process. 3, 2-7;
Haghtalab A., Marzban R., **2011**. *Viscoelastic properties of nanosilica-filled polypropylene in the molten state: Effect of particle size.* Adv. Polym. Tech. 30, 203-218;
Han C.D., **2007**. *Rheology and Processing of polymeric materials, Vol.1 Polymer Rheology*. Oxford University Press;

Hodder P., Franck A., **2005**. *A new tool for measuring extensional viscosity*. in *Annual Transactions of the Nordic Rheology Society*. vol. 13, Aho J. (ed), Juvenes Print, Tampere;
Kasehagen L.J., Macosko C.W., **1998**. *Nonlinear shear and extensional rheology of long-chain randomly branched polybutadiene*. J. Rheol. 42, 1303-1328;
Keller A., **1968**. *Polymer crystals*. Rep. Prog. Phys. 31, 623-704;
Kim J.-K., Mai Y.-W., **1991**. *High Strength, High Fracture Toughness Fibre Composites with Interface Control – A Review.* Comp. Sci. Tech. 41, 333-378;
Krause T.H., Kalinka G., Auer C., Hinrichsen G., **1994**. *Computer simulation of crystallization kinetics in fiber-reinforced composites.* J. Appl. Polym. Sci. 51, 399-406;
Lau S.-F., Suzuki H., Wunderlich B., **1984**. *The thermodynamic properties of polytetrafluoroethylene.* J. Polym. Sci. Polym. Phys. Ed. 22, 379-405;
Lau H.C., Bhattacharya S.N., Field G.J., **1998**. *Melt Strength of Polypropylene: Its Relevance to Thermoforming*. Polym. Eng. Sci. 38, 1915-1923;
Laun H.M., Münstedt H., **1978**. *Elongational behaviour of a low density polyethylene melt I. Strain rate and stress dependence of viscosity and recoverable strain in the steady-state. Comparison with shear data. Influence of interfacial tension.* Rheol. Acta 17, 415-425;
Léopoldès J., Barrès C., Leblanc J.L., Georget P., **2004**. *Influence of Filler-Rubber Interactions on the Viscoelastic Properties of Carbon-Black-Filled Rubber Compounds*. J. Appl. Polym. Sci. 91, 577-588;
Li J.X., Cheung W.L., Jia D., **1999**. *A study on the heat of fusion of β-polypropylene*. Polymer 40, 1219-1222;
Lin L., Argon A.S., **1994**. *Review: Structure and plastic deformation of polyethylene.* J. Mater. Sci. 29, 294-323;
Lin Y., Chen H., Chan C.-M., Wu J., **2010**. *The toughening mechanism of polypropylene/calcium carbonate nanocomposites.* Polymer 51, 3277-3284;
Lippits D.R., Rastogi S., Talebi S., Bailly C.M.E., **2006**. *Formation of entanglements in initially disentangled polymer melts.* Macromolecules 39, 8882-8885;
Lovell S.E., Ferry J.D., **1961**. *Influence of molecular weight distribution on viscoelastic properties of polymers as expressed by the rouse and zimm theories.* J. Phys. Chem. 65, 2274-2276;
Macosko C.W., **1994**. *Rheology: Principles, Measurements, and Applications*. Wiley-VCH, New York;
Manas-Zloczower I., Tadmor Z.Sunder J., **1994**. *Mixing and compounding of polymers. Theory and practice*. Hanser, New York;

Martuscelli E., Musto P., Ragosta G., **1996**. *Advanced routes for polymer toughening.* Elsevier, Amsterdam;

Masirek R., **2007**. *Role of spatial confinement in nucleation of polymer crystallization.* PhD Thesis, Lodz, Poland;

Masirek R. Piorkowska E., **2010**. *Nucleation of crystallization in isotactic polypropylene and polyoxymethylene with poly(tetrafluoroethylene) particles.* Eur. Polym. J. 46, 1436-1445;

Mehl N.A., Rebenfeld L., **1993a**. *Computer simulation of crystallization kinetics and morphology in fiber-reinforced thermoplastic composites. II. Three-dimensional case.* J. Polym. Sci. Part B: Polym. Phys. 31, 187-193;

Mehl N.A., Rebenfeld L., **1993b**. *Computer simulation of crystallization kinetics and morphology in fiber-reinforced thermoplastic composites. II. Two-dimensional case.* J. Polym. Sci. Part B: Polym. Phys. 31, 1677-1686;

Meissner J., **1972**. *Development of a Uniaxial Extensional Rheometer for the Uniaxial Extension of Polymer Melts.* Trans. Soc. Rheol. 16, 405-420;

Meissner J., **1985**. *Experimental aspects in polymer melt elongational rheology.* Chem. Eng. Commun. 33, 159-180;

Mittal V., **2010**. *Optimization of polymer nanocomposite properties.* Wiley-VCH Verlag, Weinhein;

Münstedt H., **1975**. *Viscoelasticity of polystyrene melts in tensile creep experiments.* Rheol. Acta 14, 1077-1088;

Münstedt H., Laun H.M., **1981**. *Elongational properties and molecular structure of polyethylene melts.* Rheol. Acta 20, 211-221;

Münstedt H., Kurzbeck S., Egersdörfer L., **1998**. *Influence of molecular structure on rheological properties of polyethylenes Part II. Elongational behavior.* Rheol. Acta 37, 21-29;

Nazockdast E., Nazockdast H., Goharpey F., **2008**. *Linear and Nonlinear Melt-State Viscoelastic Properties of Polypropylene/Organoclay Nanocomposites.* Polym. Eng. Sci. 48, 1240-1249;

Osman M.A., Atallah A., **2005**. *Interparticle and particle –matrix interactions in polyethylene reinforcement and viscoelasticity.* Polymer 46, 9476-9488;

Osman M.A., Atallah A., **2006**. *Effect of the particle size on the viscoelastic properties of filled polyethylene*. Polymer 47, 2357-2368;

Perkins W.G., **1999**. *Polymer Toughness and Impact Resistance.* Polym. Eng. Sci. 39, 2445-2460;

Philips P.J., **1990**. *Polymer crystals*. Rep. Prog. Phys. 53, 549-604;

Piorkowska E., **2001**. *Modeling of crystallization kinetics in fiber reinforced composites*. Macromol. Symp. 169, 143-148;

Piorkowska E., Galeski A., Haudin J.-M., **2006.** *Critical assessment of overall crystallization kinetics theories and predictions.* Prog. Polym. Sci. 31, 549-575;

Pucciariello R., Villani V., Mancusi C., **1999**. *On melt-crystallization of polytetrafluoroethylene and of random fluorinated copolymers of tetrafluoroethylene.* J. Appl. Polym. Sci. 74, 1607-1613;

Pucciariello R., Villani V., **2004**. *Melt and crystallization behavior of poly(tetrafluoroethylene) by temperature modulated calorimetry*. Polymer 45, 2031-2039;

Raos G., Moreno M., Elli S., **2006**. *Computational experiments on filled rubber viscoelasticity: what is the role of particle-particle interactions?* Macromolecules 39, 6744-6751;

Rastogi S., Spoelstra A.B., Goossens J.G.P., Lemstra P.J., **1997**. *Chain Mobility in Polymer Systems: on the Borderline between Solid ans Melt. 1. Lamellar Doubling during Annealing of Polyethylene.* Macromolecules 30, 7880-7889;

Spitael P., Macosko C.W., **2004**. *Strain Hardening in Polypropylenes and Its Role in Extrusion Foaming*. Polym. Eng. Sci. 44, 2090-2100;

Takahashi M., Isaki T., Takigawa T., Masuda J., **1993**. *Measurement of biaxial and uniaxial extensional flow behavior of polymer melts at constant strain rates.* J. Rheol. 37, 827-846;

Toda A., Hikosaka M., Yamada K., **2002**. *Superheating of the melting kinetics in polymer crystals: a possible nucleation mechanism.* Polymer 43, 1667-1679;

Van der Meer D.W., Milazzo D., Sanguineti A., Vancso G.J., **2005**. *Oriented Crystallization and Mechanical Properties of Polypropylene Nucleated on Fibrillated Polytetrafluoroethylene Scaffolds.* Polym. Eng. Sci. 45, 458-468;

Wagner M.H., Bastian H., Hachmann P., Meissner J., Kurzbeck S., Münstedt H., **2000**. *The strain-hardening behaviour of linear and long-chain-branched polyolefin melts in extensional flows.* Rheol. Acta 39, 97-109;

Walter R., Friedrich K., Privalko V., Savadori A., **1997**. *On Modulus and Fracture Toughness of Rigid Particulate Filled High Density Polyethylene.* J. Adhesion 64, 87-109;

Wang C., Hwang L.M., **1996**. *Transcrystallization of PTFE Fiber/PP Composites (I) Crystallization Kinetics and Morphology.* J. Polym. Sci. Part B: Polym. Phys. 34, 47-56;
Wang C., Liu C.R., **1999**. *Transcrystallization of polypropylene composites: nucleation ability of fibers.* Polymer 40, 289-298;
Wittmann J.C., Smith P., **1991**. *Highly oriented thin films of poly(tetrafluoroethylene) as a substrate for oriented growth of materials.* Nature 352, 414-417;
Wu S., **1990**. *Chain Structure, Phase Morphology, and Toughness Relationships in Polymers and Blends*. Polym. Eng. Sci. 30, 753-761;
Wu S., **1992**. *Control of Intrinsic Brittleness and Toughness of Polymers and Blends by Chemical Structure: A Review.* Polym. Inter. 29, 229-247;
Wunderlich B., **1976**. *Macromolecular Physics, Volume 2 Crystal nucleation, Growth, Annealing.* Academic Press, Inc., New York;
Wunderlich B., **1980**. *Macromolecular Physics, Volume 3 Crystal Melting.* Academic Press, Inc., New York;
Yamaguchi M., Suzuki K., **2002**. *Enhanced Strain Hardening in Elongational Viscosity for HDPE/Crosslinked HDPE Blend. II. Processablility of Thermoforming.* J. Appl. Polym. Sci. 86, 79-83;
Yang J., Williams R., Peterson K., Geil P.H., Long T.-C., Xu P., **2005**. *Morphology evolution in polytetrafluoroethylene as a function of melt time and temperature. Part III. Effect of prior deformation.* Polymer 46, 8723-8733;

3.9 Nomenclature

Letters of the Roman Alphabet

a	Diameter of liquid drop
B	Width of an ellipsoid
C	Degree of crystallinity
Ca	Capillary number
Ca_{crit}	Critical capillary number
d	Density
D	Deformation of liquid drop
D_c	Chamber diameter
D_s	Screw diameter
E	Modulus of elasticity
E'	Storage modulus from bending
E''	Loss modulus from bending
e_f	Efficiency parameter
f_c	Hermans orientation parameters of crystalline phase
f_a	Hermans orientation parameters of amorphous phase
G'	Storage modulus (from shearing)
G''	Loss modulus (from shearing)
H	Rotor clearance
ΔH_m	Heat of melting (or melting enthalpy or enthalpy of fusion)
ΔH_m^0	Heat of melting of 100% crystalline polymer
k	Parameter (shear sensitivity to the normal stress)
l	Lamellae thickness
L	Length of an ellipsoid
M_n	Number-average molecular weight
M_w	Weight-average molecular weight
n	Coefficient (exponent value in the Avrami equation)
N_c	Rotor speed
N_s	Screw speed
p	Viscosity ratio
R	Local radius of a drop
R_{av}	Average spherulite radius
R_0	Radius of an undisturbed thread
$R(z)$	Radius of a disturbance
$\bar{R}$	Average radius of disturbed thread
$tan\ \delta$	Loss factor, (= G'' / G')
t_b	Disintegration time of a liquid thread
T_c	Crystallization peak temperature
T_g	Glass transition temperature
T_m	Melting peak temperature
T_m^0	Equilibrium melting temperature
T_{ons}	Onset melting temperature
T_r	Trouton ratio
U_I	Izod impact strength
X_m	Dominant wave number
x	Rotation angle

Capital Greek Letters

ϕ	Orientation angle
Ω	Dimensionless growth rate of a disturbance
Ω_m	Dimensionless growth rate of dominant disturbance

Lower Case Greek Letters

α	Disturbance amplitude
α_0	Original disturbance amplitude
$\alpha(t)$	Conversion degree
β	Growth rate of a disturbance
γ	Total shear
$\dot{\gamma}$	Shear rate
$\dot{\gamma}_{chamber}$	Local average shear rate in a chamber
$\dot{\gamma}_{flight}$	Shear rate over the flight
δ	Flight clearance
ε	Total strain (or strain)
$\dot{\varepsilon}$	Strain rate (or Hencky rate)
ε_b	Elongation at break
η_c	Viscosity of a matrix (or a continuous phase)
η_E^+	Transient extensional viscosity
η_s	Steady shear viscosity
η_S^+	Transient shear viscosity
λ	Disturbance wavelength
λ_m	Wavelength of dominant disturbance
ω	Angular frequency
ω_c	Cross-over frequency ($G'=G''$)
τ	Shear stress
τ_c	Critical resolved shear stress
τ_0	Critical resolved shear stress in the absence of any normal stress on the slip planes
σ	Interfacial tension
σ_b	Stress at break
σ_e	Basal surface free energy
σ/R	Interfacial stress
σ_n	Resolved stress normal to the slip plane
σ_s	Yield stress
σ_y	Compressive yield stress

3.10 List of patents and papers

Patents:

K. Jurczuk, A. Galeski, E. Piorkowska-Galeska, Polish Patent Application No. P-390607, *Polimerowe nanokompozyty włókniste is sposób ich otrzymywania*, 4-03-2010;

K. Jurczuk, A. Galeski, E. Piorkowska-Galeska, European Patent Application No. EP-11460010, *All-polymer fibrillar nanocomposites and method for manufacture of thereof*, 6-03-2011;

Papers at various stages of publication that resulted from PhD thesis investigations:

1. All-polymer nanocomposites with nanofibrillar inclusions generated *in situ* during compounding.

   Macromolecules IF 4.838

2. Polytetrafluoroethylene nanofibers as rheology modifiers for thermoplastic polymers.

   Journal of Rheology IF 3.117

3. Role of polytetrafluoroethylene nanofibers in strain hardening.

   European Polymer Journal IF 2.517

4. Continuous extrusion foaming of polypropylene/polytetrafluoroethylene nanocomposites.

   Colloid and Polymer Science IF 2.443

3.11 Summary

Polymer nanocomposites represent a new and attractive alternative to conventionally filled polymers. The virtue of polymer nanocomposites is neither solely based on the mechanical enhancement of the neat resin nor based on the direct replacement of current filler or blend technology. Rather, its importance comes from providing value-added properties not present in the neat resin, without sacrificing the resin's inherent processability and mechanical properties or by adding excessive weight. Polymer-polymer composites are rear and known only when ready-made nanofibers or nanodroplets are dispersed in the matrix. Previous attempts of formation of polymer nanocomposites with fibrillar inclusions by compounding were unsuccessful, because it was impossible to deform a solidified polymer inclusions during compounding, while in a molten state impossible to preserve the shape of extended threads because of capillary instabilities leading to their breakup into droplets.

A new idea which has been exploited in this thesis was to use crystalline polymer inclusions and deform them into nanofibers during compounding by shearing via second polymer being in the molten state. It is known that deformation of polymer crystals to large strains is possible when the density of entanglements persisting in the amorphous phase is drastically reduced. Hence, selection of a polymer for the studies was based on the low chain entanglement of the polymer forming crystals. Crystallization during polymerization of tetrafluoroethylene enables formation of polytetrafluoroethylene (PTFE) with large chain-extended crystals having high melting temperature (higher than its equilibrium melting temperature) suggesting low entanglement state. Because of reduced density of entanglements and crystals with extended chains, deformation process of polytetrafluoroethylene by shearing is possible and easy, so PTFE crystalline powder has been chosen as crystalline polymer inclusions for further studies. A range of polymer matrices was used including various polypropylenes, high density polyethylene, low density polyethylene and polystyrene.

The main objective of this thesis was to generate nanofibers of polytetrafluoroethylene *in situ* during compounding solid PTFE particles with thermoplastic matrix being in a molten state. The influence of a type of polytetrafluoroethylene, polymer matrix and its viscosity, as well as processing parameters including shear rate and mixing time on the deformation of PTFE crystals into nanofibers ,

has been studied. Other objective of the thesis was to analyze an effect of generated PTFE nanofibers on the thermal, mechanical, and rheological properties of studied materials.

On the basis of performed experimental studies it has been concluded that polytetrafluoroethylene nanofibers can be generated *in situ* during compounding solid PTFE particles with molten polymer matrix if critical conditions of fibrillation described below are fulfilled:

(a) polytetrafluoroethylene consists of chain-extended crystals with melting temperature higher than equilibrium melting temperature being in the range 332÷336 ^{o}C;

(b) In order to deform PTFE crystals embedded in a polymer matrix a critical shear stress, in a slip plane of the PTFE crystal slip systems should be resolved, a shear stress of the order of few MPa must be reached and exceeded.

(c) Formation of PTFE nanofibers was observed in all molten polymers used as a matrix, provided that a sufficient shear stress was imposed on the composite either during compounding or in the shearing rheometer.

It has been shown that larger the deformation ratios and shear rates, and longer the compounding times enable the formation of thinner and stronger polytetrafluoroethylene nanofibers that are in the form of entangled network, which in turns drastically changes thermal, mechanical and rheological properties of generated 'all polymer' nanocomposites, especially causes:

(a) acceleration of crystallization of isotactic polypropylene with simultaneous elevation of its crystallization temperature, diminution of the spherulites sizes and their alteration (spherulites of isotactic polypropylene grow perpendicular to the surface of PTFE nanofibers);

(b) increase in Izod impact strength and stiffness of studied materials and elevation of glass transition temperature of atactic polystyrene;

(c) alternation of the relaxation dynamics of isotactic polypropylene chains and in consequence increase in storage modulus more than in loss modulus;

(d) significant increase in strain hardening of molten linear polymers like isotactic polypropylene and high density polyethylene that exhibit no strain hardening itself;

(e) increase in the melt strength of nanocomposites compared to neat polymers.

The results of the thesis enabled a fabrication of new generation of ‘all polymer’ nanocomposites reinforced by polytetrafluoroethylene nanofibers with wide potential applications. Simplicity of fabrication just by shearing the dispersed crystalline inclusions in another molten polymers would play very important role in minimizing the costs, hazardous exposure to nanofillers and environmental impact, all being usually very high when dealing with ready made nanofillers.